The mechanisms of exercise-induced improvements in whole-body glycemia in RabGAP-deficient mice

Inaugural-Dissertation

zur Erlangung des Doktorgrades

der Mathematisch-Naturwissenschaftlichen Fakultät

der Heinrich-Heine-Universität Düsseldorf

vorgelegt von

Lena Espelage

aus Lohne

Düsseldorf, März 2023

aus dem Institut für Klinische Biochemie und Pathobiochemie
des Deutschen Diabetes-Zentrums (DDZ)
Leibniz-Zentrum für Diabetes-Forschung
an der Heinrich-Heine-Universität Düsseldorf

Gedruckt mit der Genehmigung der
Mathematisch-Naturwissenschaftlichen Fakultät der
Heinrich-Heine-Universität Düsseldorf

Berichterstatter:

1. Prof. Dr. Hadi Al-Hasani
2. Prof. Dr. Christine R. Rose

Tag der mündlichen Prüfung: 24.07.2023

Summary

The Rab-GTPase-activating protein (RabGAP) TBC1D4 is a regulator of glucose uptake into skeletal muscle and white adipose tissue (WAT) by mediating GLUT4 translocation to the plasma membrane. Recently, a common loss-of-function variant in the *TBC1D4* gene (p.Arg684Ter) was identified in the indigenous Greenlandic population that confers *TBC1D4* depletion specifically in muscular tissues. Furthermore, homozygous p.Arg684Ter allele carriers exhibit postprandial hyperglycemia and an increased risk to develop type 2 diabetes mellitus. Whole-body *Tbc1d4*-deficient mice (D4KO) reflect the human phenotype in demonstrating postprandial hyperglycemia caused by impaired insulin-stimulated glucose uptake into oxidative skeletal muscle fibers and WAT, accompanied with reduced GLUT4 abundance. Interestingly, physical activity improves glucose homeostasis particularly in homozygous p.Arg684Ter allele carriers, implicating the relevance of a skeletal muscle TBC1D4-independent pathway. In D4KO mice, regular exercise training results in enhanced insulin-stimulated glucose uptake and a restored GLUT4 abundance into primary white adipocytes, but not in skeletal muscle.

The present study investigated the individual contribution of skeletal muscle and WAT in exercise-mediated improvements in whole-body glycemia, previously observed in D4KO mice. Therefore, skeletal muscle-specific (mD4KO) and white adipocyte-specific *Tbc1d4*-deficient (aD4KO) mice were metabolically characterized after a chronic exercise intervention. We demonstrated that tissue-specific TBC1D4 ablation in skeletal muscle or adipose tissue alone did not lead to pronounced improvements in WAT after a chronic exercise intervention. While mD4KO mice displayed an impaired glucose transport and reduced GLUT4 abundance in skeletal muscle, aD4KO mice exhibited impairments in glucose uptake exclusively in the WAT. Both tissue-specific knockout mouse lines were characterized by postprandial hyperglycemia, but only mD4KO animals had improved postprandial glycemia in response to chronic exercise. However, aD4KO mice were glucose intolerant, which was restored after the training intervention. Therefore, both tissues in concordance might be responsible for the exercise-mediated improvements observed in trained whole-body D4KO mice. We suggest that the *Tbc1d4*-deficient skeletal muscle secretes a factor in response to the chronic exercise intervention that affects insulin sensitivity of *Tbc1d4*-deficient WAT. The performed transcriptome analysis in *Gastrocnemius* muscle of mD4KO mice provided evidence that TBC1D4 might regulate vesicle trafficking by linking trans-Golgi-network and endosome-derived vesicles, which might bridges the gap to *Tbc1d4*-deficient WAT, improving its insulin sensitivity.

Further investigations will aim to clarify the complex interaction in skeletal muscle-adipocyte crosstalk. Thereby, focusing on *Tbc1d4*-deficient WAT and its presumably altered signal transduction, which might contribute to the observed improved insulin sensitivity after chronic exercise.

Zusammenfassung

Das Rab-GTPase-aktivierende Protein (RabGAP) TBC1D4 spielt eine wichtige Rolle in der Regulierung der Glukoseaufnahme in die Skelettmuskulatur und ins weiße Fettgewebe (WAT), da es die Translokation von GLUT4 zur Plasmamembran koordiniert. In der indigenen Grönländischen Population wurde kürzlich eine weit verbreitete *loss-of-function* Variante im *TBC1D4* Gen (p.Arg684Ter) identifiziert, die zu einer skelettmuskel-spezifischen *TBC1D4* Depletion führt. Homozygote Allelträger dieser Variante zeigen eine postprandiale Hyperglykämie, sowie ein erhöhtes Risiko an Typ 2 Diabetes mellitus zu erkranken. Ganzkörper *Tbc1d4*-defiziente Mäuse (D4KO) spiegeln diesen humanen Phänotyp, da sie ebenfalls eine postprandiale Hyperglykämie aufweisen, bedingt durch eine gestörte Insulin-stimulierte Glukoseaufnahme in oxidative Muskelfasern und ins WAT, einhergehend mit einer verringerten GLUT4 Abundanz. Nach sportlicher Aktivität verbessert sich die Glukosehomöostase interessanterweise ausschließlich in homozygoten p.Arg684Ter Allelträgern, das auf einen TBC1D4-unabhängigen Signalweg im Skelettmuskel schließen lässt. Ebenfalls D4KO Mäuse zeigen nach einem chronischen Ausdauertraining eine verstärkte Insulin-stimulierte Glukoseaufnahme. Zudem ist die GLUT4 Abundanz im WAT wiederhergestellt, allerdings nicht im Skelettmuskel.

Der individuelle Beitrag der Skelettmuskulatur und des WAT bezüglich der verbesserten Ganzkörper-Glyklämie nach körperlicher Aktivität wurde in der hier vorliegenden Studie untersucht. Dazu wurden Skelettmuskel-spezifische (mD4KO) und Adipozyten-spezifische *Tbc1d4*-defiziente (aD4KO) Mäuse nach einer chronischen Trainingsintervention metabolisch charakterisiert. Die gewebsspezifische TBC1D4 Defizienz in Muskel und WAT führte nach dem chronischen Training zu keiner verbesserten Insulinsensitivität des WAT. Dies deutet darauf hin, dass beide Gewebe im Zusammenspiel für die TBC1D4-abhängigen Verbesserungen der Ganzkörper-Glykämie in trainierten D4KO Mäusen verantwortlich sind. mD4KO Mäuse zeigten nach der Trainingsintervention eine Verbesserung in der postprandialen Hyperglykämie, wohingegen dies nicht bei aD4KO Mäusen beobachtet wurde. Wir nehmen an, dass der *Tbc1d4*-defiziente Muskel nach dem Training einen Faktor sekretiert, der die postprandialen Blutglukosespiegel verbessert. Die in der vorliegenden Arbeit durchgeführte Transkriptomanalyse des *Gastrocnemius* Muskels von mD4KO Mäusen liefert Beweise, dass TBC1D4 möglicherweise den Vesikeltransport reguliert, in dem es das Trans-Golgi-Netzwerk mit Endosom-assoziierten Vesikeln verknüpft und so die Insulinsensitivität des *Tb1d4*-defizienten WAT verbessern könnte.

Künftige Untersuchungen zielen darauf die komplexe Interaktion zwischen Skelettmuskulatur und WAT weiter aufzuklären. Dafür wird *Tbc1d4*-defizientes WAT hinsichtlich einer veränderten Signaltransduktion untersucht, das möglichlichweise die Insulinsensitivität nach chronischem Training verbessert.

Table of contents

1 Introduction

1.1 *Diabetes mellitus*

Diabetes mellitus is a group of metabolic diseases characterized by chronically increased blood glucose levels (hyperglycemia), due to impaired insulin secretion and/or reduced insulin sensitivity (DeFronzo et al., 2015). In 2021, 537 million adults (between 20 and 79 years) worldwide suffered from diabetes mellitus and it is estimated that this number will rise up to 783 million cases by 2045 (IDF, 2021). Diabetes mellitus is one of the leading causes of death, as 6.7 million people died in 2021 due to this disease. In Germany, around 6.2 million adults (between 20 and 79 years) currently suffer from diabetes, which accounts for an age-adjusted prevalence of 6.9 % (IDF, 2021).

Besides gestational diabetes and other specific forms, diabetes mellitus is classified into two main types: type 1 diabetes mellitus (T1DM) usually develops during childhood and adolescence and is associated with an absolute insulin deficiency (Gale, 2005, Atkinson et al., 2014). The complete degradation of insulin-producing pancreatic β-cells in the islets of Langerhans is the cause of this autoimmune disease, resulting in the need for a lifelong insulin substitution (Bluestone et al., 2010, Atkinson et al., 2014).

In comparison, T2DM usually occurs during adulthood and is associated with insulin resistance in peripheral tissues, impaired insulin secretion and obesity (Roden and Shulman, 2019, Stumvoll et al., 2005). Due to impaired insulin sensitivity and a relative insulin deficiency, insulin-stimulated glucose uptake into peripheral tissues like skeletal muscle or adipose tissue is decreased, leading to continuously rising blood glucose levels (Czech, 2017, Czech, 2020, Galicia-Garcia et al., 2020). An interaction between genetic predisposition, risk factors (obesity, hypertension and dyslipidemia) and lifestyle factors (sedentary lifestyle and smoking) are leading causes for the manifestation of T2DM (Collaboration, 2016, Galicia-Garcia et al., 2020, Wong et al., 2016, Maddatu et al., 2017).

Untreated or insufficiently treated T1DM and T2DM lead to serious short-term and long-term complications. The ketoacidotic coma is a characteristic complication for T1DM patients, as the absolute insulin deficiency leads to dramatically increased blood glucose levels if untreated (>250 mg/dl) (Evans, 2019, Kitabchi et al., 2009). Symptoms are polyuria and metabolic acidosis, as ketone bodies are produced in an uncontrolled manner, thus leading to the acidification of the blood, a life-threatening situation (Fayfman et al., 2017, Miles et al., 1980). In conditions of relative insulin deficiency, for instance in patients with T2DM, the hyperosmolar coma presents a severe short-term complication. Relative insulin deficiency leads to blood glucose levels higher than 600 mg/dl, resulting

in dehydration, polyuria and altered level of consciousness (Kitabchi et al., 2009, Fayfman et al., 2017). Likewise, hypoglycemia leads to severe complications, as low blood glucose levels result in confusion, seizures, loss of consciousness or death (Kittah and Vella, 2017, Cryer, 2007). Complications due to increased blood glucose levels that develop over time affect many organ systems. The main common long-term complications in T2DM are nephropathy, neuropathy, retinopathy and cardiomyopathy (Emerging Risk Factors et al., 2010, Vinik et al., 2013, Jindal et al., 2013, Wang and Lo, 2018).

1.2 Obesity and insulin resistance

T2DM is strongly associated with obesity and peripheral insulin resistance (Haslam, 2010). Obesity is defined as an abnormal or excessive fat accumulation with a body mass index (BMI) >30 kg/m² (WHO, 2000). According to the World Health Organization (WHO), in 2016 more than 1.9 billion adults were overweight with a BMI >25 kg/m². Of these, over 650 million individuals were obese. Thereby, the worldwide obesity rate has been nearly tripled since 1975 (WHO, 2021). In Germany, 67 % of male and 53 % of female individuals were overweight in 2016, among those one fourth was classified as obese (Schienkiewitz et al., 2017). The increased obesity prevalence is attributed to environmental factors, such as an excessive energy intake of a high-caloric diet and a sedentary lifestyle (Dunstan et al., 2012, Barazzoni et al., 2018). In addition, the individual genetic predisposition accounts for the steadily increasing number of obese people (Prasad and Groop, 2015).

A common consequence of obesity is insulin resistance, defined as impaired insulin action in insulin-target tissues like the skeletal muscle or the adipose tissue (Petersen and Shulman, 2018, Lustig et al., 2022). Thereby, insulin fails to induce insulin signaling, leading to reduced glucose uptake and further rising blood glucose levels. In order to compensate hyperglycemia, insulin production in pancreatic β-cells is increased, which results eventually in hyperinsulinemia (Elton et al., 1994, Friedman et al., 1994, da Silva Rosa et al., 2020). T2DM develops when pancreatic β-cells fail to compensate for the insulin resistance in peripheral tissues (Goodpaster and Sparks, 2017). Various reasons lead to the development of insulin resistance. A causative role in the development of insulin resistance has been observed for elevated levels of plasma free fatty acid (FFA) (Guerreiro et al., 2022). Insulin resistant individuals display increased plasma FFA concentration as insulin is not able to inhibit lipolysis in adipose tissue appropriately (Abdul-Ghani and DeFronzo, 2010, Groop et al., 1989, Groop et al., 1991). Simultaneously, obese individuals display an increased entry of FFAs into diverse non-adipose tissues such as the skeletal muscle, without correspondingly enhanced lipid oxidation, thus intramyocellular lipids (IMCL) accumulate (Shulman, 2014, Barazzoni et al., 2018, Bell et al., 2010). Due to the partial

degradation of FFAs within skeletal muscle, bioactive lipid molecules, such as diacylglycerols (DAGs) and ceramides accumulate and further induce impairments in insulin action, for instance via the activation of atypical PKC isoforms and protein phosphatase 2A, which leads to phosphorylation of serine residues of IRS-1 and AKT dephosphorylation (Itani et al., 2000, Dobrowsky et al., 1993, da Silva Rosa et al., 2020, Laurens and Moro, 2016). Moreover, pro-inflammatory cytokines releasing immune cells (for instance macrophages and T-cells) have been observed in adipose tissue and skeletal muscle of obese individuals, resulting in local muscle inflammation that further promotes insulin resistance by disrupting insulin-stimulated tyrosine phosphorylation of IR or IRS, or by downregulating molecules involved in insulin signaling (Wu and Ballantyne, 2020, Wu and Ballantyne, 2017)

1.3 Energy metabolism in skeletal muscle and adipose tissue

1.3.1 Skeletal muscle anatomy

Skeletal muscles account for about 40 % of total body weight in lean humans and affect the movement such as locomotion and maintaining posture (Frontera and Ochala, 2015). Moreover, skeletal muscle is built in a bundles-with-bundles structure. Overall, skeletal muscle consists of fibers that are bundled into fascicles, each of them containing 10 to 100 muscle fibers that are individual muscle cells, called myocytes (Mukund and Subramaniam, 2020). Muscle fibers are long protein bundles composed of thin and thick filaments. Thin filaments contain mainly actin, tropomyosin and troponin, whereas thick filaments consist mainly of myosin. These filaments occur in repeated basic functional units (sarcomeres), which are necessary for skeletal muscle contraction (Frontera and Ochala, 2015, Mukund and Subramaniam, 2020).

Skeletal muscle consists of two major fiber types, namely slow-twitch (type I) and fast-twitch (type II) fibers (Frontera and Ochala, 2015, Schiaffino and Reggiani, 2011). Slow-twitch or type I muscle fibers are resistant to fatigue, as they are mostly relying on oxidative metabolism, because of their high mitochondrial and oxidative enzyme content (Chen et al., 2022). Moreover, they are saturated with mitochondria and myoglobin, thus appearing with a red color (Schiaffino, 2018). Type I fibers are found more abundantly in endurance athletes, as they are contracting for a long period with little force generation (Mukund and Subramaniam, 2020). In comparison, fast-twitch or type II fibers demonstrate a high capacity of glycolytic enzymes to ensure adequate ATP generation (Sawano and Mizunoya, 2022). They are further divided into the subtypes IIA, IIB, and IIX due to their expression patterns of myosin heavy chain isoforms (Schiaffino, 2018). Fast-twitch fibers exhibit a low myoglobin and mitochondrial content, but are abundant in glycolytic enzymes, which give them their characteristic

light color (Mukund and Subramaniam, 2020, Schiaffino, 2018). As these fiber types exhibit faster contraction times due to a rapid level of calcium release and uptake by the sarcoplasmic reticulum, they are fatiguing easier than type I fibers, thus are more abundant in strength and power athletes (Mukund and Subramaniam, 2020, Frontera and Ochala, 2015).

1.3.2 Adipose tissue anatomy

Adipose tissue accounts for 20-28 % of the total body mass in lean humans (Thompson et al., 2012). As the potentially largest endocrine organ, it plays a pivotal role in the regulation of physiological functions, including metabolic homeostasis, appetite, angiogenesis, immunity and the cardiovascular system (Coelho et al., 2013). Adipose tissue is usually divided into white (WAT), brown (BAT), and beige adipose tissue (BeAT). WAT is mainly located either subcutaneously (subcutaneous white adipose tissue, scWAT) or in the abdominal cavity (visceral white adipose tissue, visWAT) (Aldiss et al., 2018). scWAT is located under the skin and accounts for the majority of WAT in humans, whereas visWAT is found around the kidneys, intestines, vasculature, and heart (Despres and Lemieux, 2006). Moreover, visWAT possesses a greater cardio-metabolic risk following expansion (Despres and Lemieux, 2006). The main function of WAT is to store and mobilize energy via the accumulation of triglycerides and the oxidation of fatty acids (Mu et al., 2021, Morigny et al., 2021). In comparison, BAT is located primarily in the supraclavicular region and expends energy for thermogenesis when it is activated, a process known as “non-shivering thermogenesis” (Cannon and Nedergaard, 2004, Sacks and Symonds, 2013). Thereby, oxidative metabolism is uncoupled in favor of heat production via uncoupling protein 1 (UCP1), a protein located in the inner membrane of the mitochondria (Sacks and Symonds, 2013, Fedorenko et al., 2012). BeAT is located in WAT and possesses similarities to BAT, as it also produces heat (Shao et al., 2019).

1.3.3 Metabolic flexibility and fuel selection

Metabolic flexibility is defined as the capacity of organisms to accordingly adapt fuel oxidation to fuel availability during alterations in energy demand (Goodpaster and Sparks, 2017, Mengeste et al., 2021). In healthy individuals during fasting conditions, FFAs serve as principal fuel source for energy production in skeletal muscle (Chomentowski et al., 2011). In the absence of insulin, skeletal muscle glucose uptake is decreased, whereas simultaneously lipolysis in adipose tissue is increased. FFAs are released into the circulation and, in turn, taken up by skeletal muscle for energy generation via fatty

acid oxidation (FAO) (Rynders et al., 2018, Hue and Taegtmeyer, 2009). Thereby, fuel oxidation switches from glucose to fatty acid oxidation. In contrast, during postprandial conditions blood glucose levels are rising, stimulating the secretion of insulin from the pancreatic β-cells. Consequently, skeletal muscle glucose uptake is initiated and glucose further oxidized for energy production, whereas lipid oxidation is prevented (Rynders et al., 2018, Chomentowski et al., 2011, Hue and Taegtmeyer, 2009). Moreover, insulin inhibits lipolysis in adipose tissue, thus reducing FFA levels in the blood stream. Beside the nutritional status, physical activity requires a tremendous degree of metabolic flexibility in order to ensure fuel availability and utilization in response to the increased energy demand (Egan and Zierath, 2013, Hawley et al., 2014).

1.3.4 Glucose uptake into skeletal muscle and adipose tissue

Skeletal muscle and adipose tissue are the main tissues for glucose disposal in response to insulin stimulation. Approximately 80 % of the blood glucose is taken up by skeletal muscle, while adipose tissue accounts for around 10 % of whole-body glucose uptake (Ng et al., 2012). Insulin-stimulated glucose uptake into skeletal muscle and adipose tissue is facilitated via the glucose transporter type 4 (GLUT4; gene name *SLC2A4*). In skeletal muscle, both insulin and muscle contraction induce glucose uptake via enhanced GLUT4 translocation to the plasma membrane (Fazakerley et al., 2022). Although adipose tissue plays only a minor role in whole-body glucose uptake compared to skeletal muscle, insulin-stimulated adipose tissue glucose uptake has an important impact on whole-body glycemia. Adipose tissue-specific GLUT4 knockout mice display glucose intolerance and IR, and *in vivo* glucose uptake into adipose tissue is reduced by approximately 50 % in these animals. Individual animals even developed severe IR and diabetes, emphasizing the importance of adipose tissue in regulating whole-body glycemia (Minokoshi et al., 2003, James et al., 1985). Interestingly, *in vivo* glucose uptake into skeletal muscle is also impaired in these animals, indicating an important inter-organ crosstalk between these two tissue types (Abel et al., 2001).

In response to carbohydrate intake, blood glucose levels increase, leading to the release of insulin into the blood stream from pancreatic β-cells (Campbell and Newgard, 2021). Then, insulin binds to the insulin receptor (IR) that is located in the cell membrane of skeletal muscle and adipose tissue. The IR is a tyrosine kinase and built as a hetero-tetramer, consisting of two extracellular α- and two intracellular β-subunits, covalently connected via disulfide bridges. Insulin binds to the α-subunits, thereby initiating a conformational receptor change, leading to the autophosphorylation of various tyrosine residues of the β-subunits (Boucher et al., 2014). The activated tyrosine kinase phosphorylates different insulin receptor substrates (IRS), thereby activating phosphatidylinositol-3’-kinase (PI3K) that

in turn phosphorylates phosphatidylinositol (4,5)-bisphosphate (PIP_2) to phosphatidylinositol (3,4,5)-trisphosphate (PIP_3) (Boucher et al., 2014). PIP_3 recruits the protein kinase B (PKB = AKT) to the plasma membrane, where it is activated via phosphorylation by 3-phosphoinositide-dependent kinase 1 (PDK1). In skeletal muscle as well as in adipose tissue, activated AKT phosphorylates the Rab-GTPase-activating proteins (RabGAPs) TBC1D1 and TBC1D4 (also known as Akt substrate of 160 kDa = AS160) (Miinea et al., 2005, Sano et al., 2003, Chavez et al., 2008). Phosphorylation of both RabGAPs leads to the activation of Rab (Ras related in brain) proteins, that promote the translocation of GLUT4-containing storage vesicles (GSVs) to the plasma membrane, resulting in the fusion of GLUT4 with the plasma membrane, hence initiating the glucose transport into the cell (Fazakerley et al., 2022).

Beside insulin stimulation, skeletal muscle contraction leads to increased glucose uptake into skeletal muscle (Richter et al., 2021). In response to skeletal muscle contraction, for instance during exercise, intracellular calcium concentration increases, triggering the interaction of the myofibrillar actin-myosin complex and thereby causing ATP-dependent muscle contraction (Mukund and Subramaniam, 2020). The increasing ATP demand in contracting skeletal muscle fibers increases the AMP:ATP-ratio, thus activating the AMP depending protein kinase (AMPK) via one of its upstream kinase liver kinase B1 (LKB1). AMPK in turn phosphorylates the two RabGAPs TBC1D1 and TBC1D4 at various sites, leading to GLUT4 translocation and increased glucose influx into the cell (Richter and Hargreaves, 2013). Figure 1 summarizes the insulin- and contraction-stimulated glucose uptake into skeletal muscle

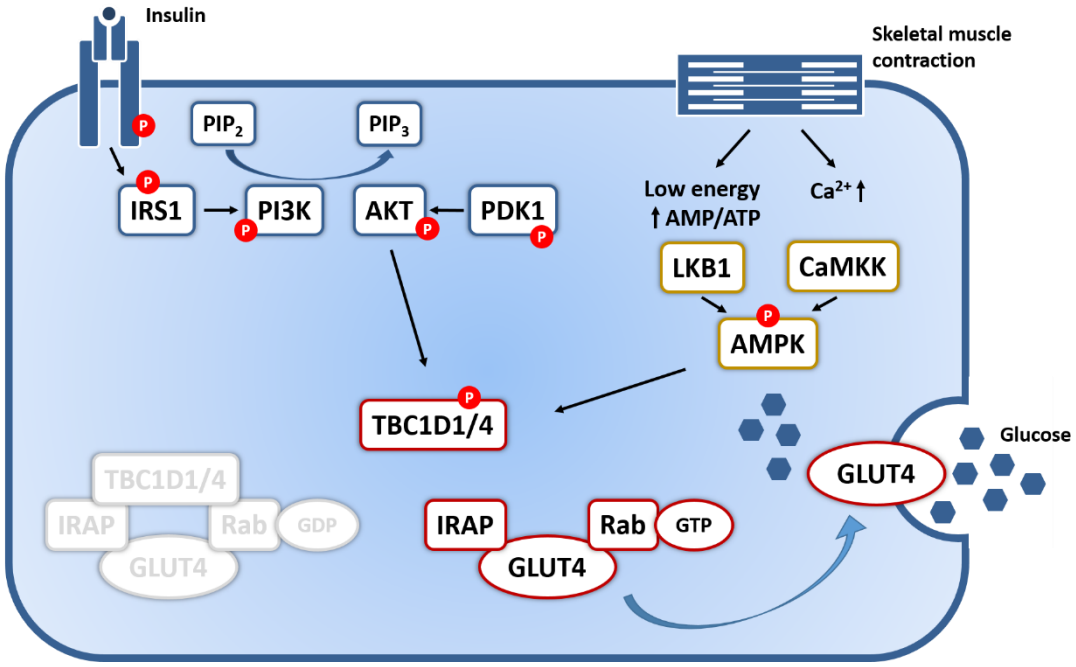

Figure 1: Insulin- and contraction-stimulated glucose uptake into skeletal muscle. Insulin binds to the IR, which leads to its autophosphorylation, resulting in the phosphorylation of IRS1, which in turn phosphorylates PI3K. PI3K catalyzes the conversion of PIP_2 to PIP_3, which recruits AKT to the plasma membrane, where it is activated via phosphorylation by PDK1. Activated AKT phosphorylates the RabGAPs TBC1D1 and TBC1D4. In the unphosphorylated state, both RabGAPs catalyze GTP hydrolysis, thereby Rab proteins remain in their more inactive GDP-bound conformational state and inhibiting GLUT4 translocation. Upon phosphorylation, RabGAP function is inhibited, thus Rab proteins are in their more active GTP-bound state, leading to the translocation of GLUT4 to the plasma membrane. Beside insulin stimulation, skeletal muscle contraction initiates a phosphorylation cascade, resulting in enhanced glucose uptake, independently of insulin. Due to the high energy demand during contraction, the AMP/ATP ratio increases, as well as the intracellular Ca^{2+} concentration that lead to the activation of LKB1 and CaMKK, which in turn phosphorylate AMPK. Activated AMPK then phosphorylates to two RabGAPs, which leads to the translocation of GLUT4 containing storage vesicles to the plasma membrane, hence increasing glucose influx. IR = insulin receptor; IRS1 = insulin receptor substrate 1; PI3K = phosphoinositide 3-kinase; PIP_2 = phosphatidylinositol-4,5-bisphosphate; PIP_3 = phosphatidylinositol-3,4,5-trisphosphate; AKT = protein kinase B; PDK1 = phosphoinositide-dependent kinase 1; RabGAP = Rab-GTPase-activating protein; Rab = Ras related in brain; GTP = guanosine triphosphate; GDP = guanosine diphosphate; AMP = adenosine monophosphate; ATP = adenosine triphosphate; LKB1 = liver kinase 1; CaMKK = calcium/calmodulin-dependent protein kinase kinase; AMPK = AMP-activated kinase.

1.3.5 Glucose metabolism in insulin-responsive peripheral tissues

Glucose serves as an important energy source for skeletal muscle and adipose tissue in the form of ATP. Following glucose uptake, it is directly phosphorylated to G6P via hexokinase II, the predominant hexokinase isoform expressed in skeletal muscle (Ritov and Kelley, 2001). During glycolysis, G6P is further metabolized to pyruvate, which in turn enters the mitochondria under aerobic conditions to be converted via pyruvate dehydrogenase (PDH) into acetyl-CoA, the starting point of the tricarboxylic acid (TCA) cycle (Dashty, 2013). Throughout the diverse reaction steps during the TCA cycle, NADH and $FADH_2$ are obtained, which are needed for the oxidative phosphorylation to generate ATP. Under anaerobic conditions, for instance during exercise, pyruvate is converted to lactate, then released into

the circulation and finally taken up by hepatocytes, to be further metabolized for either gluconeogenesis or re-oxidized to pyruvate and acetyl-CoA for energy supply (Yang et al., 2020).

Besides entering the glycolytic pathway, glucose is stored in the form of glycogen in skeletal muscle and liver upon insulin stimulation (Zhang et al., 2021, Hers, 1976). Relative to its weight, liver has the highest glycogen content in the body with up to 10 %, whereas skeletal muscle glycogen content makes up to 1-2 % of total skeletal muscle mass (Wasserman, 2009, den Otter and van Boxtel, 1971, Knuiman et al., 2015). In the postprandial state, glycogen synthesis is initiated with the conversion of G6P to glucose-1-phosphate (G1P) that is subsequently metabolized to uridine diphosphate (UDP)-glucose and further synthesized to glycogen via glycogen synthase (GS) (Adeva-Andany et al., 2016). During long-term fasting conditions, liver glycogen is broken down to G6P and eventually dephosphorylated to glucose by glucose-6-phosphatase in the cytosol of hepatocytes (McGarry et al., 1987). Furthermore, the gluconeogenic pathway is triggered during fasting that exclusively occurs in the liver. Skeletal muscle or adipose tissue deriving non-carbohydrate metabolites, such as lactate, glycerol and glycogenic amino acids, are transported into the liver and serve as precursors for gluconeogenesis (Sen and Das, 2018, Zhang et al., 2018). Finally, glucose is released into the blood stream to maintain glucose homeostasis.

1.3.6 Lipid metabolism in skeletal muscle and adipose tissue

Besides glucose, lipids serve as important energy source for skeletal muscle and adipose tissue. In postprandial conditions, plasma FFA are taken up by the adipose tissue and stored as triacylglycerols (triglyerides) that are hydrolyzed for internal energy consumption or released into circulation for further substrate utilization (Smith and Kahn, 2016). In case of an oversupply of dietary carbohydrates, adipose tissue and mainly the liver are able to synthesize the excess of carbohydrates into fatty acids, called "*de novo* lipogenesis" (DNL) (Ameer et al., 2014). The DNL pathway involves the conversion of glycolysis-derived pyruvate to acetyl-CoA that further enters the TCA cycle. The resulting citrate enters the cytosol and is converted again to acetyl-CoA, which is subsequently converted to malonyl-CoA that serves as the substrate for the generation of saturated palmitate. The generated palmitate is further elongated to complex long-chain fatty acids (LCFA) that are stored as triglycerides, which in turn provide energy via β-oxidation (Ameer et al., 2014, Frayn et al., 2006). During conditions of high energy demand, for instance fasting or exercise, triglycerides are metabolized in the mitochondrial β-oxidation for the generation of acetyl-CoA. In adipose tissue, lipolysis is increased, leading to the release of lipids as non-esterified free fatty acids (NEFAs) into the circulation. After the depletion of glycogen stores, skeletal muscle takes up NEFAs as an additional fuel source via fatty acid transporters, such as fatty

acid translocase (FAT/CD36) or fatty acid transport proteins (FATP1 and FATP4). Within the muscle cells, fatty acids are further stored as triglycerides or directly converted to acetyl-CoA in the mitochondrial β-oxidation, in order to fuel TCA cycle and the oxidative phosphorylation pathway (Watt and Hoy, 2012).

1.3.7 Disturbed glucose and lipid metabolism in T2DM in skeletal muscle and adipose tissue

Insulin resistance is associated with metabolic inflexibility, thereby the highly regulated glucose and lipid metabolism is disturbed, leading to the progress of T2DM. Insulin is no longer able to suppress lipolysis in adipose tissue, thus plasma FFAs are chronically elevated, which are then in turn taken up by skeletal muscle (Sangwung et al., 2020). Interestingly, obese individuals express an increased abundance of fatty acid transporters, such as FAT/CD36, leading to the increased influx of FFAs into skeletal muscle. Within the myocytes, FFAs accumulate in the form of IMCL (Bergman and Goodpaster, 2020, Hulver et al., 2003, Coen et al., 2013). Eventually, increased IMCL accumulation results in mitochondrial dysfunction, characterized by impaired mitochondrial function, reduced mitochondrial biogenesis and content, impaired autophagy and reduced FAO activity (Bergman and Goodpaster, 2020, Roden, 2005, Sangwung et al., 2020, Coen et al., 2013). Additionally, several mitochondrial enzymes show a reduced activity due to insulin resistance. It has been shown, that CPT-1 activity is reduced, leading to an impaired mitochondrial import of FFA, thereby promoting accumulation of IMCL (Colberg et al., 1995). In addition, β-hydroxy-acyl-CoA dehydrogenase activity, a key enzyme of FAO, is decreased, which results in the partial degradation of FFAs that further promotes mitochondrial dysfunction (Consitt et al., 2009). As a consequence of the partial FFA degradation, harmful lipid metabolites, such as diacylglycerols (DAGs) and ceramides accumulate within the myocytes (Goodpaster and Sparks, 2017, Kelley et al., 1999). They are playing key roles in the dysregulated phosphorylation of IR, IRS and AKT, hence further promoting insulin resistance (Bergman and Goodpaster, 2020, Zick, 2005, Dobrowsky et al., 1993, Sangwung et al., 2020). Moreover, lipid metabolites are shown to engage stress-activated serine kinases like JNK and non-typical PKC isoforms, thus attenuating insulin signaling by hyperphosphorylation of serine/threonine residues of the IR (Bergman and Goodpaster, 2020, Perreault et al., 2018, Kellerer et al., 1998, Itani et al., 2000).

Due to the impairments in the insulin signaling cascade, insulin-stimulated glucose uptake into skeletal muscle and adipose tissue is impaired, thereby contributing to hyperglycemia and insulin resistance

(Sangwung et al., 2020, Yu et al., 2002, Li et al., 2004). Taken these data into account, the importance of an intact insulin signaling for the regulation of glucose and lipid metabolism is indispensable.

1.4 Chronic exercise

1.4.1 Role of chronic exercise in the prevention and treatment of T2DM

Chronic exercise training is an effective tool in the prevention and treatment of T2DM. Beneficial effects are observed in patients with T2DM, including positive impacts on body composition (reduced total body fat and visceral adipose tissue), cardio-metabolic risk factors (improved lipid profile and blood pressure), and in particular on whole-body glucose homeostasis (reduced plasma fasting glucose levels, reduced plasma insulin levels, improved insulin sensitivity) (Balducci et al., 2012, Magkos et al., 2020, Kadoglou et al., 2007). The risk to develop insulin resistance, impaired glucose tolerance and T2DM is reduced in individuals maintaining a physically active lifestyle, as exercise interventions prevent the onset of T2DM (Pan et al., 1997, Zanuso et al., 2010). However, the combination of exercise training together with a diet intervention led to even more remarkable improvements in the reduction of T2DM prevalence (Ried-Larsen et al., 2019, Johansen et al., 2017, Tuomilehto et al., 2001, Boule et al., 2001). These findings suggest that an increase in physical activity, together with a comprehensive lifestyle modification program, is probably an important contributor to T2DM remission (Magkos et al., 2020)

1.4.2 Exercise types

Exercise is usually divided into endurance and resistant exercise. Endurance (or aerobic) exercise is characterized by the contraction of diverse muscle groups at a high frequency for a longer duration, but a relatively low workload, for instance during low-speed running. This exercise mode aims towards an elevated skeletal muscle oxidation and ameliorated endurance capacity, resulting in enhanced cardiac output, maximal oxygen consumption and mitochondrial biogenesis (Roden, 2012, Hughes et al., 2018). In contrast, resistant exercise involves the contraction of defined muscle groups at a low frequency, but with a heavy work load, e.g. during weight lifting. Thereby, muscle size increases and the strength improves (Hughes et al., 2018). However, both exercise types have shown to contribute toward the delayed onset of age-related diseases such as insulin resistance and T2DM. Therefore, a combination of endurance and resistant exercise training is recommended for the prevention and

treatment of T2DM (Pesta et al., 2017, Colberg et al., 2016). Apart from endurance and resistance training, further training modes positively contribute to overall health. For instance, high intensity interval training (HIIT), characterized by relatively short bouts of repeated vigorous activity, interspersed by periods of rest or low-intensity exercise for recovery (Gibala and Jones, 2013), has been shown to efficiently reduce total fat mass (Kolnes et al., 2021) and is effective for reducing postprandial glycemia and insulinemia, particularly in individuals with impaired glucose tolerance (Khalafi et al., 2022).

1.4.3 Metabolic regulations and adaptations during endurance exercise

In order to ensure energy supply during physical activity, ATP generation via metabolic pathways is mandatory to maintain activity of enzymes involved in membrane excitability, sarcoplasmic reticulum calcium handling, and myofilament cross-bridge cycling (Hargreaves and Spriet, 2020). Endurance activities that are lasting several minutes to hours, carbohydrate (muscle glycogen and blood glucose) and fat (muscle triglyceride and LCFA) oxidation provide almost all the ATP, in order to guarantee skeletal muscle contraction (Hawley and Leckey, 2015, van Loon et al., 2001, Romijn et al., 1993). The enhanced glucose and fatty acid oxidation is accompanied with increased skeletal muscle uptake of both metabolites (Ahlborg et al., 1974, Wasserman, 2009). Oxidized glucose derives from an increased liver output due to hepatic glycogen stores and gluconeogenesis from precursors, such as lactate, glycerol and certain amino acids (Wasserman, 2009, Coggan et al., 1995, Richter et al., 2021).

The overall endurance performance improves due to increased oxidative capacity, as neural function (maximal voluntary contraction, rate of force development) is ameliorated and an increase in type IIa muscle fibers is seen (Aagaard and Andersen, 2010, Aagaard et al., 2007). Moreover, skeletal muscle hypertrophy and growth is observed due to aerobic training (Konopka and Harber, 2014). Additionally, several molecules (Ca^{2+}, AMP, ADP, $P_{i'}$) are generated during skeletal muscle contraction that have direct effects on metabolic pathways, kinases and signaling cascades. One important player is the AMPK, an energy sensing enzyme activated during exercise that is crucial for regulating skeletal muscle glucose uptake in response to exercise (McConell, 2020). It is hypothesized that AMPK's major role may be regulating glucose uptake after, rather than during exercise, due to its contribution to GLUT4 endocytosis instead of exocytosis (Kjobsted et al., 2019b, Yang and Holman, 2005). Moreover, it is mediating some of the key adaptive responses to exercise in skeletal muscle, such as mitochondrial biogenesis and enhanced GLUT4 expression (Hargreaves and Spriet, 2020, Stuart et al., 2010). Elevated levels of mitochondrial markers, such as PGC1α, referred to as master regulator of mitochondrial biogenesis, display a fundamental component of endurance exercise induced adaptations (Pilegaard

et al., 2003, Little et al., 2010, Jacobs et al., 2013). Recently, p53 has been shown to be elevated in response to aerobic exercise, thereby emerging as key player in substrate metabolism and controlling mitochondrial biogenesis (Granata et al., 2016, Saleem et al., 2009, Saleem and Hood, 2013). Moreover, citrate synthase activity, the predominant marker used to determine alterations in mitochondrial content, is increased after endurance exercise, which further supports the increased oxidative capacity (Granata et al., 2016, Hughes et al., 2018). In addition, improved endurance performance is attributed to enhanced fatigue resistance, as proteins involved in mitochondrial ATP production, TCA cycle, FFA transport and oxidation, glycolytic metabolism, glucose transport and glycogen synthesis, are increased (Egan and Zierath, 2013). For instance, increased protein levels of hexokinase II and GLUT4 have been observed after chronic exercise training, both crucial players in glucose metabolism (Raun et al., 2020, Kleinert et al., 2018). Moreover, it is believed that insulin-stimulated GLUT4 translocation is increased as well, since insulin-stimulated phosphorylation of AKT and TBC1D4 is potentiated in response to exercise training (Hansen et al., 2020, Vind et al., 2011, Sylow et al., 2021, Bienso et al., 2015).

Likewise, adipose tissue in particular benefits from endurance exercise, not only purely due to reduced visceral and subcutaneous fat mass (Ibanez et al., 2005, Kirwan et al., 2017, Mu et al., 2021). Insulin sensitivity in scWAT is improved after exercise training, evaluated by the suppression of lipolysis, accompanied by increased protein expression of IR and hexokinase II (Richter et al., 2021, Riis et al., 2019). In conditions of obesity, adipose tissue is known to be low-grade inflamed (Wu and Ballantyne, 2017). Exercise training has shown to decrease inflammation as cytokine production is suppressed and infiltration of immune cells is reduced (Dandona et al., 2003, Balducci et al., 2010). Hence, leading to the normalization of adipokine signaling (Jorge et al., 2011, Kirwan et al., 2017). Moreover, browning, a process exclusively observed in white adipose tissue represents a major adaptation to endurance exercise (Mu et al., 2021). Browning is defined as a phenotypic switch in adipose tissue from energy storing white adipocytes towards more thermogenic adipocytes, thereby improving insulin sensitivity (Aldiss et al., 2018, Wu et al., 2014). Within this process, UCP1 plays a crucial role, as it mediates the uncoupling of oxidative metabolism from ATP production to heat production (Cannon and Nedergaard, 2004, Fedorenko et al., 2012). After exercise training, an increase in *Ucp1* expression in scWAT has been observed (Mu et al., 2021, Bostrom et al., 2012). Taken these data together, chronic exercise is an effective tool for the improvement of overall and tissue-specific insulin sensitivity.

1.5 Rab-GTPase-activating proteins (RabGAP)

1.5.1 Structure and function of the RabGAP TBC1D4

TBC1D4 belongs to the family of Rab-GTPase-activating proteins (RabGAPs) and is a crucial player in GLUT4 translocation, and thereby in insulin signaling and skeletal muscle contraction metabolism (Chadt et al., 2015, de Wendt et al., 2021, Espelage et al., 2020). This RabGAP contains two N-terminal phosphotyrosine binding domains (PTB), a calmodulin-binding domain (CBD), and a C-terminal GAP domain, which is responsible for its GTP hydrolysis activity (Mafakheri et al., 2018). TBC1D4 has a length of about 1298 amino acids, a size of 160 kDa and is primarily abundant in oxidative skeletal muscle fibers (*Soleus*), adipose tissue and the heart (Wang et al., 2013, Dokas et al., 2013, Sakamoto and Holman, 2008). Two predominant *TBC1D4* gene isoforms are known. The long isoform, exhibiting the additional exons 11 and 12, and the short isoform that is lacking these exons. The short *TBC1D4* isoform is widely expressed, whereas the long isoform is primarily expressed in skeletal muscle and the heart (Moltke et al., 2014, Binsch et al., 2023). Moreover, the RabGAP TBC1D4 is a downstream substrate of AKT and AMPK, thus becoming phosphorylated in response to insulin stimulation and skeletal muscle contraction at specific serine (Ser) and threonine (Thr) residues, which results in association with 14-3-3 proteins (Mafakheri et al., 2018). Thereby, it has been shown that TBC1D4 is phosphorylated via AKT at Ser^{318}, Ser^{570}, and Thr^{642}, whereas AMPK phosphorylates TBC1D4 at Ser^{588} and Ser^{751}. In contrast, Ser^{341}, Thr^{642} and Ser^{704} were found to be phosphorylated by both, AKT and AMPK (Figure 2) (Mafakheri et al., 2018, Taylor et al., 2008, Kramer et al., 2006, Cartee, 2015, Treebak et al., 2014).

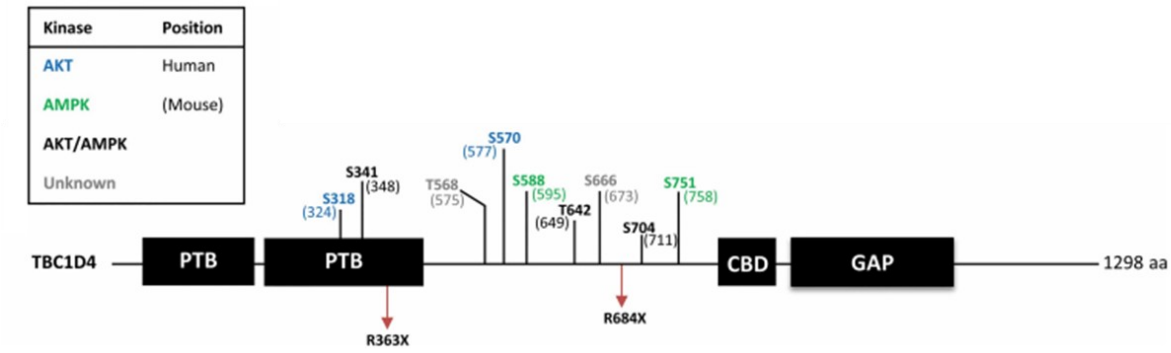

Figure 2: Structure and phosphorylation sites of TBC1D4. TBC1D4 consists of two PTB-binding domains, a CBD domain and the functional GAP domain. Several serine and threonine phosphorylation sites have been reported that are phosphorylated via AKT and/or AMPK. Blue marked residues represent AKT phosphorylation sites and green marked sites display AMPK phosphorylation sites. Moreover, several residues are found to be phosphorylated by both, thereby marked in black. Of note, murine phosphorylation sites are displayed in brackets. PTB = phosphotyrosine binding domain; CBD = calmodulin binding domain; GAP = GTPase activating protein. Modified from Mafakheri et al. 2018.

The exact mechanism of RabGAP-mediated GLUT4 translocation is still not fully understood. However, there is evidence that inhibiting the interaction between RabGAPs and Rab-GTPases is crucial in this process (Mafakheri et al., 2018). Rab-GTPases are small 21 kDa sized proteins that play an important role in vesicle formation, vesicle docking, vesicle trafficking, and vesicle fusion with the plasma membrane (Zerial and McBride, 2001, Stenmark, 2009, Pfeffer, 2017). Rab proteins are active in their GTP-bound conformational state, which is promoted via guanine nucleotide exchange factors (GEFs) that catalyze GDP release and subsequently GTP binding to the Rab proteins (Figure 3) (Pfeffer and Aivazian, 2004, Barr and Lambright, 2010). Thereby, active GTP-bound Rab proteins trigger the redistribution of GLUT4 from GSVs to the plasma membrane, eventually enabling glucose influx into the cell (Zerial and McBride, 2001). At basal conditions, RabGAPs catalyze GTP hydrolysis of Rab-GTPases, thereby maintaining them in their inactive GDP-bound conformational state. Inactive GDP-bound Rab proteins prevent the translocation and fusion of GSVs to the plasma membrane (Mafakheri et al., 2018). Recent findings provide evidence that TBC1D4 phosphorylation inhibits the interaction with the cytoplasmic tail of the GLUT4-vesicle resident protein insulin-regulated aminopeptidase (IRAP), thereby leading to the dissociation of TBC1D4 from the GSVs, thus transferring Rab proteins into their active GTP-bound conformational state (Eickelschulte et al., 2021).

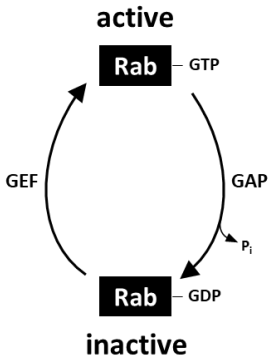

Figure 3: Rab GTPase conformational states. Rab GTPases constantly cycle between their active GTP-bound state and their inactive GDP-bound conformational state. GEFs initiate the GTP loading, whereas GAPs hydrolyze GTP to GDP, thereby inactivating the Rab proteins. Rab = Ras related in brain; GEF = Guanine nucleotide exchange factor; GAP = GTPase-activating protein.

1.5.2 The impact of TBC1D4 to human metabolic phenotypes and diseases

TBC1D4 has been observed to play a crucial role in human skeletal muscle insulin resistance. A TBC1D4 mutation, coding for a truncated protein lacking the GAP domain, confers postprandial hyperinsulinemia in humans. This mutant has been shown to bind *in vitro* wildtype (WT) TBC1D4, thus inhibiting GLUT4 translocation (Dash et al., 2009). Moreover, a *TBC1D4* nonsense loss-of-function

variant in the Greenlandic Island population is associated with postprandial hyperglycemia and increased prevalence to develop T2DM in homozygous allele carriers (Moltke et al., 2014). This *TBC1D4* p.Arg684Ter variant is specifically affecting the long TBC1D4 isoform, primarily expressed in skeletal muscle. Thus, individuals carrying this nonsense variant display a muscle-specific depletion of *TBC1D4*, resulting in postprandial insulin resistance. Other tissues like liver or adipose tissue are not affected by the p.Arg684Ter variant, as they are expressing the short *TBC1D4* isoform (Andersen and Hansen, 2018). Interestingly, in homozygous allele carriers, a reduced GLUT4 protein abundance was observed, which is likely secondary to the lack of TBC1D4 (Moltke et al., 2014). Likewise, a disruption of the *TBC1D4* gene is also common among North American Inuit from Canada and Alaska, resulting in exclusively elevated postprandial blood glucose levels (Manousaki et al., 2016). The *TBC1D4* gene mutation may have been induced by evolutionary adaptive processes to the traditional Inuit diet that was low in carbohydrates and consisted mostly of fish and marine mammals like seals. Thus, prolonged postprandial hyperglycemia might have been advantageous (Andersen and Hansen, 2018). Interestingly, a recent study has shown that physical activity attenuates postprandial hyperglycemia in homozygous allele carriers of the previously described *TBC1D4* loss-of-function mutation (Schnurr et al., 2021).

1.5.3 The role of *Tbc1d4*-deficiency on glucose and lipid metabolism in animal models

In order to investigate the role of TBC1D4 in whole-body metabolism, genetically modified animal models have been used in a number of studies. Thus, emphasizing the crucial role of TBC1D4 in insulin sensitivity, as whole-body *Tbc1d4* deficiency leads to impairments in insulin sensitivity and glucose tolerance in rodents (Espelage et al., 2020). In detail, insulin-stimulated glucose uptake into oxidative *Soleus* muscle and primary white adipocytes are severely impaired due to the TBC1D4 knockout (KO) and a reduction in the GLUT4 abundance has been observed (Chadt et al., 2015, de Wendt et al., 2021, Zhou et al., 2017). Of note, mRNA levels of *Slc2a4* are unaffected due to the *Tbc1d4* efficiency, showing RabGAP deficiency-associated depletion of skeletal muscle GLUT4 seems to appear as a result of posttranslational miss-sorting process (Chadt et al., 2015, Xie et al., 2016). Additionally, TBC1D4 is considered as signaling hub between glucose and lipid metabolism, since *Tbc1d4*-deficient mice preferably use lipids as energy substrates, simultaneously exert an elevated FAO *in vivo* (Chadt et al., 2015). This enhanced lipid use may be a result from altered trafficking and/or abundance of proteins involved in fatty acid transport and oxidation (Espelage et al., 2020, Miklosz et al., 2016). Thus, it is shown that D4KO animals display in skeletal muscle an increased level of FAT/CD36 and fatty acid-binding protein (FABPpm) (Miklosz et al., 2016). Interestingly, TBC1D4 also plays a central role in the

enhancement of skeletal muscle insulin sensitivity after exercise and enhanced insulin-stimulated TBC1D4 phosphorylation is linked to elevated glucose uptake in response to insulin (Wang et al., 2018, Kjobsted et al., 2019a).

1.6 Organ crosstalk between skeletal muscle and adipose tissue

The organ crosstalk between skeletal muscle and adipose tissue is mediated via numerous circulating factors. In response to external stimuli, for instance exercise, both tissues secrete various proteins, which are termed “exerkines” or “myokines” and “adipokines”, respectively to their organ of origin (Pedersen et al., 2004, Pedersen and Febbraio, 2012, Priest and Tontonoz, 2019). Thus, it has been shown that myokines mediate exercise-induced beige adipose tissue development, as irisin is reported to brown WAT in mice (Severinsen and Pedersen, 2020). Moreover, the exercise-mediated release of the myokine Interleukin (IL)-6 has been shown to enhance lipolysis and FAO in rodents, which further demonstrates the close crosstalk between skeletal muscle and adipose tissue (Pedersen and Febbraio, 2008). Likewise, WAT-derived adipokines, such as adiponectin and leptin play important roles in whole-body energy homeostasis and influence skeletal muscle by promoting fatty acid uptake and oxidation, mitochondrial function and biogenesis, glucose uptake and muscle regeneration (Li et al., 2011, Krause et al., 2019, Kahn et al., 2019). Interestingly, transplantation of trained WAT in sedentary mice results in an improvement of glucose uptake in skeletal muscle and whole-body metabolism, possibly due to an altered adipokine profile in WAT after training (Stanford et al., 2015), emphasizing the key role of adipose tissue-skeletal muscle connectivity in glucose homeostasis (Kotani et al., 2004).

1.7 Protein secretion

Protein transport from their site of synthesis in the cytoplasm to their functional location is an essential characteristic of all living cells (Sarvas et al., 2004). Hence, the delivery of soluble proteins and cargoes to the extracellular space is indispensable (Viotti, 2016). The majority of secretory proteins reach their destination conventionally via the transport through the endoplasmic reticulum (ER) to the Golgi apparatus, further to the plasma membrane, where they are eventually released into the extracellular space (Rabouille, 2017). This secretion pathway is defined as the “classic” or “conventional” protein secretion, initiated by the recognition of signal peptides (Kim et al., 2018b, Ferro-Novick and Brose, 2013). The newly synthesized proteins exit the ER, reaching the Golgi network before being dispatched to the plasma membrane, lysosome, endosome or peroxisome (Gee et al., 2018, Viotti, 2016). The

fusion of vesicular intermediates and organelles is mediated among other things by Rab proteins and their regulators (Kim et al., 2018b, Mellman and Warren, 2000). However, several proteins reach their destinations via the unconventional protein secretion pathway that comprises cargos without a signal peptide that are able to translocate across the plasma membrane, and cargos with signal peptides that reach the plasma membrane by bypassing the Golgi apparatus, despite entering the ER (Rabouille, 2017, Kim et al., 2018b, Rabouille et al., 2012). However, proteins could still function in the extracellular matrix, despite being secreted, for instance via proteolytic ectodomain shedding, a post-translation modification (Lichtenthaler et al., 2018). Thereby, proteases cleave a membrane protein close to or within its transmembrane domain, leading to the release of the soluble extracellular domain (ectodomain). The cleaved ectodomain substrate may be eventually secreted (Lichtenthaler et al., 2018, Kapeller et al., 1973, Black, 1980). Several studies have shown that ectodomain shedding influences many processes, such as cholesterol homeostasis, inflammatory disorders or Alzheimer's disease (Lichtenthaler et al., 2018).

1.7.1 RabGAPs and their involvement in protein secretion

The small Rab-GTPases are known to serve as master regulators of membrane trafficking. Thereby, they are controlling several different aspects of vesicular transport, such as vesicle tethering, docking and fusion with the plasma membrane (Novick, 2016, Grosshans et al., 2006). As already described in chapter 1.5.1, Rab proteins are regulated by specific proteins: GEFs catalyze the GTP-binding to Rab proteins, thereby transforming them into their active form, while GAPs promote GTP hydrolysis, hence converting the Rabs into their inactive state (Novick, 2016). This leads to the assumption that also GAPs play an essential role in protein secretion. Interestingly, it has been shown in yeast that the RabGAPs Gyp5p and Gyl1p recruit Rvs167p to the small-bud tip, where it plays a role in polarized exocytosis (Prigent et al., 2011). Over the past years, the focus of investigations has been set on the role of Rab-GTPases in secretory pathways. Studies in yeast have shown that several human Rab homologs play important roles in the protein secretion (Novick, 2016, Jedd et al., 1997). Of special interest, Sec4, a Rab8 homolog, drives the docking and fusion of vesicles to the plasma membrane (Grosshans et al., 2006, Jin et al., 2011, Walch-Solimena et al., 1997). Moreover, Rab8 itself has also been implicated in the traffic from endosomes to the basolateral membranes of polarized cells (Ang et al., 2003, Henry and Sheff, 2008). At least in makrophages, TBC1D4 has shown to regulate cargo secretion in a Rab14-dependent manner (Weimershaus et al., 2018). Therefore, it cannot be ruled out that TBC1D4 plays also an essential role in the skeletal muscle protein secretion pathway.

1.8 Aim of the thesis

Several studies have shown the important role of TBC1D4 in whole-body glycemia. Whole-body D4KO mice exhibit postprandial hyperglycemia, impaired glucose tolerance, and reduced insulin-stimulated glucose uptake in *Soleus* and primary white adipocytes, accompanied by a reduction in GLUT4 protein abundance (Chadt et al., 2015, de Wendt et al., 2021, Springer PhD thesis, 2018). Interestingly, a recent study in our grouo showed that whole-body glycemia was restored, at least in part, after chronic exercise training of D4KO mice, associated with increased insulin-stimulated glucose uptake and GLUT4 abundance in primary white adipocytes (Springer PhD thesis, 2018). In order to investigate this mechanism further, and the contribution of muscle and fat tissue to the phenotype, muscle-specific (mD4KO) and adipocyte-specific *Tbc1d4*-deficient (aD4KO) mice were generated using the Cre/LoxP technology and the following key questions were addressed in this study:

1. **What is the contribution of skeletal muscle and adipose tissue to the metabolic phenotype of D4KO?**
2. **How does chronic exercise training affect *Tbc1d4*-deficient skeletal muscle and adipose tissue?**
3. **Does an inducible *Tbc1d4* knockout recapitulate the phenotype of whole-body *Tbc1d4*-deficient mice?**

2 Material & Methods

2.1 Material

2.1.1 Mouse strains

All mouse strains used throughout the study are listed in Table 1.

Table 1: Mouse strains

Strain	Abbreviation	Genetic modification	Supplier
Flp deleter mouse/N	Flp		Dr. Thomas Wunderlich, Dr. Karina Schöfisch (MPI Cologne, Germany)
B6.FVB-Tg(Adipoq-cre)^{1Evdr}/J	Adipoq-Cre	Adiponectin Cre recombinase	Jackson Laboratory (Bar Harbor, Maine, USA)
B6.Cg-Tg(ACTA1-cre)^{79Jme}/J	HSA-Cre	Human skeletal actin Cre recombinase	Jackson Laboratory (Bar Harbor, Maine, USA)
Inducible HSA-Cre-ER	HSA-Cre-ER	Inducible human skeletal actin Cre recombinase	Prof. Dr. Jørgen Wojtaszewski, Dr. Rasmus Kjøbsted (Kopenhagen, Denmark)
B6.*Tbc1d4*^{tm1}	Floxed	Floxed *Tbc1d4* gene	German Diabetes Center (DDZ), Düsseldorf, Germany
B6.*Tbc1d4*^{tm1}-Tg(ACTA1-cre)^{79Jme}/J	mD4KO	Muscle-specific *Tbc1d4*-deficiency	DDZ, Düsseldorf, Germany
B6.*Tbc1d4*^{tm1}-Tg(*Adipoq-cre*)^{1Evdr}/J	aD4KO	Adipocyte-specific *Tbc1d4*-deficiency	DDZ, Düsseldorf, Germany

2.1.2 Mouse diet

Animals were fed a standard chow diet (SD) purchased from Ssniff (Soest, Germany). Table 2 summarizes the dietary composition.

Table 2: Composition of mouse diet

Diet (Cat.-No.)	Fat (cal %)	Protein (cal %)	Carbohydrate (cal %)	Total calorie content (kcal/g)
SD (V1126)	11	36	53	3,3

2.1.3 Genotyping primers

Table 3 displays the used primers for the genotyping.

Table 3: Genotyping primers

Primer	Sequence (5' → 3')
Adiponectin-Cre	Fwd: CTAGGCCACAGAATTGAAAGATCT
	Rev: GTAGGTGGAAATTCTAGCATCATCC
	Col F: TCCAATTTACTGACCGTACACCAA
	Col R: CCTGATCCTGGCAATTTCGGCTA
Floxed	Tbc1d4fl_geno_Fwd9: CTGTGAAGCCAAGCAGAGGA
	CSD-loxF: GAGATGGCGCAACGCAATTAATG
	CSD-R: GTAGGGACCTAGTGATGGTGGTCTC
HSA-Cre conventional	Fwd: GCGGTCTGGCAGTAAAAACTATC
	Rev: GTGAAACAGCATTGCTGTCACTT
HSA-Cre inducible	Fwd: AAGCAGAGGGCTTCCCCAACA
	Rev: CTTCCTCTTCTTCTTGGGCATGGT
LacZ	Fwd: ATCACGACGCGCTGTATC
	Rev: ACATCGGGCAAATAATATCG

2.1.4 Antibodies

Following antibodies were used during the Western Blot (Table 4).

Table 4: Antibodies

Name	Host Species	Supplier	Order. #	Dillution used in TBS-T
AS160/TBC1D4	Rabbit	Abcam (Cambridge, UK)	#ab189890	1:1000 + 5 % milk powder
GAPDH	Rabbit	Cell Signaling (Danvers, MA, USA)	#2118	1:5000 + 5 % milk powder
GLUT4	Rabbit	Custom-made (Prof. Al-Hasani DDZ, Düsseldorf)		1:2000 + 5 % milk powder
TBC1D1	Rabbit	Cell Signaling (Danvers, MA, USA)	#4629	1:1000 + 5 % milk powder
Anti-Rabbit-HRP	Goat	Dianova (Hamburg, Germany)	111-035-003	1:20.000 + 5 % milk powder 1:5000 + 5 % milk powder

2.1.5 Reaction Kits

The following table displays the used reaction kits in the present thesis (Table 5).

Table 5: Reaction Kits

Reaction Kit	Supplier
BCA Protein Assay Kit	Pierce (Rockford, IL, USA)
miRNeasy Mini Kit	Qiagen (Hilden, Germany)
RNase-free DNase Set	Qiagen (Hilden, Germany)
Western Lightning ECL Enhanced Chemiluminescence Substrate	PerkinElmer (Waltham, MA, USA)

2.1.6 Molecular weight size markers

Following molecular weight size markers were used in the present thesis (Table 6).

Table 6: Molecular weight size markers

Molecular weight size marker	Supplier
50 bp DNA ladder	Thermo Scientific (Peqlab, Wilmington MA, USA)
100 bp DNA ladder	Thermo Scientific (Peqlab, Wilmington MA, USA)
1 kb DNA ladder	Thermo Scientific (Peqlab, Wilmington MA, USA)
PageRuler Prestained Protein Ladder	Thermo Scientific (Peqlab, Wilmington MA, USA)

2.1.7 Chemicals

Table 7 summarizes the used chemicals.

Table 7: Chemicals

Chemical	Supplier
2-deoxyglucose	Sigma-Aldrich (St. Louis, MO, USA)
2-propanol	Applichem (Darmstadt, Germany)
5x HF Buffer	Mobidiag (Espo, Finland)
6x DNA Loading Dye	Thermo Scientific (Peqlab, Wilmington MA, USA)
10x Green Buffer	Thermo Scientific (Peqlab, Wilmington MA, USA)
Acrylamid 4K Solution (37. 5:1; 30 %)	Applichem (Darmstadt, Germany)
Actraprid Penfill Insulim human	Novo Nordisk (Bagsværd, Denmark)
Adenosine	Sigma-Aldrich (St. Louis, MO, USA)
Albumin Fraction V (BSA)	Merck (Darmstadt, Germany)
Ammonium persulfate (APS)	Serva (Heidelberg, Germany)
Avertin (2,2,-Tribromoethanol)	Sigma-Aldrich (St. Louis, MO, USA)
Bromophenol blue	Applichem (Darmstadt, Germany)
Calcium chloride dehydrate ($CaCl_2 \cdot 2\ H_2O$)	Merck (Darmstadt, Germany)
Chloroform	Applichem (Darmstadt, Germany)
Collagenase Type 1	Worthington Biochemical (Lakewood, NJ, USA)
Corn Oil	Sigma-Aldrich (St. Louis, MO, USA)
D-(+)-Glucose	Sigma-Aldrich (St. Louis, MO, USA)
Deoxynucleoside Triphosphate Set (dNTPs)	Roche (Mannheim, Germany)

Dimethylsulfoxide (DMSO)	Applichem (Darmstadt, Germany)
Dinonyl Phthalate	PHYWE (Göttingen, Germany)
Dithiothreitol (DTT)	Carl Roth (Karlsruhe, Germany)
Dream Taq Polymerase	Thermo Scientific (Peqlab, Wilmington MA, USA)
Ethanol, absolute (EtOH)	Merck (Darmstadt, Germany)
Ethylenediaminetetraacetic acid (EDTA)	Carl Roth (Karlsruhe, Germany)
Ethylene glycol bis (2-aminoethylether)-N, N, N', N'-tetra acetic acid (EGTA)	Carl Roth (Karlsruhe, Germany)
Glucose (20 %)	B Braun (Melsungen, Germany)
Glycerol	MP Biomedicals (Santa Ana, CA, USA)
Glycine	Applichem (Darmstadt, Germany)
HD Green fluorescent dye	Intas Science Imaging (Göttingen, Germany)
HEPES 4-(2-hydroxyethyl)-1-piperazineethanesulfonic acid	Sigma-Aldrich (St. Louis, MO, USA)
Heptane (Isomers)	Carl Roth (Karlsruhe, Germany)
Hydrochloric acid (HCL)	Carl Roth (Karlsruhe, Germany)
Magnesium sulfate heptahydrate ($MgSO_4 \cdot 7 H_2O$)	Merck (Darmstadt, Germany)
Mannitol	Applichem (Darmstadt, Germany)
Methanol	Carl Roth (Karlsruhe, Germany)
Phosphatase inhibitor tablets (PhosSTOP)	Roche (Mannheim, Germany)
Potassium chloride (KCl)	Merck (Darmstadt, Germany)
Potassium dihydrogen phosphate (KH_2PO_4)	Merck (Darmstadt, Germany)
Powdered milk	Carl Roth (Karlsruhe, Germany)
Proteinase Inhibitor Cocktail (cOmplete)	Roche (Mannheim, Germany)
Proteinase K	Carl Roth (Karlsruhe, Germany)
Pyruvate	Applichem (Darmstadt, Germany)
Rotiszint eco plus	Carl Roth (Karlsruhe, Germany)
Sodium acetate	Sigma-Aldrich (St. Louis, MO, USA)
Sodium chloride (NaCl)	Carl Roth (Karlsruhe, Germany)
Sodium dodecyl sulfate (SDS)	Carl Roth (Karlsruhe, Germany)
Sodium hydrogen carbonate ($NaHCO_3$)	Merck (Darmstadt, Germany)
Sodium sulfate (Na_2SO_4)	Merck (Darmstadt, Germany)
Sulphuric acid	Carl Roth (Karlsruhe, Germany)

Tamoxifen	Sigma-Aldrich (St. Louis, MO, USA)
N, N, N', N'-Tetramethylendiamine (TEMED)	Carl Roth (Karlsruhe, Germany)
Tris	Carl Roth (Karlsruhe, Germany)
Triton X-100	Sigma-Aldrich (St. Louis, MO, USA)
TRIzol™ RNA Isolation Reagent	Thermo Scientific (Peqlab, Wilmington, MA, USA)
Tween 20	Applichem (Darmstadt, Germany)

2.1.8 Radioactive isotopes

Radiolabeled chemicals were used for *ex vivo* experiments to measure glucose uptake into skeletal muscle and primary white adipocytes and are listed in Table 8.

Table 8: Radioactive chemicals

Radiolabeled Chemical	Supplier
[^{3}H]-2-deoxyglucose	Hartmann Analytic (Brunswick, Germany)
[^{14}C]-D-glucose	Hartmann Analytic (Brunswick, Germany)
[^{14}C]-mannitol	PerkinElmer (Waltham, MA, USA)

2.1.9 Buffers and solutions

Following buffers and solutions were used in the present thesis (Table 9).

Table 9: Buffers and solutions

Buffer and solution	Ingredients
DNA Isolation	
DNA lysis buffer	0.1 M Tris-HCl (pH 8.0), 0.2 M NaCl, 5 mM EDTA, 0.4 % SDS
TE buffer	10 mM Tris-HCl (pH 8.0), 1 mM EDTA
Glucose uptake into primary white adipocytes	
Krebs-Ringer-Bicarbonate HEPES buffer (KRBH)	Stock I: 118.5 mM NaCl, 4.7 mM KCl, 1.2 mM KH_2PO_4, 25 mM $NaHCO_3$, gassing with carbogen gas for 20 min on ice; +Stock II: 2.5 mM $CaCl_2 \cdot 2$ H2O, 1.2 mM $MgSO_4 \cdot 7$ H_2O, 5 mM HEPES, gassing

	with carbogen gas for 10 min on ice, 1 % BSA finally added
Lipid extract solution	78 Vol. % 2-propanol, 20 Vol. % heptane, 2 Vol. % sulphuric acid
Glucose uptake into isolated skeletal muscle	
Avertin solution	5 ml MQ water, 250 µl Avertin
Krebs-Henseleit buffer (KHB)	Stock I: 118.5 mM NaCl, 4.7 mM KCl, 1.2 mM KH_2PO_4, 25 mM $NaHCO_3$, gassing with carbogen gas for 20 min on ice; +Stock II: 2.5 mM $CaCl_2 \cdot 2 H_2O$, 1.2 mM $MgSO_4 \cdot 7 H_2O$, 5 mM HEPES, gassing with carbogen gas for 10 min on ice, 1 % BSA finally added
Hot incubation buffer	19 mM Mannitol, 1 mM 2-deoxyglucose with/without 120 nM Insulin, 2.5 µCi/ml [3H]-2-deoxyglucose, 0.7 µCi/ml [14C]-mannitol
Incubation buffer	15 mM Mannitol, 5 mM Glucose with/without 120 nM Insulin (solved in KHB)
Recovery buffer	15 mM Mannitol, 5 mM Glucose (solved in KHB)
Rinse buffer	20 mM Mannitol, with/without 120 nM Insulin (solved in KHB)
Protein and Western Blot analysis	
Blocking solution	5 % powdered milk, TBS-Tween (1x)
Electrophoresis buffer	25 mM Tris, 192 mM glycine, 0.1 % SDS, 20 Vol % glycerol, 8 & SDS, 10 mM EDTA,

Laemmli sample buffer (4x LSB)	0.25 M Tris, 6 % DTT, 0.2 % bromophenol blue (pH 6.8)
Separating gel buffer	1.5 M Tris, 0.4 % SDS (pH 8.8)
Stacking gel buffer	0.5 M Tris, 0.4 % SDS (pH 6.8)
TBS-Tween buffer (TBS-T, 1x)	10 mM Tris, 150 mM NaCl, 0.05 Vol. % Tween 20
Transfer buffer	25 mM Tris, 192 mM glycine, 20 % methanol
***Ex vivo* induction of skeletal muscle contraction**	
Tension buffer	15 mM mannitol, 8 mM pyruvate (solved in KHB without BSA)

2.1.10 Devices

Table 10 displays the used devices.

Table 10: Devices

Device	Supplier
Centrifuge 5415 C	Eppendorf (Hamburg, Germany)
Centrifuge 5424 R	Eppendorf (Hamburg, Germany)
ChemiDoc XRS+	Bio-Rad Laboratories (Munich, Germany)
Contour Glucometer	Bayer (Leverkusen, Germany)
GelDoc XR+	Bio-Rad Laboratories (Munich, Germany)
iMARK Microplate Reader	Bio-Rad Laboratories (Munich, Germany)
Microbeta Counter	PerkinElmer (Waltham, MA, USA)
NanoDrop 2000	Thermo Scientific (Peqlab, Wilmington, MA, USA)
Thermomixer Compact	Eppendorf (Hamburg, Germany)
TissueLyser II	Qiagen (Hilden, Germany)
Treadmill systems	TSE Systems (Bad Homburg, Germany)
Whole Body Composition Analyzer	Echo MRI (Houston, TX, USA)

2.1.11 Software

Following software were used throughout the present thesis (Table 11).

Table 11: Software

Software	Supplier
GraphPad Prism 9	GraphPad Software Inc (San Diego, CA, USA)
Image Lab	Bio-Rad Laboratories (Munich, Germany)
Microplate Manager 6	Bio-Rad Laboratories (Munich, Germany)
NanoDrop 2000	Thermo Scientific (Peqlab, Wilmington, MA, USA)
Phenomaster	TSE Systems (Bad Homburg, Germany)

2.2 Methods

2.2.1 Study design

The experimental time line for the tissue-specific training study is represented in Figure 5. Female mD4KO and floxed littermates as well as male mD4KO, aD4KO and floxed controls were randomly assigned to either the training or sedentary cohort. The four-week chronic exercise training on treadmills (2.2.2.4) started in week-of-life 12. Glucose tolerance was determined via an intraperitoneal (i. p.) glucose tolerance test (GTT) (2.2.2.5) in week 14 and insulin sensitivity via an i. p. insulin tolerance test (ITT) (2.2.2.6) in week 15, respectively. To determine the exercise capacity of the mice, a physical capacity test (2.2.2.7) was performed in week 15. The body composition (2.2.2.8) was measured before (week 8) and after (week 16) the four-week exercise training. Moreover, in the same week a fasting and refeeding experiment (2.2.2.9) has been performed. In the final week 17, insulin stimulated glucose uptake was measured *ex vivo* in *Soleus* muscle (2.2.2.10) and isolated primary white adipocytes (2.2.2.11) from white adipose tissue. The remaining tissues were harvested during *ex vivo* measurements and stored at -80 °C for further processing.

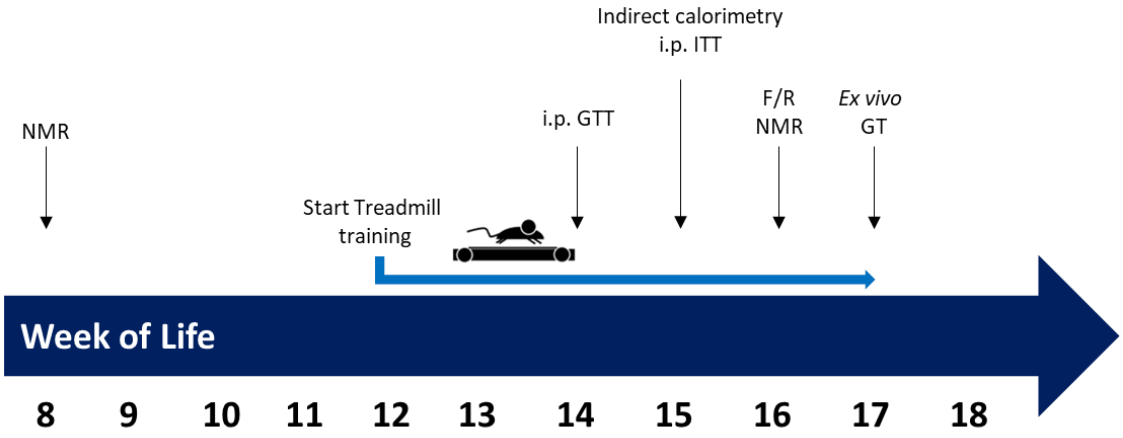

Figure 4: Study design for the four-week treadmill training with tissue-specific *Tbc1d4*-deficient mice. Chronic exercise training intervention started at week of life 12, on three days a week, with one exercise bout per day. i.p. GTT = intraperitoneal glucose tolerance test; i.p. ITT = intraperitoneal insulin tolerance test; F/R = Fasting and refeeding experiment; NMR = nuclear magnetic resonance; GT = glucose transport.

2.2.2 Animal experiments

2.2.2.1 General animal housing

Mice were kept in Makrolon type III-cages (EBECO, Castrop-Rauxel, Germany) in groups of up to six mice per cage. The environmental temperature was 22 °C and the mice were exposed to a 12 hours light-dark cycle with lights on from 6 am to 6 pm. Unless otherwise mentioned, all animals had *ad libitum* access to diet and water. All experiments were approved by the Ethics Committee of the State Agency of Nature, Environment and Consumer Protection (LANUV, North Rhine-Westphalia, Germany; reference numbers 81-02.04.2018.A160 and 84-02.04.2017.A102).

2.2.2.2 Generation of skeletal muscle-specific and adipocyte-specific *Tbc1d4*-deficient animals

To generate tissue-specific *Tbc1d4*-deficient animals, several breeding steps were necessary. *Tbc1d4*^{tm1a} mice were commercially acquired from the Knockout Mouse Project (KOMP) repository. These animals exhibited a neomycin resistance cassette for the initial selection of embryonic stem cells, and a LacZ reporter gene to verify gene expression. Both genetic elements were flanked by flippase recognition target (*FRT*) sites. The aim of the first breeding step was to remove these genetic elements. Therefore, *Tbc1d4*^{tm1a} animals were crossed with flippase (Flp) deleter mice that overexpressed the Flp recombinase. Flp binds to the *FRT* sites, thereby removing the neomycin resistance cassette and the LacZ reporter gene (Figure 5). Afterwards, a backcrossing step with C57BL/6J animals was necessary to remove the *Flp* transgene from the colony (*Tbc1d4*^{tm1c}).

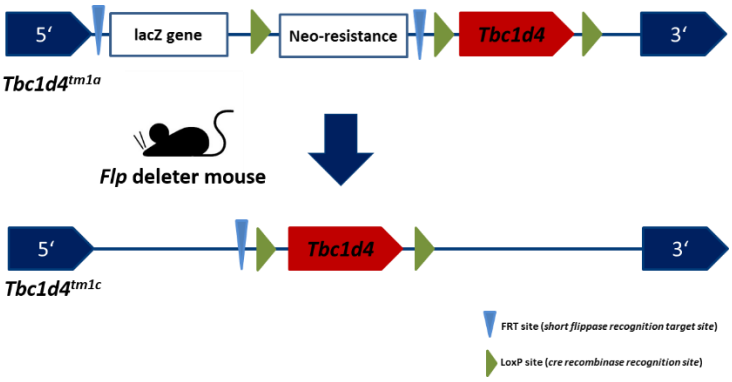

Figure 5: Removal of the neomycin resistance cassette and LacZ reporter gene. In order to remove both genetic elements required for the initial selection of embryonic stem cells, *Tbc1d4*^{tm1a} mice were crossed with animals overexpression the Flp recombinase. Flp binds to the *FRT* sites that flank the LacZ gene and neomyocin resistance cassette, thereby removing both genetic elements. Flp = flippase; FRT = flippase recoginition target.

Then, *Tbc1d4*^{tm1c} animals were crossed with mice overexpressing a tissue-specific Cre recombinase. The Cre enzyme targets LoxP sites, a 34 bp consensus sequence that flanks the gene-of-interest, in our study the *Tbc1d4* gene. Thereby, the LoxP flanked DNA is excised, creating two types of DNA with circular, excised and inactivated *Tbc1d4* gene (Kim et al., 2018a) (Figure 6). For the generation of conventional mD4KO animals, *Tbc1d4*^{tm1a} mice were mated with B6.Cg-Tg(ACTA1-cre)^{79Jme}/J animals that are overexpressing a conventional human skeletal muscle actin (HSA)-Cre recombinase. Furthermore, adipocyte-specific *Tbc1d4*-deficient mice (aD4KO) were characterized in this thesis. Thus, *Tbc1d4*^{tm1a} animals were crossed with B6.FVB-Tg(Adipoq-cre)^{1Evdr}/J mice.

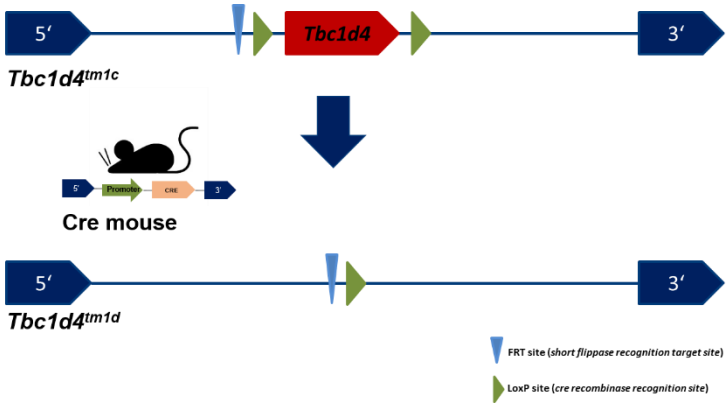

Figure 6: Generation of conventional tissue-specific *Tbc1d4* knockout mice. *Tbc1d4*^{tm1c} mice are crossed with animals overexpressing the tissue-specific Cre recombinase. The Cre enzyme targets LoxP sites, thereby the LoxP flanked DNA is excised.

To generate inducible muscle-specific *Tbc1d4*-deficient mice (mD4KO.ind), *Tbc1d4*^{tm1c} animals were mated with mice overexpressing a human skeletal actin (HSA)-Cre recombinase that is fused with mutant estrogen receptor ligand-binding domains (CreER). These CreER fusion proteins are tamoxifen sensitive but estrogen insensitive, thereby sequestered in the cytoplasm in an inactive form in the

absence of tamoxifen. In response to tamoxifen administration, a conformation change is induced, leading to the nuclear translocation and activation of Cre recombinase, thus allowing excision of floxed DNA sequences (Andersson et al., 2010) (Figure 7).

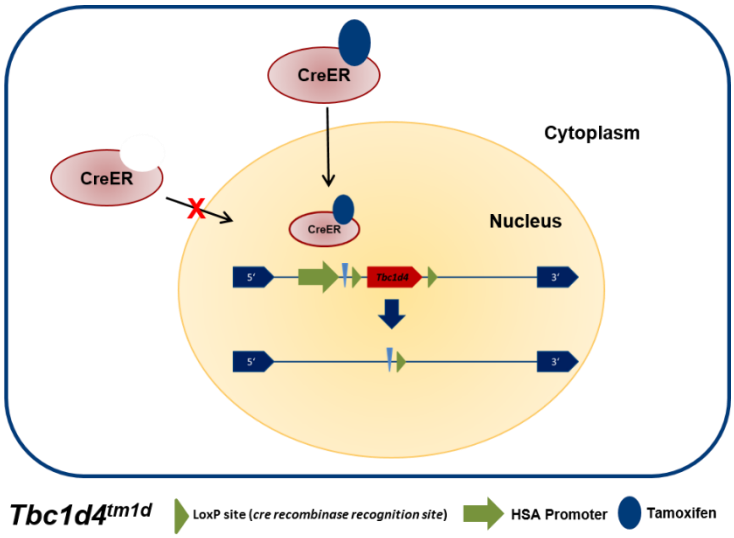

Figure 7: Generation of inducible *Tbc1d4* knockout mice. In the absence of tamoxifen, the CreER fusion protein is sequestered in an inactive form in the cytoplasm. In response to tamoxifen injection, a conformation change is induced, leading to the nuclear translocation and activation of the Cre recombinase, thus allowing excision of the floxed DNA sequences. CreER = Cre estrogen receptor ligand-binding domain.

Tbc1d4^{tm1c} mice, without the overexpression of a tissue-specific Cre recombinase served as control animals.

2.2.2.3 Tamoxifen treatment

To induce a skeletal muscle-specific *Tbc1d4* knockout, the selective estrogen receptor modulator tamoxifen was used. In the absence of tamoxifen, the Cre-ER fusion protein is sequestered in the cytoplasm in an inactive form by heat shock protein 90 (Hsp90), leading to the expression of the respective target gene. After tamoxifen is administered, it binds to the ER, which induces a conformational change in the ER and promotes the release from Hsp90. Consequently, nuclear translocation and Cre recombinase activation is promoted. Thereby, the respective target gene is excised (McCarthy et al., 2012, Andersson et al., 2010). Tamoxifen (Table 7) was disolved in corn oil to receive a final concentration of 30 mg/ml. In order to solve tamoxifen appropriately, the mixture was incubated for 1 hour at 55 °C and 1400 rpm in a Thermomixer (Table 10) and vortexed every 3-5 minutes for 30 seconds. 100 µl tamoxifen were administrated intraperitoneally into each mouse on alternate three days. Before each injection, the tamoxifen solution was warmed to 37 °C.

2.2.2.4 Chronic exercise treadmill training

The chronic exercise training intervention was carried out with a four-lane treadmill system (Table 10). Tissue-specific D4KO mice and floxed littermates performed a chronic exercise training intervention for four weeks with three training days per week and one training unit per day. Each training unit started with a 5 minutes warm-up at 6-9 m/min running, followed by a 55 minutes running period with increasing speed and duration levels. During the following weeks, speed, duration and inclination were constantly increased up to a final exercise bout of 60 minutes at 12 m/min to 22 m/min running at an inclination of 13 °. During the training intervention, mice were motivated to run by pushing them carefully with a paper tissue from behind. This exercise protocol was modified from previously established treadmill experiments within our institute (Springer PhD thesis, 2018). A detailed protocol of the chronic exercise training intervention is shown in the supplemental section (Supplemental Table 1).

2.2.2.5 Intraperitoneal glucose tolerance test (i.p.GTT)

The ability to dispose a glucose load is defined as glucose tolerance, whereas in glucose intolerant conditions this ability is impaired (Ahrén, 2013). In the present study, glucose tolerance was measured via an intraperitoneal glucose tolerance test (i.p.GTT). During the experiment, mice were kept individually in cages without access to the diet but with *ad libitum* access to water. After 16 hours of fasting, mice were weighed and basal blood glucose levels were determined with a glucometer (Table 10). For this purpose, a small portion of the tail tip was cut with a scalpel to obtain one drop of blood. Subsequent to these baseline measurements, sterile glucose (2 g/kg body weight, 20 % solution) was injected intraperitoneally into each mouse and blood glucose levels were determined from the tail tip without further incision at 15, 30, 60 and 120 minutes after injection.

2.2.2.6 Intraperitoneal insulin tolerance test (i.p.ITT)

To assess whole-body insulin sensitivity, an intraperitoneal insulin tolerance test (i.p.ITT) was performed. During the i.p.ITT random fed mice were kept individually in cages without food, but *ad libitum* access to water. Basal blood glucose levels were determined with a glucometer (Table 10) as described in 2.2.2.5. Afterwards, mice were injected intraperitoneally with human recombinant insulin (1 U/kg body weight; Actrapid, Novo Nordisk), and blood glucose levels were determined at 15, 30 and 60 minutes following the injections.

2.2.2.7 Physical capacity test

Physical fitness of the animals was assessed with an one-lane calorimetric treadmill system (Table 10). These treadmills possess air-tight covers and are connected to a calorimetric control unit, thereby allowing to monitor oxygen consumption (VO_2), carbon dioxide production (VCO_2) and respiratory exchange ratio (RER; ratio VCO_2/VO_2) during the running. The measurements were conducted at a flow-rate of 0.4 l/min and a sample flow rate of 0.25 l/min. Calorimetric parameters were recorded every 5 seconds by the PhenoMaster software (Table 11). The determination of the physical fitness (= running performance) started with a 2 minutes warm-up phase at 9 m/min running speed and an inclination of 5°. The speed increased constantly every two minutes until mice reached exhaustion. Exhaustion was defined as the time point where the mice were unable to remain running on the treadmill, despite pushing them forward with sliders. In order to calculate the maximal oxygen consumption (VO_{2max}), the average of 30 seconds of the VO_2 plateau was determined.

2.2.2.8 Body composition

Body weight was measured using scales (Sartorius, Göttingen, Germany). To determine body composition of the mice, nuclear magnetic resonance (NMR) spectroscopy (Table 10) was used. Therefore, mice were placed in tubes (20 cm in diameter) to fix them. Then, the tube was inserted into the NMR device and the measurement lasted 60 seconds. Here, nuclei of atoms are exposed to a magnetic field and absorb electromagnetic radiation, then re-emitting it at a specific frequency that depends on the strength of the magnetic field and the magnetic properties of the isotope. Thus, based on this frequency, the proportion of the respective tissues can be determined.

2.2.2.9 Fasting and Refeeding

To measure postprandial blood glucose levels, mice were subjected to a fasting and refeeding experiment. After a 16 hours-fasting period, basal blood glucose levels were measured with a glucometer from tail vene blood (Table 10). Then, mice had access to the standard diet for 1, 2 hours and 4 hours, respectively, and blood glucose levels were determined at every time point. In addition, 30 µl blood samples were collected in microvettes at each time point (Microvette CB 300 LH, Sarstedt, Nümbrecht, Germany) by gently massaging the tail tip. Blood samples were centrifuged at 2000 x g for 5 minutes and 4 °C and plasma was collected and stored at -80 °C for further analysis.

2.2.2.10 *Ex vivo* insulin-stimulated glucose uptake in isolated skeletal muscles

Skeletal muscle glucose uptake was determined *ex vivo* by the accumulation of [^{3}H]-2-deoxyglucose (Table 8) in skeletal muscle with the use of [^{14}C]-mannitol (Table 8) as marker for the extracellular space. Previously to the experiment, mice were fasted for 4 hours and then anesthetized via intraperitoneal injection of 500 mg/kg Avertin [2,2,2-tribromoethanol], in order to isolate skeletal muscles from living mice. Intact isolated *Soleus* muscles were placed in glass vials and incubated in different buffers (Table 9) at 30 °C in a shaking water bath under constant gassing with carbogen gas (95 % O_2, 5 % CO_2). After dissection of the *Soleus* muscles, mice were sacrificed by cervical dislocation for collecting the remaining tissues. First, *Soleus* muscles were incubated in recovery buffer (Table 9) for 30 minutes, following further 30 minutes incubation in incubation buffer (Table 9). From here on, one *Soleus* per animal was incubated at basal conditions, whereas the second muscle was incubated at insulin-stimulated conditions, by adding 120 mM insulin (Table 7) to the respective buffer. Next, *Soleus* muscles were placed in new glass vials containing rinse buffer (Table 9) for another 10 minutes at basal or insulin-stimulated conditions. Afterwards, *Soleus* muscles were incubated for 20 minutes in radioactive "hot" buffer (Table 9) containing isotope-labeled [^{3}H]-2-deoxyglucose and [^{14}C]-mannitol. After these incubation phases, the tendons of each muscle were removed with a scalpel, the muscles frozen in liquid nitrogen and stored at -20 °C for further analysis. For scintillation counting, *Soleus* muscles were homogenized on ice in 300 µl ice-cold lysis buffer (Table 9) containing 100 µl/ml phosphatase inhibitor (Table 7) and 40 µl/ml proteinase inhibitor (Table 7). The procedure of generating cleared protein lysates is described in detail in chapter 2.2.4.1. In the meantime, 2 ml reaction tubes were filled with 1.5 ml scintillation liquid (Table 7) and 40 µl of the cleared protein lysate was transferred into each tube. Subsequently, the radioactivity of the incorporated [^{3}H]-2-deoxyglucose and [^{14}C-]-mannitol was counted in a scintillation counter (Table 10). The resulting counts per minute (cpm) were normalized to the protein concentration of the muscle lysates via BCA analysis (2.2.4.2). The calculation of the glucose uptake also takes into account the amount of extracellularly bound [^{3}H]-2-deoxyglucose, which is determined by subtracting the values of [^{14}C-]-mannitol as marker for the extracellular space from the measured data points of the intracellular [^{3}H]-2-deoxyglucose (Mackrell and Cartee, 2012). Final values for skeletal muscle glucose uptake are expressed as nmol/mg/protein/20 minutes of [^{3}H]-2-deoxyglucose incubation.

2.2.2.11 *Ex vivo* insulin-stimulated glucose uptake in isolated primary white adipocytes

Glucose uptake into primary white adipocytes was conducted *ex vivo* via the determination of incorporated radioactively labelled [^{14}C]-D-glucose into mature adipocytes from WAT. Before the start

of the experiment, mice were fasted for 4 hours and anesthetized via intraperitoneal injection of 500 mg/kg Avertin (Table 7). Primary adipocyte cells were isolated whilst dissecting one fat pad per mice and immediately transferring it to vials with 3 ml of pre-warmed (37 °C) KRBH buffer with 5 % BSA and 200 nM adenosine (Table 7). The fat pad was mechanically minced with scissors and 6 mg collagenase was added to each vial. During the collagenase digest, the samples were incubated for 1 hour at 37 °C and 1400 rpm in a shaking water bath. The obtained cell lysates were filtered through 400 µm polyamide nylon meshs into a falcon tubes and centrifuged at 50 x g for 1 minute at room temperature (RT). The lower aqueous phase was carefully discarded and the cells were washed twice with 5 ml of fresh KRBH buffer by shortly centrifuging the cells in between the washing steps. Afterwards, the remaining adipocyte cells were taken up into 3 ml KRBH buffer. Then, 200 µl of the adipocyte suspension was incubated with 200 µl KRBH buffer with or without 120 nM insulin (Table 7) for 30 minutes at 37 °C in a shaking water bath. In addition, 200 µl of the adipocyte suspension was transferred to 2.7 ml lipid extract solution (Table 9) and stored overnight at 4 °C for later lipid weight determination. After insulin incubation, the adipocyte cell suspension was incubated for another 30 minutes with 0.1 µCi/µl [^{14}C]-D-glucose at 37 °C. In order to stop the glucose uptake and to remove excess radioactivity, 280 µl of the adipocyte cell suspension was transferred to small tubes containing 125 µl dinonyl phthalate oil and centrifuged at 9391 x g for 10 minutes at RT. Afterwards, the tubes were cut in the middle and the upper adipocyte cells-containing piece of the tube was placed in counting vials filled with 3 ml scintillation liquid (Table 7). The tubes were thoroughly vortexed and the radioactivity of the incorporated [^{14}C]-D-glucose was measured in a scintillation counter (Table 10). The resulting cpm were normalized to the lipid weight of the samples as 1.2 ml heptane and 800 µl ddH_2O were added to the overnight lipid extract solution and centrifuged at 201 x g for 5 minutes at RT. Then, 1 ml of the supernatant was transferred to tared glass tubes (Rotilabo-test tubes, Carl Roth, Karlsruhe, Germany) and the lipid samples were dried and evaporated by heating and gassing them with nitrogen for 15 minutes using Reacti-Therm and Reacti-Vap Evaporatin Unit (Pierce, Rockford, IL, USA). In order to calculate glucose uptake as cpm/mg lipid, the weight of the dried lipids was determined. Samples at basal and insulin-stimulated conditions, respectively, were measured in quintuple. As the glucose uptake experiment was carried out in parallel to the skeletal muscle glucose uptake, this assay was performed by the two research group technical assistants Anette Kurowski and Heidrun Podini.

2.2.3 Molecular biology methods

2.2.3.1 Isolation of genomic DNA from mouse tail tips

In order to determine the genotype of each animal, genomic DNA was isolated from mouse tissue that was collected during the ear notching process to distinguish individual animals throughout the intervention period. 200 µl DNA lysis buffer (Table 9) containing 10 µl Proteinase K was added to the mouse tissue and lysed overnight at 1200 rpm at 55 °C in a Thermomixer (Table 10). The next day, the lysate was centrifuged in a table centrifuge (Table 10) at RT for 1 minute at 16,000 x g to pellet the cell debris. The supernatant was collected in a fresh 1.5 ml tube and subsequently, 200 µl 100 % isopropanol was added and the tubes were vortexed for 2 sec. Afterwards, the tubes were centrifuged for 10 min at 20,000 x g at RT. The supernatant was discarded and the DNA pellet washed with 200 µl 75 % ethanol, as the tube was vortexed and centrifuged for 5 min at 20,000 x g at RT. Subsequently, the supernatant was removed again and the pellet was dried in the thermomixer at 55 °C and 1200 rpm for 15 minutes. Afterwards, 100 µl TE buffer (Table 9) was added and incubated for 5 minutes at 55 °C and 1200 rpm. At the end, the tube was vortexed again and the DNA concentration was determined with the NanoDrop device (Table 10).

2.2.3.2 Determination of nuclei acid concentration

To determine the concentration of the isolated genomic DNA, a NanoDrop device (Table 10) was used. The measurement was conducted according to the instructions of the manufacturer. For DNA concentration measurements, 1 µl of sample were used. For further analysis, the DNA concentration was adjusted to 10 ng/µl.

2.2.3.3 Polymerase chain reaction (PCR)

To determine the genotype of the experimental animals, a Polymerase chain reaction (PCR) was performed to amplify a genetic region of interest. First, DNA was denaturated at 98 °C; thereby double-stranded DNA became single-stranded DNA as hydrogen bonds between the nucleic bases were broken. Afterwards, primers annealed at 65 °C and the elongation step followed, where a DNA polymerase complemented the second DNA strand at 72 °C. With the help of dNTPs and forward and reverse primer, the DNA polymerase synthesized the complementary strand.
To verify the success of the removed LacZ reporter gene and neomycin resistance cassette, a LacZ PCR was performed. In this study, mD4KO and aD4KO mice were investigated (2.2.2.2). To distinguish

between the HSA- and Adiponectin-Cre recombinase, two different PCR reactions were performed. Additionally a Floxed PCR was carried out, to determine whether animals displayed Floxed *Tbc1d4* alleles. Following tables display the reaction setups with a total reaction volume of 20 µl that were used to genotype tissue-specific *Tbc1d4*-deficient mice.

Table 12 displays the reaction setup for genotyping the LacZ gene

Table 12: Reaction setup for the LacZ PCR reaction

Compound	Volume (µl)	Stock Concentration
MQ H_2O	8.8	
10x GrennGoTaq-Buffer	4	
dNTPs	2	8 mM
LacZ 2_small_F	0.5	10 nM
LacZ_2_small_R	0.5	10 nM
Dream Taq Green	0.2	2 U/µl
DNA	4	10 ng/µl

The reaction setup for genotyping HSA-Cre is displayed in table 13.

Table 13: Reaction setup for conventional HSA-Cre PCR

Compound	Volume (µl)	Stock Concentration
MQ H_2O	7.8	
10x GreenGoTaq-Buffer	4.0	
dNTPs	2.0	8 mM
Cre F (oIMR1084)	1.0	10 nM
Cre R (oIMR1085)	1.0	10 nM
Dream Taq Green	0.2	2 U/µl
DNA	4.0	10 ng/µl

Table 14 summarizes the reaction setup for genotyping Adiponectin-Cre.

Table 14: Reaction setup for Adiponectin-Cre PCR

Compound	Volume (µl)	Stock Concentration
MQ H_2O	5.8	
5x HF Buffer	4.0	
dNTPs	2.0	8 mM
iIMR7338	1.0	10 nM
iIMR7339	1.0	10 nM
Col 12249	1.0	10 nM
Col 12250	1.0	10 nM
Phusion-Polymerase	0.2	2 U/µl
DNA	4.0	10 ng/µl

The reaction setup for genotyping Floxed is summarized in table 15.

Table 15: Reaction setup for Floxed PCR

Compound	Volume (µl)	Stock Concentration
MQ H_2O	11.0	
5x HF Buffer	4.0	
DMSO	0.3	
dNTPs	0.5	8 mM
Tbc1d4fl_Geno_Fwd9	0.5	10 nM
CSD-loxF	0.5	10 nM
CSD-R	1.0	10 nM
Phusion-Polymerase	0.2	2 U/µl
DNA	2.0	10 ng/µl

Following tables depict the thermocycler programs that were used for the diverse PCR reactions.

Table 16: Genotyping thermocycler program for LacZ

	LacZ		
Step	**Temp**	**Time**	**Repeats**
Hot Start	94 °C	5 min	
Denaturation	94 °C	30 sec	34 x
Annealing	60 °C	30 sec	
Elongation	72 °C	30 sec	
	72 °C	5 min	
Storage	4 °C	∞	

Table 17: Genotyping thermocycler programs for Cre recombinase

	HSA-Cre conventional			Adiponectin-Cre		
Step	Temp	Time	Repeats	Temp	Time	Repeats
Hot Start	95 °C	5 min	-	98 °C	30 sec	-
Denaturation	95 °C	15 sec	34 x	95 °C	10 sec	29 x
Annealing	63 °C	15 sec		65 °C	30 sec	
Elongation	72 °C	15 sec		72 °C	20 sec	
	72 °C	5 min	-	72 °C	5 min	-
Storage	4 °C	∞	-	4 °C	∞	-

Table 18: Genotyping thermocycler programs for Floxed

Floxed

Step	Temp.	Time	Repeats
Hot Start	98 °C	30 sec	-
Denaturation	98 °C	15 sec	9 x
Annealing	65-55 °C	30 sec	Decrease 1 °C per cycle
Elongation	72 °C	40 sec	
Denaturation	98 °C	15 sec	35 x
Annealing	57 °C	30 sec	
Elongation	72 °C	40 sec	
	72 °C	5 min	-
Storage	4 °C	∞	-

The PCR products were subsequently visualized with an agarose gel and a UV gel imager (Table 10).

2.2.3.4 Agarose gel electrophoresis

To separate the PCR products according to their length, an agarose gel electrophoresis was performed. Therefore, 1 % (Floxed) or 2 % (LacZ, Cre) agarose gels were prepared and 4.5 µl/100 ml of the fluorescent dye HD Green (Table 7) was added. This fluorescent dye intercalates between the DNA double helix and is stimulated with UV radiation. The agarose gel was transferred to an electrophoresis chamber and a comb was added. In case of the Floxed and Adiponectin-Cre PCR, 4 µl of 6xLoading Dye was added to each PCR product. Subsequently, 20 µl of the sample was loaded on the gel and the electrophoretic separation occurred at 120 V for 30 min. The PCR fragments were visualized with the UV gel imager GelDoc (Table 10).

2.2.4 Biochemical methods

2.2.4.1 Preparation of protein lysates from mouse tissue

In order to prepare protein lysates from murine tissue, 300 µl (for *Soleus* muscle or WAT) or 500 µl (for *Gastrocnemius* muscle) ice-cold lysis buffer (Table 9) containing 100 µl/ml phosphatase inhibitor and 40 µl/ml proteinase inhibitor (Table 7), was added to the tissue. In order to prepare protein lysates from skeletal muscle, a steel ball was added to each tube. Then, the reaction tube was placed in a TissueLyser (Table 10) for 5 minutes at 25 Hz for homogenization. The supernatant was transferred

into a fresh 1.5 ml reaction tube and then centrifuged for 10 minutes at 21,000 x g and 4 °C. Subsequently, the supernatant was collected and transferred into a fresh 1.5 ml tube and stored at -2 80 °C for further use. To isolate proteins from WAT, 500 µl ice-cold lysis buffer (Table 9) was added to the tissue and incubated for 20 minutes on ice. Then the tubes were incubated rotating for further 30 minutes at 4 °C. Afterwards, the supernatant was again transferred into a fresh 1.5 ml reaction tube and centrifuged for 10 minutes at 21,000 g and 4 °C. This step was conducted twice.

2.2.4.2 Determination of protein concentration via Bicinchonic acid assay (BCA)

Protein concentrations of murine tissues were determined using the BCA method (Smith et al., 1985). This method is based on the reduction of Cu^{2+} to Cu^{+} via electron transfer. Cu^{+} is building a complex with bicinchonic acid. The measurement was conducted using the BCA Protein Assay Kit (Table 5). First, a standard curve was added to a 96-well-microtiter plate. Then, protein lysates were added to the plate in a dilution of 1:20. All standards and samples were measured in technical duplicates. Table 20 shows the pipetting scheme of the bovine serum albumin (BSA) standard curve.

Table 19: Standard curve scheme

Amount (µg/well)	Concentration (µg/µl)	BSA stock solution (µl)	MQ water (µl)
0.5	0.025	1.5	118.5
1.0	0.050	3	117.0
2.0	0.100	6	114.0
3.0	0.150	9	111.0
4.0	0.200	12	108.0
5.0	0.250	15	105.0
6.0	0.300	18	102.0
7.0	0.350	21	99.0

Then, the reaction solution was prepared by mixing solution A (containing BCA) and solution B (cupper sulfate) thoroughly in a ratio of 50:1 and adding 200 µl of the reaction solution to each well. Afterwards, the microtiter plate was incubated for 30 minutes at 37 °C and the extinction was measured at the iMARK microplate reader (Table 10) at 560 nm.

2.2.4.3 Sodium-dodecylsulfate-polyacrylamide gel electrophoresis (SDS-PAGE)

After determination of total protein concentration, protein lysates were separated electrophoretically via SDS-PAGE, according to their molecular mass. SDS was added to the protein lysates to apply a negative charge to the proteins. Thereby, proteins migrated within an electric field through a polyacrylamide gel matrix in the direction of the anode. Polyacrylamide acts as a molecular filter, thus small proteins migrated faster through the gel than big proteins. Thereby, proteins are separated according to their molecular mass.

Protein lysates were diluted with 4x Laemmli buffer (Table 9) and MQ water to a final amount of 20 µg total protein. After vortexing, samples were incubated for 30 minutes at RT. During this incubation step, the protein in the samples are denaturated and a negative charge is applied proportional to the protein mass. Next, samples were centrifuged shortly and subsequently loaded on a 12 % SDS gel (Table 21). To estimate the molecular weight of the separated protein bands, a pre-stained protein standard (Table 7) was additionally loaded on the gel. Electrophoretic separation was carried out in electrode buffer (Table 9) at initial 50 V for 15 minutes and 150 V for further 45 – 60 minutes, using the Mini-PROTEAN Tetra Vertical Electrophoresis Cell systems (Table 10).

Table 20: SDS-polyacrylamide gel preparation

Compound	Volume
Stacking gel	
Stacking gel buffer (Table 9)	780 µl
Acrylamide (30 %)	390 µl
ddH_2O	1.83 ml
Ammonium persulfate (APS)	6 µl
Tetraethylethylendiamine (TEMED)	3 µl
Separation Gel (12 %)	
Separation buffer (Table 9)	2.34 ml
Acrylamide	3 ml
ddH_2O	3.66 ml
APS	18 µl
TEMED	9 µl

2.2.4.4 Western Blot analysis and protein detection

Proteins separated during SDS-PAGE were transferred onto a membrane in an electric field using a tank blot system (Tankblot Eco-Mini, Biometra, Göttingen, Germany). The gel from the SDS-PAGE was placed in a cassette with eight Whatman papers (Whatman plc, Maidstone, UK) and two sponges that allow constant energy supply. This cassette was transferred to a tank blot system filled with transfer buffer (Table 9) and the transfer was performed at 200 mA and 4 °C for 2 hours. Negatively charged proteins were blotted onto a nitrocellulose membrane of direction to the anode. After the transfer, the membrane was incubated in 5 % blocking solution (Table 9) for 1 hour at RT in order to minimize unspecific antibody binding on the membrane surface. Afterwards, the membrane was washed thoroughly with TBS-T (Table 9), and then incubated overnight with the respective primary antibody solution (Table 4). Next day, the membrane was washed for 30 minutes with 1x TBS-T and incubated for 1 hour at RT with the respective secondary horseradish-peroxidase (HRP)-conjugated antibody (Table 4) that bound to the constant region of the primary antibody. Then, the membrane was again washed for 30 minutes at RT. Subsequently, the membrane was incubated with ECL enhanced chemiluminescent substrate (Table 7), which consisted of two components that were mixed in a 1:1 ratio. HRP catalyzed the conversion of luminol to 3-aminophtalate and the resulting emitted signal of the catalyzed reaction of HRP with the ECL substrate was detected with the transilluminator (Table 10). Quantitative analysis was carried out with the Image Lab software (Table 11). In order to normalize each band, the abundance of the housekeeping protein Glyceraldehyde 3-phosphate dehydrogenase (GAPDH) was measured and given as ratio of the sedentary Floxed control group.

2.2.5 Molecular biological methods

2.2.5.1 RNA isolation from mouse tissue

Total RNA from skeletal muscle (*Gastrocnemius*) was isolated by Trizol extraction using the miRNeasy-Mini Kit (Table 5). 700 µl Trizol and a steel ball was added to the frozen tissue (30 mg) and lysis was accomplished in the TissueLyser for 5 minutes at 25 Hz. The supernatant was transferred to the QIAshredder column, incubated for 5 minutes at RT and then centrifuged at 18,407 x g for 2 minutes at 4 °C. The supernatant was transferred to Maxtract High Density Tubes (Qiagen, Hilden, Germany), and 140 µl chloroform was added, following 3 minutes incubation at RT. Then, a centrifugation step at 12,000 x g for 15 minutes at 4 °C occurred. The resulting aqueous RNA solution was transferred to 1.5 ml reaction tubes and mixed with 1.5 volume of 70 % EtOH. Subsequently, the RNA was purified using miRNeasy-Mini columns and DNase was digested using the RNase-free DNase Set (Table 5), according to the manufacturer's instructions. Then, 350 µl RW-1 buffer was added to the column and centrifuged

for 15 seconds at 18,407 x g. 500 µl RPE buffer was added and again centrifuged at 18,407 x g for 15 seconds. This step was repeated twice. RNA was eluted with 30 µl RNase free water and a final centrifugation step at 18,407 x g for 1 minute. Concentration of the RNA eluate was measured photometrically at 260 nm using a NanoDrop device (Table 10). Isolated RNA was then provided to our in-house Genomic Unit for RNA sequencing.

2.2.5.2 RNA sequencing

After total RNA isolation, sequencing was performed at our in house genomics platform using Takara MARTer® Stranded total RNA-Seq Kit v2 according to manufacturer's instructions and Illumina NextSeq 500/550 High Output Kit v2.5 at 50 million reads per sample and paired-end (2x75). Subsequent alignment to the mouse GRCm39/mm10 genome was achieved using STAR software (version 2.7.9a) (Dobin et al., 2013) and resulting gene expression was compared among the experimental groups regarding genotype and training status using DESeq2 software (Love et al., 2014). For levels of significance, resulting p-values were corrected for multiple testing following the Benjamini-Hochberg procedure (Benjamini and Hochberg, 1995). Enrichment and canonical pathway analyses as well as potential upstream target analyses were performed using Ingenuity Pathway Analysis (IPA) software (Qjagen, Hilden, Germany) based on fold-changes and level of significance (p-value < 0.01) for all analyses. The RNA sequencing was performed by Dr. Birgit Knebel, Dr. Pia Fahlbusch and Sylvia Jacobs. Ingenuity Pathway Analysis was conducted by Dr. Christian Binsch.

2.2.6 Statistical analysis

The data for all the experiments shown in this thesis are presented as mean ± standard error of the mean (SEM). The number of mice or samples (n) used for the respective experiment is indicated in the corresponding figure legend. Significant differences between two groups with two conditions (training and genotype) were determined using two-way ANOVA with recommended Sidak or Tukey post hoc tests. Values of $p < 0.05$ were considered statistical significant and expressed in the figures as follows: * $P < 0.05$, ** $P < 0.01$, *** $P < 0.001$, **** $P < 0.0001$. GraphPad Prism 9 software was used for preparing the figures and performing the statistical analysis.

3 Results

Previous studies have shown that whole-body *Tbc1d4* deficiency in mice (D4KO) leads to impaired glucose tolerance, insulin insensitivity, postprandial hyperglycemia and impaired insulin- and contraction-stimulated glucose uptake into skeletal muscle and white adipocytes (de Wendt et al., 2021, Chadt et al., 2015, Springer PhD thesis, 2018, Xie et al., 2016). Interestingly, a recent study in our group has shown that a four weeks chronic exercise intervention on treadmills was able to rescue the initially disturbed insulin-stimulated glucose uptake into primary white adipocytes in D4KO animals (Springer PhD thesis, 2018). Since TBC1D4 is highly abundant in oxidative *Soleus* muscle and WAT, the question arises which tissue contributes to the observed rescue effect after chronic exercise in D4KO mice. Therefore, we generated both skeletal muscle- and white adipocyte-specific *Tbc1d4*-deficient mouse lines (mD4KO and aD4KO, respectively), and subjected them to a chronic exercise intervention. Before, during and after the training intervention, we assessed whole-body glycemia, physical fitness and substrate utilization in these animals.

3.1 Generation of muscle-specific *Tbc1d4* knockout mouse strains

3.1.1 Generation of inducible muscle-specific *Tbc1d4* deficiency

The generation of a muscle-specific D4KO mouse line required several breeding steps (2.2.2.2). To verify the successful deletion of the neomycin resistance cassette and the LacZ reporter gene, a LacZ PCR was performed (2.2.3.3) before and after the breeding with Flp deleter mice. The length of the LacZ PCR fragment was expected to have a size around 100 bp for heterozygous and homozygous floxed animals, before the breeding step with Flp deleter mice. Figure 8A displays the result of the LacZ PCR before and after the breeding step with Flp deleter mice. As expected, wildtype (+/+) animals did not display a band around 100 bp, whereas heterozygous (+/fl), and homozygous (fl/fl) floxed animals exhibited a band, confirming the existence of LacZ in floxed animals. After breeding with Flp deleter mice, no bands were detected in wildtype, heterozygous was well as in homozygous floxed animals, validating the successful deletion of the LacZ reporter gene.

Afterwards, floxed animals were backcrossed with C57BL/6 mice and then mated with animals overexpressing an inducible HSA-CreER recombinase to achieve a muscle-specific *Tbc1d4*-deficiency. Two different genotyping PCR reactions were performed in order to distinguish the mice regarding their modified alleles and to validate the successful generation of mD4KO animals. The first PCR reaction aimed to distinguish between WT and heterozygous or homozygous *Tbc1d4* floxed allele

carriers. The expected size of the floxed PCR fragment was around 400 bp, which was shown for sample 3, identifying this animal as homozygous for the floxed allele. In comparison, heterozygous carriers of the floxed allele (e.g. sample 2) showed two bands around 400 bp and 591 bp, whereas WT mice (sample 1) expressed a band around 591 bp (Figure 8B). The second PCR reaction performed was designed to distinguish between WT animals and transgenic mice with an overexpression of the CreER recombinase under the control of the HSA promotor. The expected fragment size of the HSA-CreER allele was around 62 bp. Sample 2 exhibited a strong band around 62 bp, identifying this sample as heterozygous overexpressing HSA-CreER recombinase. In comparison, sample 1 exhibited a faint band around 62 bp, validating this sample as wildtype (Figure 8C).

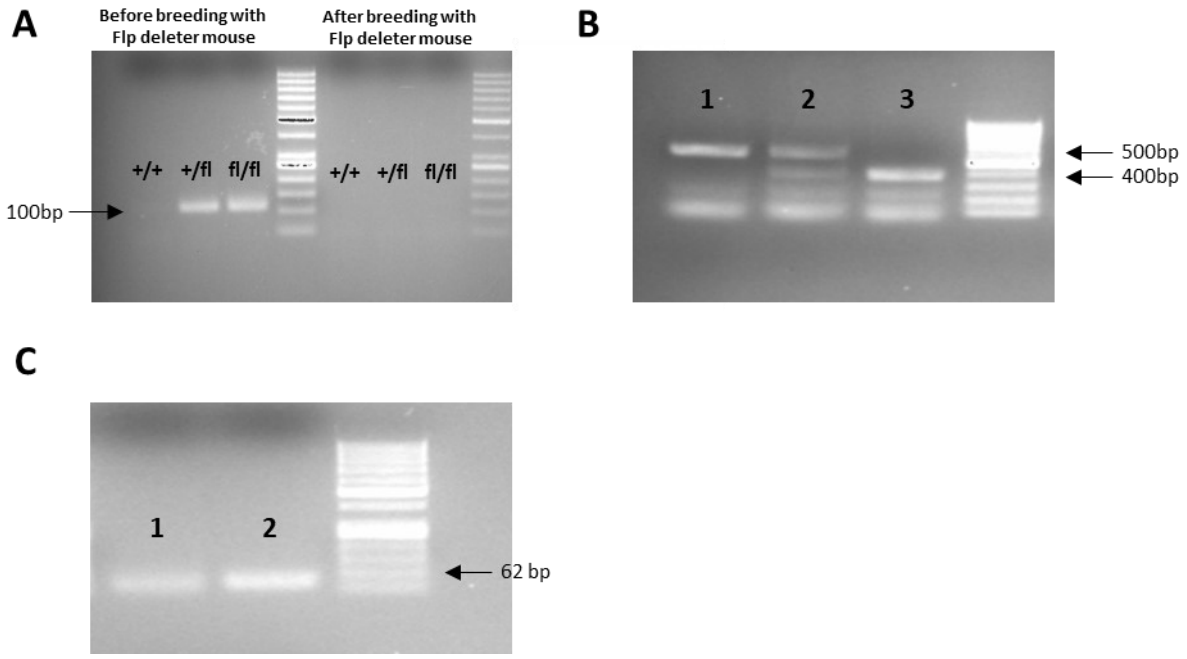

Figure 8: Generation and validation of inducible muscle-specific *Tbc1d4*-deficient mice. To generate muscle-specific *Tbc1d4*-deficient mice the LacZ reporter gene and neomycin resistance cassette were ablated via breeding with Flp deleter mice. To varify the absence of the LacZ gene, a LacZ PCR was performed before, and after mating with Flp deleter animals (**A**). Before the ablation of the LacZ gene, heterozygous and homozygous floxed animals exhibited a band around 100 bp, whereas after the mating with Flp deleter mice, no more bands were detectable. In order to identify mD4KO.indu animals, a floxed PCR (**B**) and HSA-CreER PCR (**C**) were performed. Homozygous floxed animals displayed a band around 400 bp, whereas animals overexpressing the HSA-Cre recombinase showed a clear band around 62 bp.

3.1.2 Generation of conventional muscle-specific *Tbc1d4*-deficient mice

To generate conventional mD4KO animals, homozygous floxed mice were crossed with transgenic animals overexpressing a conventional HSA-Cre recombinase. Two genotyping PCR reactions were performed in order to distinguish the mice regarding their modified alleles and to validate the successful generation of conventional mD4KO mice. Likewise to the mD4KO.ind mouse line, the first

PCR reaction aimed to distinguish between WT and heterozygous or homozygous *Tbc1d4* floxed allele carriers. Sample 3 exhibited a band around 400 bp, identifying this animal as homozygous for the floxed allele. In comparison, heterozygous carriers of the floxed allele (e.g. sample 2) showed two bands around 400 bp and 591 bp, whereas WT mice (sample 1) expressed a band around 591 bp (Figure 9A). The second PCR reaction performed distinguished between WT animals and transgenic mice with an overexpression of the conventional Cre recombinase under the control of the HSA promotor. The expected fragment size of the HSA-Cre allele was around 100 bp. Only sample 2 displayed a band around this size, identifying this sample as heterozygous overexpressing HSA-Cre recombinase. Sample 1 exhibited no band around the expected size, validating this sample as wildtype (Figure 9B).

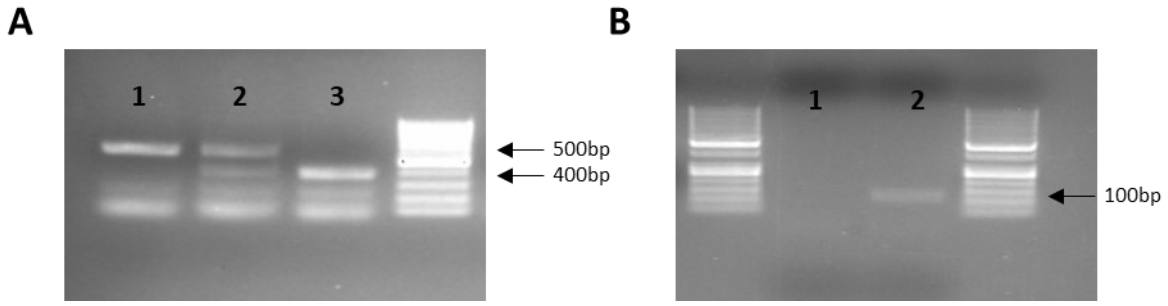

Figure 9: Generation and validation of muscle-specific *Tbc1d4*-deficient mice. In order to identify mD4KO animals two different PCR reactions were performed. The first reaction aimed to distinguish between WT and heterozygous or homozygoes *Tbc1d4* floxed allele carriers (**A**). Homozygous floxed allele carriers display a band around 400 bp. The second PCR reaction identified WT animals and transgenic mice with an overexpression of the conventional HSA-Cre recombinase, with an expected fragment size of 100 bp (**B**).

3.2 Metabolic phenotyping of mD4KO.ind mice

3.2.1 Cre recombinase induction of mD4KO.ind mice

Previous investigations in our group have shown that tamoxifen treatment induces hernia in male mice (data not shown), which was also observed by Ma and colleagues (Ma et al., 2015). Therefore, only female animals were treated with tamoxifen to induce a muscle-specific *Tbc1d4* deficiency. Muscle-specific TBC1D4 knockout was verified on protein level via Western blot technology (2.2.4.4). Protein abundance analysis revealed that in response to the tamoxifen injection, TBC1D4 protein abundance was only reduced by approximately 50 % compared to floxed control mice (Figure 10).

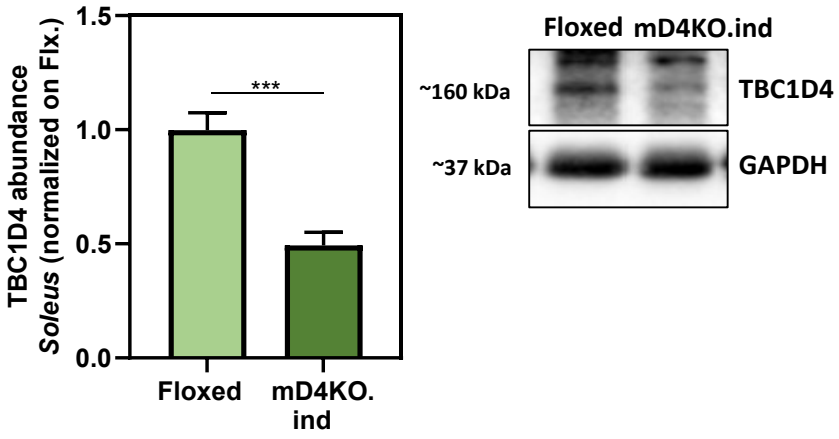

Figure 10: Validation of inducible TBC1D4 knockout. Quantification of TBC1D4 in floxed and mD4KO.ind animals. Protein abundance was normalized on GAPDH and given as ratio of the floxed group. Data are presented as mean ± SEM (n=5-7). *** P<0.001; unpaired t-test, floxed vs. mD4KO.ind. Floxed controls are displayed in light green colors, whereas mD4KO.ind are shown in dark green bars.

3.2.2 The impact of an inducible muscle-specific *Tbc1d4* knockout on glucose homeostasis

One of the most robost phenotypes observed in whole-body D4KO animals is postprandial hyperglycemia one hour after refeeding (de Wendt et al., 2021). In order to verify this phenotype in mD4KO.ind animals, a fasting and refeeding experiment (2.2.2.9) was performed. In response to the refeeding, floxed controls displayed increased blood glucose levels compared to baseline, which declined two and four hours after the refeeding (Figure 11A). Likewise, mD4KO.ind displayed elevated blood glucose levels in response to the refeeding. Surprisingly, mD4KO.ind animals displayed similar blood glucose levels one hour after refeeding compared to their floxed littermates. Likewise, no significant differences in blood glucose levels between floxed and mD4KO.ind animals were observed at other time points.

Impaired insulin-stimulated glucose uptake into the oxidative *Soleus* muscle, presumably due to reduced protein abundance of the glucose transporter GLUT4, is another characteristic phenotype observed in D4KO mice (Springer PhD thesis, 2018, Chadt et al., 2015, Wang et al., 2013, Hargett et al., 2016). Therefore, insulin-stimulated glucose uptake into intact isolated *Soleus* muscle was measured *ex vivo* (2.2.2.10). In response to insulin, floxed animals displayed a significantly increased glucose transport (Figure 11B). Similar to whole-body D4KO mice (Springer PhD thesis, 2018) mD4KO.ind animals exhibited reduced insulin-stimulated glucose uptake into *Soleus* compared to their control

littermates. However, a trend towards insulin stimulation was observable compared to basal conditions in mD4KO.ind animals. As impaired insulin-stimulated glucose uptake in whole-body D4KO mice is associated with an approximately 50 % reduction in GLUT4 protein content (Springer PhD thesis, 2018), GLUT4 abundance was determined via Western Blot technology (2.2.4.4). Interestingly, mD4KO.ind mice displayed only a mild reduction in GLUT4 protein abundance of about 25 % compared to floxed control animals (Figure 11C).

The observed phenotypes in mD4KO.ind animals were less pronounced in comparison to whole-body D4KO mice. As the abundance of skeletal muscle TBC1D4 was only ablated around 50 %, it cannot be distinguished, whether the milder effects are due to the muscle-specific *Tbc1d4* deficiency or due to the fact that TBC1D4 was still present. In order to exclude this technically limitation, conventional mD4KO animals were generated to enable the analysis of skeletal muscle *Tbc1d4* deficiency after a chronic exercise intervention.

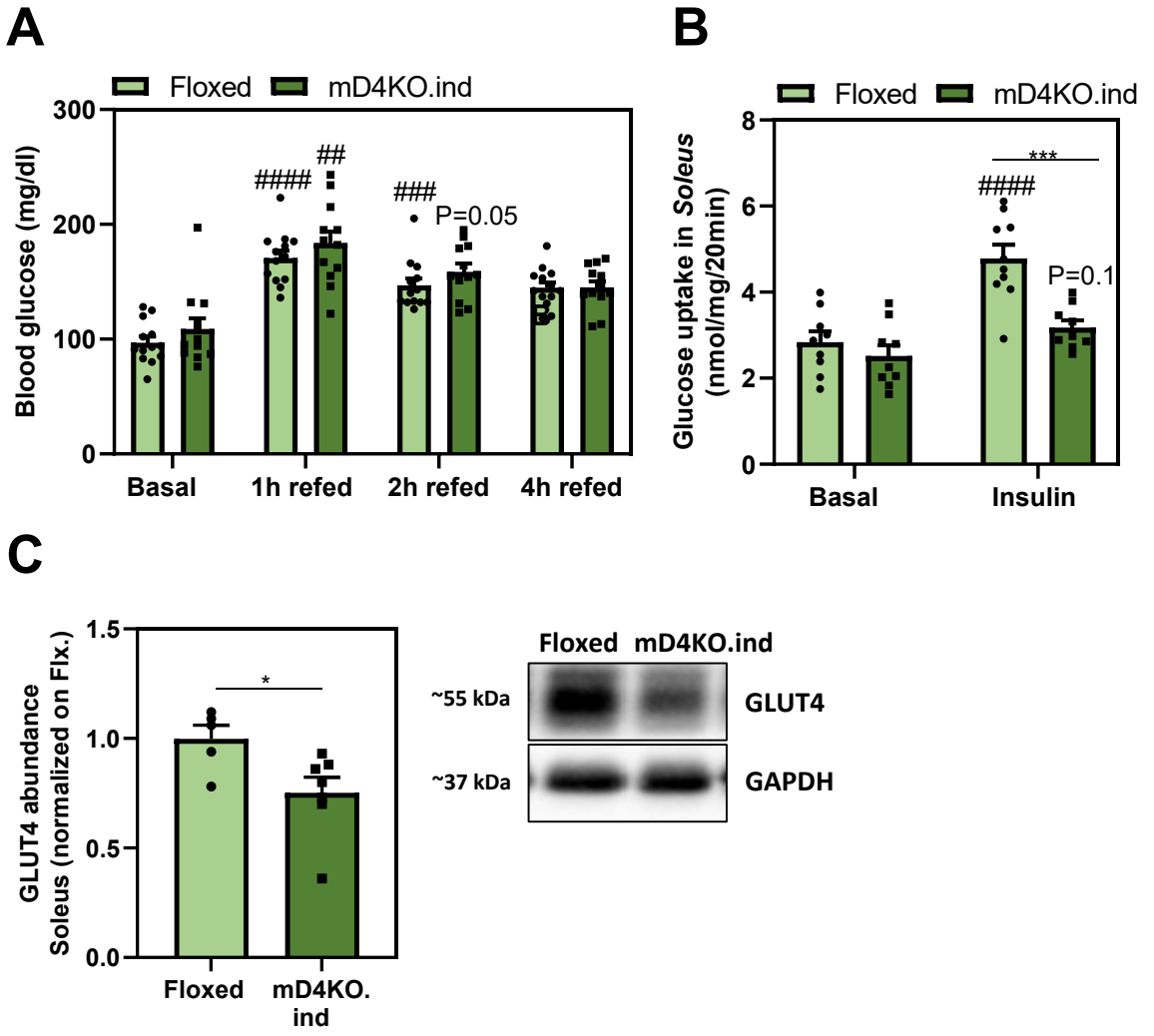

Figure 11: Phenotyping mD4KO.ind animals. Blood glucose levels after a fasting and refeeding experiment (**A**). Data are shown as mean ± SEM (n=12-13). ## P<0.01, ### P<0.001, #### P<0.0001, basal vs. refed, 2-way ANOVA with Tukey post-test; floxed vs. mD4KO.ind 2-way ANOVA with Sidak post-test. Insulin-stimulated glucose uptake into oxidative *Soleus* muscle (**B**). Data are shown as mean ± SEM (n=9-10). #### P<0.0001, Basal vs. Insulin, 2-way ANOVA with Sidak post-test; *** P<0.001, Floxed vs. mD4KO.ind, 2-way ANOVA with Sidak post-test. Western Blot quantification (**C**) of GLUT4 in floxed and mD4KO.ind animals. Protein abundance normalized on GAPDH and given as ratio of the floxed group. Data are shown as mean ± SEM (5-7). * P<0.05, unpaired t-test. Floxed controls are displayed in light green colors, whereas mD4KO.ind are shown in dark green bars.

3.3 Metabolic phenotyping of female conventional mD4KO mice subjected to a chronic exercise intervention

The following paragraph displays the phenotyping of female conventional mD4KO mice after a four weeks chronic exercise intervention.

3.3.1 Validation of muscle-specific *Tbc1d4*-deficiency

In this thesis, both female and male conventional mD4KO mice and respective floxed littermates as controls were analyzed. To verify muscle-specific *Tbc1d4*-deficiency on protein level, a Western Blot analysis was performed using TBC1D4-specific antibodies (2.2.4.4). In comparison to floxed control animals, no signal for TBC1D4 protein was present in mD4KO *Gastrocnemius* muscle. As TBC1D4 is known to be highly abundant in WAT, TBC1D4 protein abundance was also determined in this tissue to determine the specificity of the knockout. TBC1D4 protein was detected in mD4KO animals to a similar amount as in floxed control mice (Figure 12).

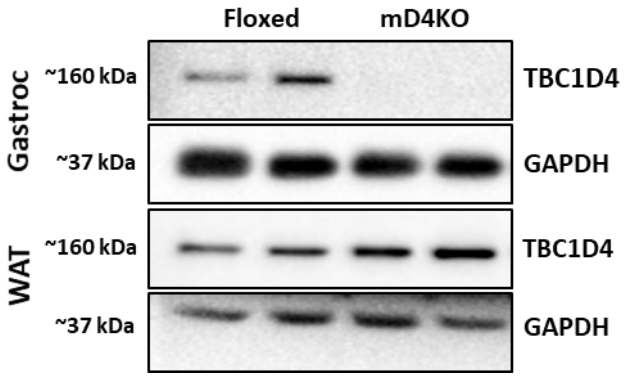

Figure 12: Validation of muscle-specific TBC1D4 ablation. Representative Western Blot of TBC1D4 in *Gastrocnemius* (*Gastroc*) muscle and white adipose tissue (WAT) in female mD4KO and floxed mice.

3.3.2 The impact of a muscle-specific *Tbc1d4* knockout on body composition in female mice after chronic exercise intervention

To measure body weight, lean and fat mass, female mD4KO mice were subjected before (week of life 8) and after the exercise training (week of life 17) to a whole body composition analyzer (NMR) (Table 10). The body composition measurements pre and post exercise are displayed in the supplement (Supplemental Figure 1). Figure 13 shows the body composition of floxed and mD4KO mice in the sedentary and trained state, respectively. No differences in body weight were observed between the genotypes or the training status (Figure 13A). Likewise, lean mass was unaltered between the groups (Figure 13B). Sedentary mD4KO mice showed an increased fat mass in the sedentary state compared to Floxed littermates. After the training period, the fat mass decreased in trained mD4KO compared to sedentary mD4KO mice, but no differences were observed between Floxed and mD4KO mice in the trained state (Figure 13C).

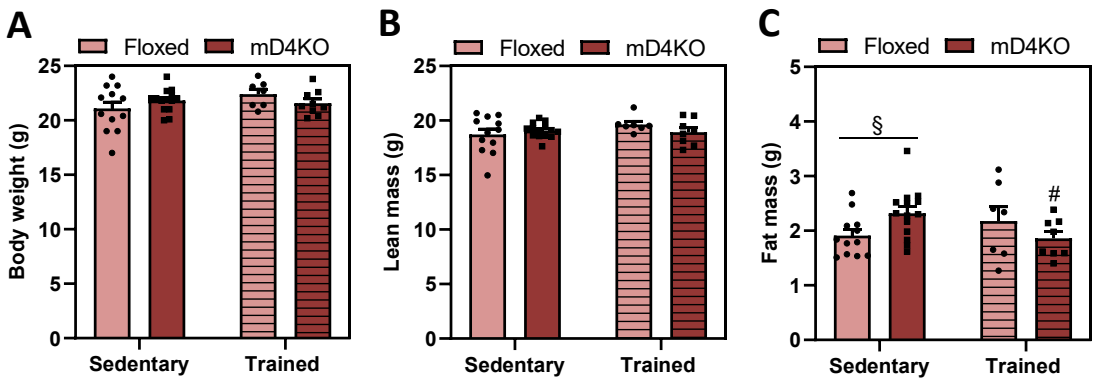

Figure 13: Body composition of female mD4KO. Body weight (**A**), Lean (**B**) and Fat mass (**C**) of sedentary and trained floxed and mD4KO mice. Data are shown as mean ± SEM (n=9-12). § P<0.05, floxed vs. mD4KO, unpaired t-test; # P<0.05, sedentary vs. trained, unpaired t-test. Pink bars represent floxed control mice, whereas red bars symbolize mD4KO animals. Additionally, striped bars demonstrate the trained status.

3.3.3 The impact of a muscle-specific *Tbc1d4* knockout on glucose homeostasis in female mice after chronic exercise intervention

Glucose tolerance was assessed via i.p.GTT after a 16 hours fasting period (2.2.2.5). Floxed and mD4KO mice showed increased blood glucose levels after i.p. injection of glucose that declined evenly over the time of the experiment (Figure 14A). No differences in the area under the curve (AUC) were observed between the groups (Figure 14B).

Insulin sensitivity was measured via i.p.ITT (2.2.2.6). After i.p. injection of insulin, blood glucose levels decreased equally in random fed floxed and mD4KO animals in the sedentary and trained state (Figure 14C). In the sedentary state, mD4KO tended towards reduced AUC compared to floxed mice (Figure 14D). However, no significant differences in trained floxed and mD4KO were observed. Baseline corrected glucose tolernace and insulin sensitivity are displayed in Supplemental Figure 2.

Postprandial blood glucose levels were determined during a fasting and refeeding experiment (2.2.2.9). After a 16 hours fasting period, sedentary and trained floxed and mD4KO animals displayed similar blood glucose levels (Figure 14E). One hour after *ad libitum* refeeding, sedentary mD4KO mice exhibited increased postprandial blood glucose levels compared to sedentary floxed animals. Interestingly, trained mD4KO mice demonstrated reduced blood glucose levels compared to sedentary littermates. Moreover, no statistical difference was observed between trained floxed and trained mD4KO mice 1 hour after refeeding. In addition, no alterations in the blood glucose levels were seen two and four hours after the refeeding when comparing genotypes and training status.

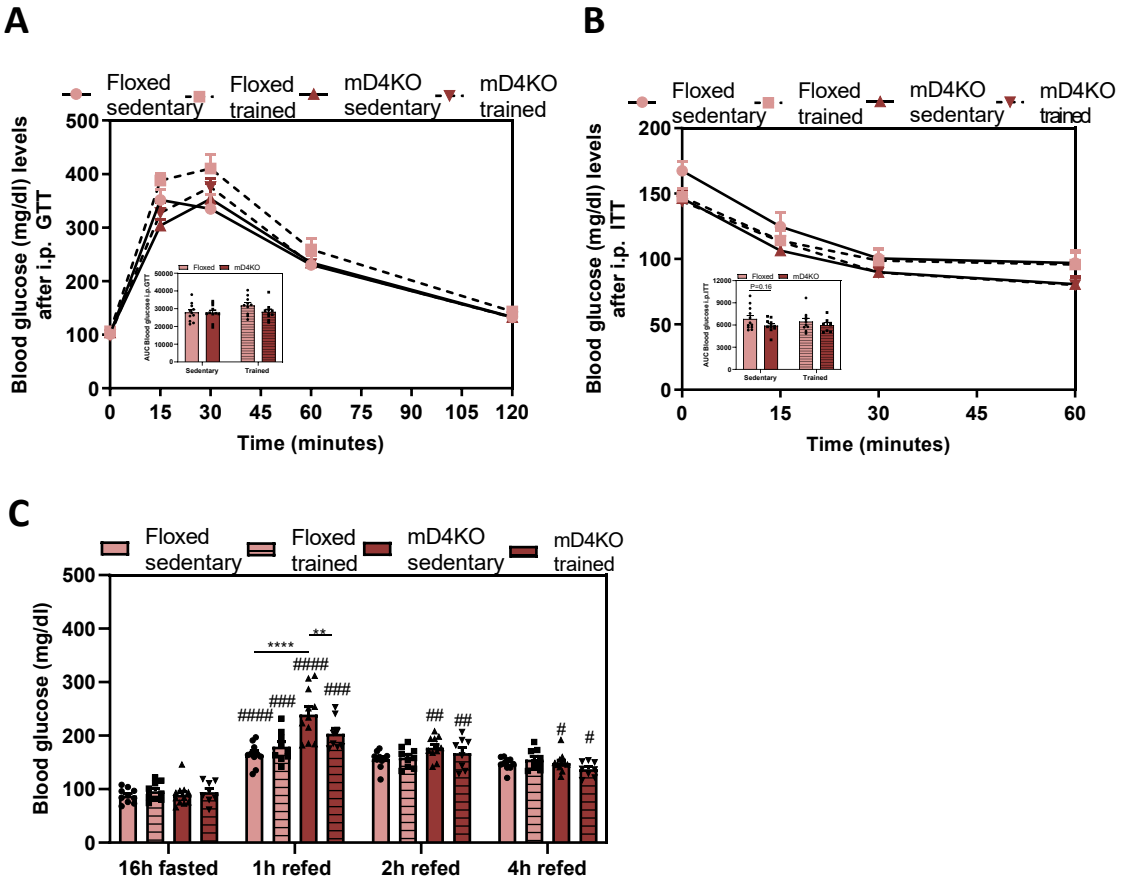

Figure 14: Glucose homeostasis in female mD4KO animals. Blood glucose levels and AUC (**A**) after an i.p.GTT. Data are shown as mean ± SEM (n=10-11). Floxed vs. mD4KO, 2-way ANOVA with Sidak post-test; sedentary vs. trained, 2-way ANOVA with Sidak post-test. Blood glucose levels after an i.p. ITT and calculated AUC (**B**). Data are shown as mean ± SEM (n=8-12). Sedentary vs. trained, 2-way ANOVA with Sidak post-test; floxed vs. mD4KO, 2-way ANOVA with Sidak post-test. Blood glucose levels after a fasting and refeeding experiment (**C**). Data are shown as mean ± SEM (n=8-11). ## P<0.01, ### P<0.001, #### P<0.0001, 16 h fasted vs. 1h refed vs. 2h refed vs. 4h refed, 2-way ANOVA with Tukey post-test; ** P<0.01, **** P<0.0001, floxed sedentary vs. floxed trained vs. mD4KO sedentary vs. mD4KO trained, 2-way ANOVA with Tukey post-test. Pink bars represent floxed control mice, whereas red bars symbolize mD4KO animals. Additionally, striped bars demonstrate the trained status.

3.3.4 The impact of a muscle-specific *Tbc1d4* knockout on exercise capacity in female mice after chronic exercise intervention

In order to determine exercise capacity after the chronic exercise intervention, time to exhaustion and maximum oxygen consumption were measured (2.2.2.7). In the sedentary state, mD4KO mice displayed a reduced time to exhaustion compared to floxed control littermates (Figure 15A). After four weeks of chronic exercise training, both floxed and mD4KO mice improved their running capacity significantly. However, trained mD4KO mice still displayed a reduced time to exhaustion compared to

trained floxed animals. The maximum oxygen consumption which is given as the VO_{2max} value was unaltered compared the genotypes and training status (Figure 15B).

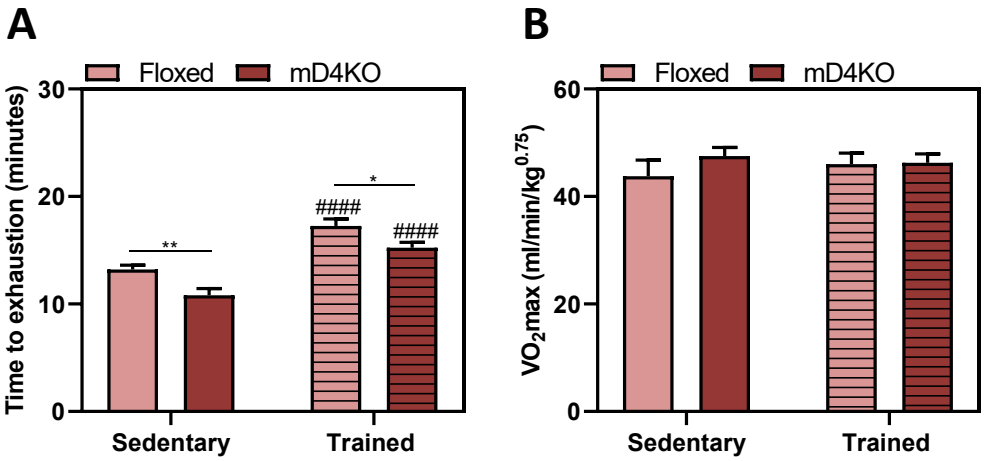

Figure 15: Exercise capacity of female mD4KO mice. Time to exhaustion (**A**) and VO_{2max} value (**B**) determined during indirect calorimetry in sedentary and trained floxed and mD4KO mice. Data are shown as mean ± SEM (n=6-12). * P<0.05, ** P<0.01, floxed vs. mD4KO, 2-way ANOVA with Sidak post-test; #### P<0.0001, sedentary vs. trained, 2-way ANOVA with Sidak post-test. Pink bars represent floxed control mice, whereas red bars symbolize mD4KO animals. Additionally, striped bars demonstrate the trained status.

3.3.5 Contribution of skeletal muscle TBC1D4 on insulin-stimulated glucose uptake into *Soleus* muscle and primary white adipocytes in female mice after chronic exercise intervention

Whole-body D4KO mice showed dramatically impaired insulin-stimulated glucose uptake into the oxidative *Soleus* muscle and primary white adipocytes, both improved after a chronic exercise intervention (Springer PhD thesis, 2018). To validate whether the knockout of *Tbc1d4* in skeletal muscle is responsible for the previously observed rescue effect, insulin-stimulated glucose uptake into *Soleus* muscle and primary white adipocytes of mD4KO and floxed mice was carried out *ex vivo* (2.2.2.10; 2.2.2.11).

In the oxidative *Soleus* muscle, basal glucose uptake was unaltered between floxed and mD4KO mice. Likewise the training intervention had no impact on basal glucose uptake (Figure 16A). In response to insulin, sedentary and trained floxed animals displayed a significantly increased glucose transport. In comparison, no insulin stimulation was observed in sedentary and trained mD4KO mice. Moreover, sedentary mD4KO mice showed a significantly impaired insulin-stimulated glucose transport compared

to sedentary floxed littermates. Interestingly, after the chronic exercise intervention, glucose transport in mD4KO mice was significantly increased, and no statistic difference was observed compared to trained floxed mice. Of note, GLUT4 abundance in *Soleus* muscle was significantly reduced in sedentary and trained mD4KO compared to their respective floxed control (Figure 16B).

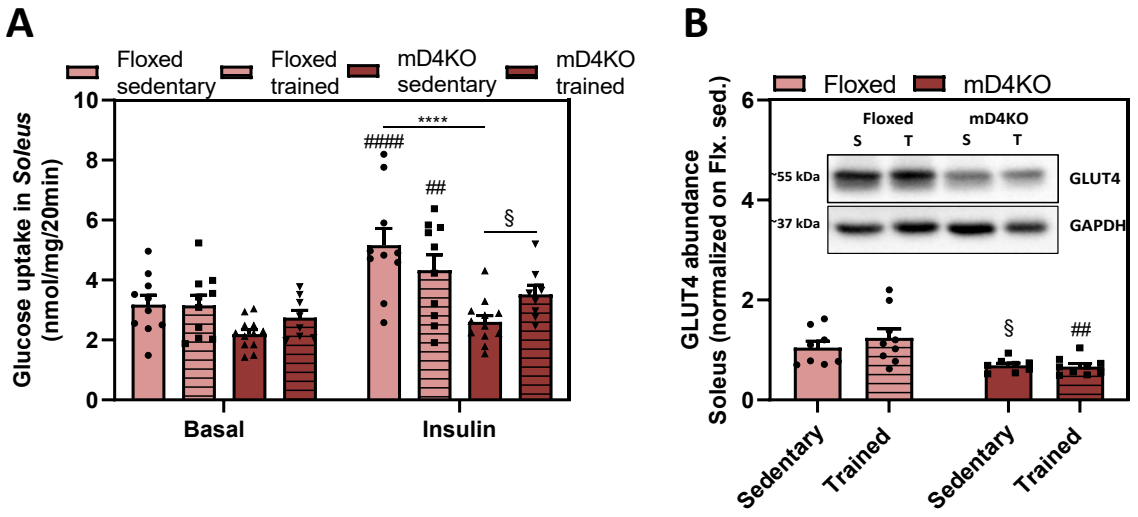

Figure 16: Insulin-stimulated glucose transport into oxidative *Soleus* muscle. Insulin-stimulated glucose uptake into *Soleus* muscle (**A**). Data are shown as mean ± SEM (n=8-12). ## P<0.01, #### P<0.0001, Basal vs. Insulin, 2-way ANOVA with Sidak post-test; **** P<0.0001, floxed sedentary vs. floxed trained vs. mD4KO sedentary vs. mD4KO trained, 2-way ANOVA with Tukey post-test; § P<0.05, mD4KO sedentary at insulin vs. mD4KO trained at insulin, unpaired t-test. Western Blot quantification of GLUT4 (**B**) in sedentary and trained floxed and mD4KO mice. Protein abundance is normalized on GAPDH and given as ratio of sedentary floxed. Data are shown as mean ± SEM (n=8-9). Sedentary vs. trained, 2-way ANOVA with Sidak post-test; ## P<0.01, floxed vs. mD4KO, 2-way ANOVA with Sidak post-test; § P<0.05, floxed sedentary vs. mD4KO sedentary, unpaired t-test. Pink bars represent floxed control mice, whereas red bars symbolize mD4KO animals. Additionally, striped bars demonstrate the trained status. S = sedentary, T = trained.

To further characterize whether the TBC1D4 deficiency in skeletal muscle is responsible for the rescue effect observed in WAT of whole-body D4KO mice, *ex vivo* [^{14}C]-D-glucose uptake was measured in isolated adipocytes from gonadal white fat depots (2.2.2.11). No alterations in basal glucose uptake were observed between the genotypes or the training status, respectively (Figure 17A). In response to insulin, all groups displayed an equally significant increase in glucose transport into primary white adipocytes. Likewise, GLUT4 abundance in WAT was unaltered between the genotypes or the training status, respectively (Figure 17B).

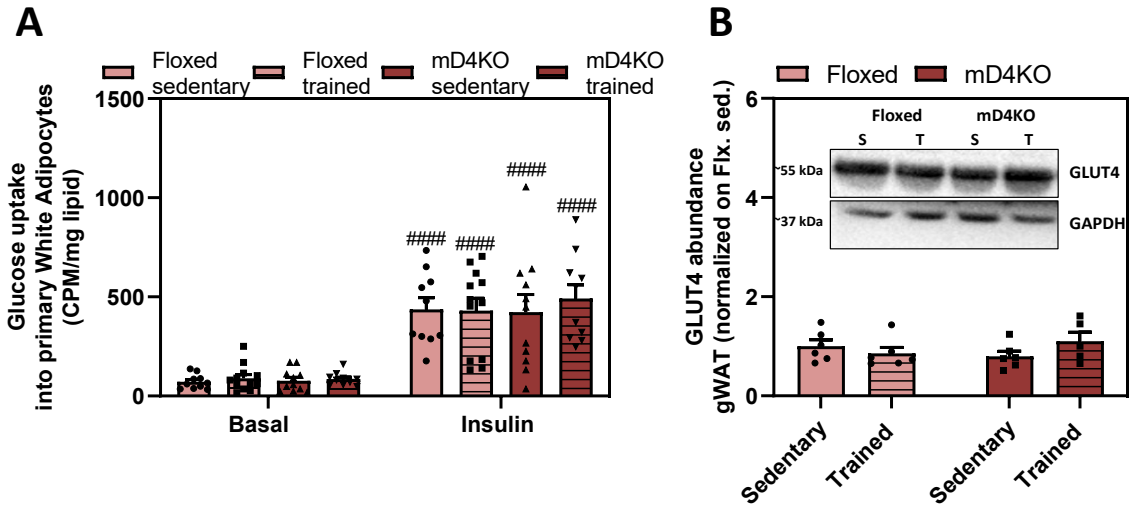

Figure 17: Insulin-stimulated glucose transport into primary white adipocytes. Insulin-stimulated glucose uptake into primary white adipocytes (**A**). Data are shown as mean ± SEM (n=10-12). #### P<0.0001, Basal vs. Insulin, 2-way ANOVA with Sidak post-test. Floxed sedentary vs. floxed trained vs. mD4KO sedentary vs. mD4KO trained, 2-way ANOVA with Tukey post-test; Western Blot quantification of GLUT4 (**B**) in WAT of sedentary and trained floxed and mD4KO mice. Protein abundance is normalized on GAPDH and given as ratio of sedentary floxed. Data are shown as mean ± SEM (n=5-6). Floxed vs. mD4KO, 2-way ANOVA with Sidak post-test; Sedentary vs. Trained, 2-way ANOVA with Sidak post-test. Pink bars represent floxed control mice, whereas red bars symbolize mD4KO animals. Additionally, striped bars demonstrate the trained status. S = sedentary, T = trained.

3.4 Metabolic phenotyping of male conventional mD4KO mice subjected to chronic exercise intervention

Besides female mD4KO, male mD4KO mice were also metabolically characterized before, during and after a four weeks chronic exercise intervention.

3.4.1 Validation of muscle-specific *Tbc1d4*-deficiency

In this thesis, both female and male conventional mD4KO mice and respective floxed littermates as controls were analyzed. To verify muscle-specific *Tbc1d4*-deficiency on protein level, a Western blot analysis was performed using TBC1D4-specific antibodies (2.2.4.4). In comparison to floxed control animals, no signal for TBC1D4 protein was present in female as well as male mD4KO *Gastrocnemius* muscle. As TBC1D4 is known to be highly abundant in WAT, TBC1D4 protein abundance was also determined in this tissue to determine the specificity of the knockout. TBC1D4 protein was detected in female and male mD4KO animals to a similar amount as in floxed control mice (Figure 18).

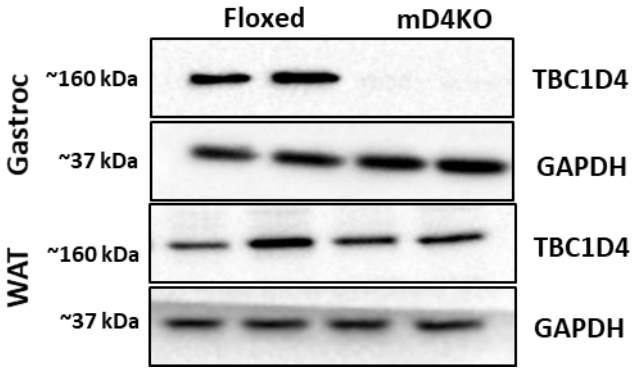

Figure 18: Validation muscle-specific *Tbc1d4*-defiency. Representative Western Blot of TBC1D4 in *Gastrocnemius* (*Gastroc*) muscle and white adipose tissue (WAT) male mD4KO mice.

3.4.2 The impact of a muscle-specific *Tbc1d4* knockout on body composition in male mice after chronic exercise intervention

To determine body composition of floxed and mD4KO mice during the four weeks chronic exercise intervention, a NMR analyzer was used (Table 10). Body composition was analyzed before (week of life 8) and after (week of life 17) the chronic exercise intervention. The body composition analysis between pre and post exercise is displayed in the supplement (Supplemental Figure 3). Figure 19 displays the body composition of sedentary and trained male floxed controls and mD4KO mice. No differences were seen in the body weight between floxed and mD4KO mice in the sedentary as well as in the trained state (Figure 19A). Likewise, lean mass did not differ between the genotypes or the training status, respectively (Figure 19B). No alterations in fat mass between sedentary floxed and mD4KO mice were observed (Figure 19C). After the training period, both floxed and mD4KO mice displayed significantly reduced fat mass compared to their sedentary littermates. Within the trained cohort, no differences between floxed and mD4KO mice were determined.

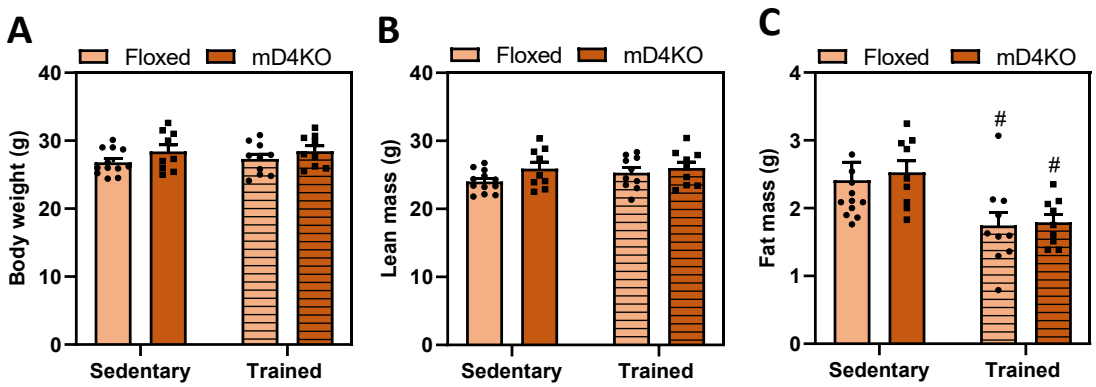

Figure 19: Body composition of male mD4KO animals. Body weight (**A**), Lean (**B**) and Fat mass (**C**) of sedentary and trained floxed and mD4KO mice. Data are shown as mean ± SEM (n=9-12). Floxed vs. mD4KO, 2-way ANOVA with Sidak post-test. # P<0.05, sedentary vs. trained, 2-way ANOVA with Sidak post-test. Light orange bars represent floxed controls and dark orange bars display mD4KO mice. Additionally, striped bars show the trained situation.

3.4.3 The impact of a muscle-specific *Tbc1d4* knockout on glucose homeostasis in male mice after chronic exercise intervention

Glucose tolerance was measured via an i.p.GTT (2.2.2.5) and glucose levels were determined. Floxed and mD4KO mice displayed a similar time course during the GTT, and no differences in the AUC were measured between the genotypes or the training status, respectively (Figure 20A).

To determine insulin sensitivity, an i.p.ITT was carried out (2.2.2.6). In response to the insulin injection, blood glucose levels decreased over time. No differences in the AUC between sedentary or trained floxed and mD4KO mice (Figure 20B). Baseline corrected glucose tolerance and insulin sensitivity is displayed in Supplemental Figure 4.

To analyze postprandial blood glucose levels, a fasting and refeeding experiment was performed (2.2.2.9). After 16 hours of fasting, sedentary mD4KO mice displayed reduced blood glucose levels compared to sedentary floxed controls (Figure 20C). Moreover, sedentary mD4KO animals showed decreased blood glucose levels compared to their trained littermates. One hour after refeeding, sedentary mD4KO displayed increased postprandial blood glucose levels compared to sedentary floxed animals. Interestingly, the elevated postprandial blood glucose levels in the mD4KO mice were rescued after the training intervention, as blood glucose levels of trained mD4KO mice were significantly lower compared to sedentary mD4KO. Two and four hours after refeeding, respectively, no differences in blood glucose levels were observed between the four groups.

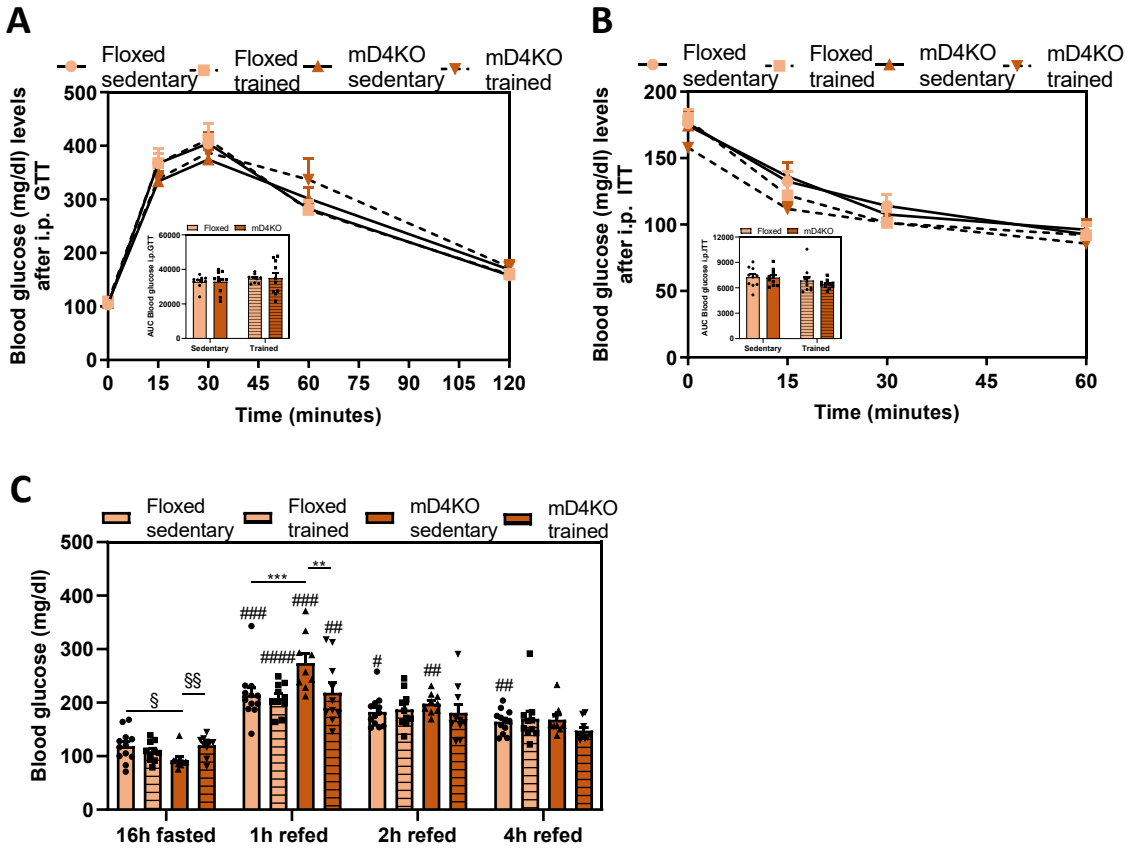

Figure 20: Glucose homeostasis in male mD4KO animals. Blood glucose levels and AUC (**A**) after an i.p.GTT. Data are shown as mean ± SEM (n=10-11). floxed vs. mD4KO, 2-way ANOVA with Sidak post-test; sedentary vs. trained, 2-way ANOVA with Sidak post-test. Blood glucose levels after an i.p. ITT and calculated AUC (**B**). Data are shown as mean ± SEM (n=10-11). Sedentary vs. trained, 2-way ANOVA with Sidak post-test; floxed vs. mD4KO, 2-way ANOVA with Sidak post-test. Blood glucose levels after a fasting and refeeding experiment (**C**). Data are shown as mean ± SEM (n=9-12). # P<0.05, ## P<0.01, ### P<0.001, #### P<0.0001, 16 h fasted vs. 1h refed vs. 2h refed vs. 4h refed, 2-way ANOVA with Tukey post-test; ** P<0.01, *** P<0.001, floxed sedentary vs. floxed trained vs. mD4KO sedentary vs. mD4KO trained, 2-way ANOVA with Tukey post-test. § P<0.05, floxed sedentary at 16 h fasted vs. mD4KO sedentary at 16 h fasted; §§ P<0.01, mD4KO sedentary at 16 h fasted vs. mD4KO trained at 16 h fasted, unpaired t-test. Light orange bars represent floxed controls and dark orange bars display mD4KO mice. Additionally, striped bars demonstrate the trained status.

3.4.4 The impact of a muscle-specific *Tbc1d4* knockout on exercise capacity in male mice after chronic exercise intervention

In order to determine exercise capacity, animals were subjected to a running protocol on calorimetric treadmills to measure time to exhaustion and maximum oxygen consumption (2.2.2.7). In the sedentary state, no alterations between floxed and mD4KO animals were observed (Figure 21A). Likewise, within the trained group, no differences between the genotypes were seen. However, in comparison to sedentary littermates, trained floxed and mD4KO showed a significantly increased running capacity.

The maximum oxygen consumption, given as the VO_{2max} value, was unaltered in the sedentary state between floxed and mD4KO mice (Figure 21B). After the chronic exercise intervention, floxed animals displayed a significant increase in the VO_{2max} value. In contrast, no different VO_{2max} value between trained and sedentary mD4KO mice were observed. Moreover, trained mD4KO exhibited an impaired maximum oxygen consumption compared to trained floxed controls.

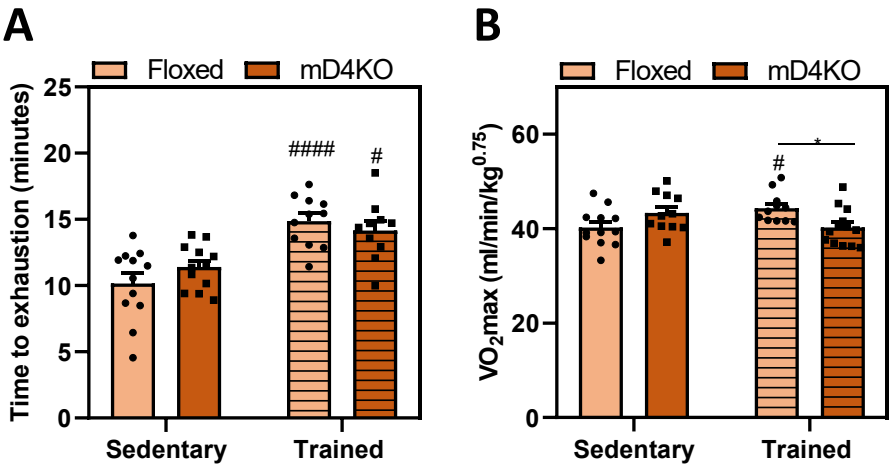

Figure 21: Exercise capacity of male mD4KO mice. Time to exhaustion (**A**) and VO_{2max} value (**B**) determined during indirect calorimetry in sedentary and trained floxed and mD4KO mice. Data are shown as mean ± SEM (n=8-12). * P<0.05, floxed vs. mD4KO, 2-way ANOVA with Sidak post-test; # P<0.05, #### P<0.0001, sedentary vs. trained, 2-way ANOVA with Sidak post-test. Light orange bars represent floxed controls and dark orange bars display mD4KO mice. Additionally, striped bars demonstrate the trained status.

3.4.5 The contribution of skeletal muscle TBC1D4 on insulin-stimulated glucose uptake into *Soleus* muscle and primary white adipocytes in male mice after chronic exercise intervention

Insulin-stimulated glucose uptake into isolated *Soleus* muscle was measured *ex vivo* using [^{3}H]-2-deoxyglucose and, in addition, [^{14}C]-mannitol as marker for the extracellular space (2.2.2.10). In the basal state, sedentary mD4KO displayed reduced glucose transport compared to sedentary floxed controls (Figure 22A). In response to insulin, sedentary and trained floxed animals showed a significantly increased glucose uptake. However, neither sedentary nor trained mD4KO mice showed an insulin response. Moreover, sedentary and trained mD4KO demonstrated significantly impaired insulin-stimulated glucose transport compared to their respective controls. Noteworthy, GLUT4 abundance in the *Soleus* muscle was reduced in mD4KO compared to Floxed controls in the sedentary as well as in the trained state (Figure 22B).

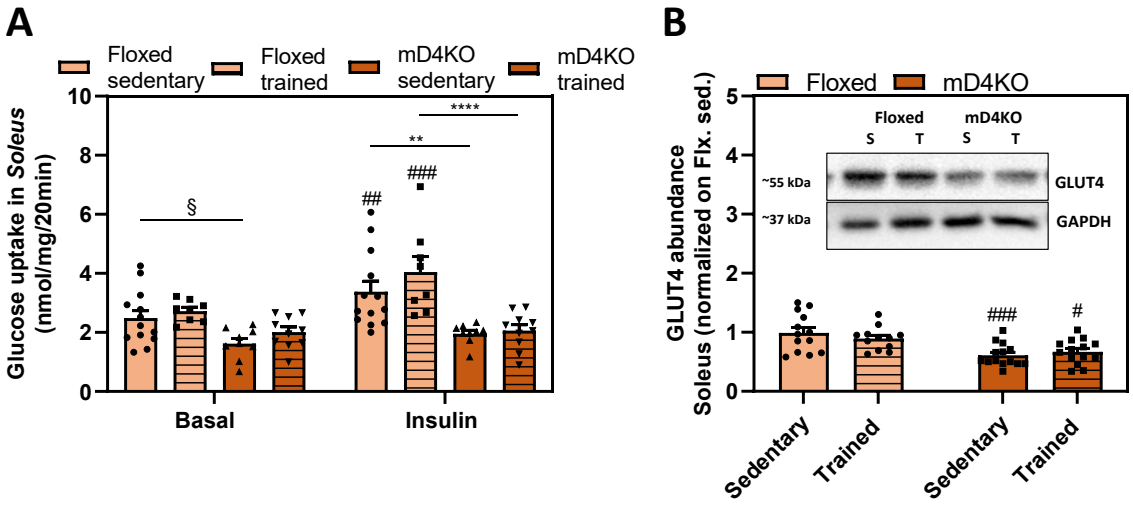

Figure 22: Insulin-stimulated glucose transport into oxidative *Soleus* muscle. Insulin-stimulated glucose uptake into *Soleus* muscle (**A**). Data are shown as mean ± SEM (n=8-13). ## P<0.01, ### P<0.001; Basal vs. Insulin, 2-way ANOVA with Sidak post-test; ** P<0.01, **** P<0.0001, floxed vs. mD4KO, 2-way ANOVA with Tukey post-test; § P<0.05, sedentary floxed at basal vs. sedentary mD4KO at basal, unpaired t-test. Western Blot quantification of GLUT4 (**B**) in sedentary and trained floxed and mD4KO mice. Protein abundance is normalized on GAPDH and given as ratio of sedentary Floxed. Data are shown as mean ± SEM (n=12-14). # P<0.05, ### P<0.001, floxed vs. mD4KO, 2-way ANOVA with Sidak post-test; Sedentary vs. trained, 2-way ANOVA with Sidak post-test. Light orange bars represent floxed controls and dark orange bars display mD4KO mice. Additionally, striped bars demonstrate the trained status. S = sedentary, T = trained.

Next, insulin-stimulated glucose uptake into primary white adipocytes was determined *ex vivo* using [^{14}C]-D-glucose (2.2.2.11). No alterations between the genotypes or the training status, respectively were observed at basal condition (Figure 23A). In response to insulin, floxed as well as mD4KO mice exhibited significantly increased glucose uptake in both the sedentary and trained state. Interestingly, trained floxed animals presented a significantly increased glucose transport compared to their sedentary littermates. In comparison, glucose transport into primary white adipocytes was unchanged in trained mD4KO, compared to sedentary animals. Moreover, GLUT4 protein level remained unaltered between the genotypes and the training status (Figure 23B).

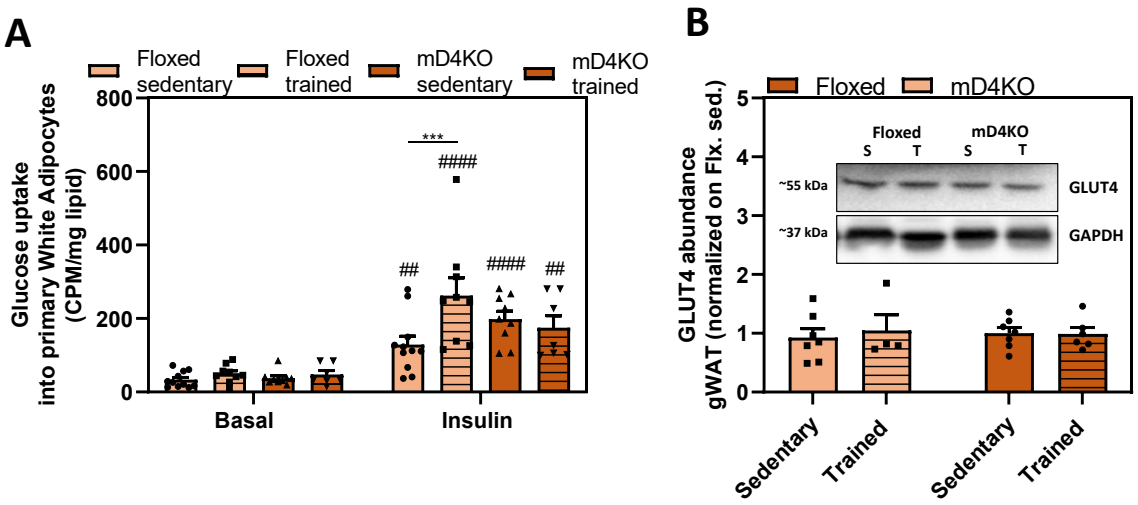

Figure 23: Insulin-stimulated glucose transport into primary white adipocytes. Insulin-stimulated glucose uptake into primary white adipocytes (**A**). Data are shown as mean ± SEM (n=7-11). ## P<0.01, #### P<0.0001, Basal vs. Insulin, 2-way ANOVA with Sidak post-test. Floxed sedentary vs. floxed trained vs. mD4KO sedentary vs. mD4KO trained, 2-way ANOVA with Tukey post-test; Western Blot quantification of GLUT4 (**B**) in WAT of sedentary and trained floxed and mD4KO mice. Protein abundance is normalized on GAPDH and given as ratio of sedentary floxed. Data are shown as mean ± SEM (n=5-7). Floxed vs. mD4KO, 2-way ANOVA with Sidak post-test; sedentary vs. trained, 2-way ANOVA with Sidak post-test. Light orange bars represent floxed control mice, whereas dark orange bars symbolize mD4KO animals. Additionally, striped bars demonstrate the trained status. S = sedentary, T = trained.

3.5 Metabolic phenotyping of aD4KO mice subjected to chronic exercise intervention

As TBC1D4 is also highly abundant in WAT, adipocyte-specific TBC1D4 KO (aD4KO) mice were generated to verify whether a deficiency of *Tbc1d4* in WAT is accountable for the rescue effect in glycemic control previously observed in whole-body D4KO mice after chronic exercise training.

3.5.1 Generation and validation of aD4KO mice

To genotype aD4KO animals, a mouse line carrying floxed *Tbc1d4* alleles was bred with a transgenic strain overexpressing a Cre recombinase under the control of an adiponectin promotor. Both gene loci were analyzed via specific PCR reactions in order to determine the respective genotype of the aD4KO mice. In order to distinguish between WT and heterozygous or homozygous *Tbc1d4* floxed allele carriers, a floxed PCR reaction was performed (2.2.3.3). Homozygous *Tbc1d4* floxed allele carriers exhibit a band around 400 bp, which was seen in sample 3. In comparison, sample 2 displayed two

bands around 400 bp and 591 bp, classifying this animal as heterozygous carrier for the floxed allele, while sample 3 was identified as WT mice, as it expressed a band around 591 bp (Figure 24A). The second PCR reaction aimed to distinguish between WT animals and transgenic mice with a heterozygous overexpression of the Cre recombinase under the control of the adiponectin promotor. The expected fragment sizes of the adiponectin-Cre allele was around 324 bp and 531 bp. Only sample 2 displayed both bands at the expected sizes, identifying this sample as heterozygous overexpressing adiponectin-Cre recombinase. Sample 1 exhibited a band around 324 bp, validating this sample as wildtype (Figure 24B).

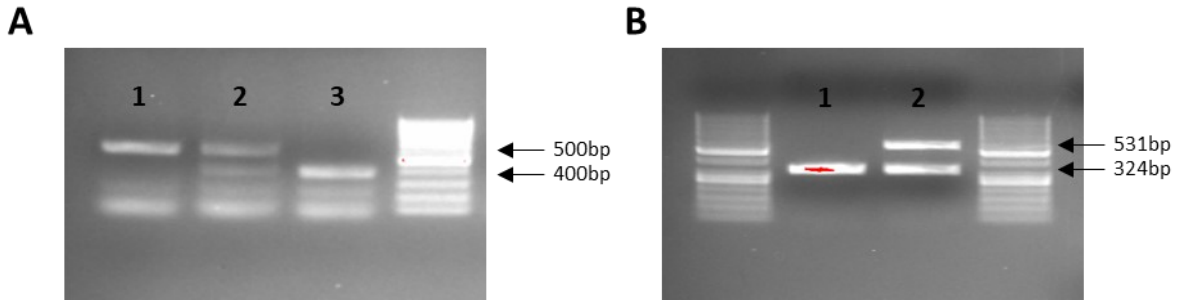

Figure 24: Validation of adipocyte-specific *Tbc1d4*-deficient mice. In order to identify aD4KO mice two different PCR reactions were performed. The first reaction aimed to distinguish between WT and heterozygous or homozygous Tbc1d4 floxed allele carriers (A). Homozygous floxed allele carriers display a band around 400 bp. The second PCR reaction identified WT animals and transgenic mice overexpressing adiponectin-Cre recombinase, with two expected fragments around 324 bp and 531 bp (B).

On protein level, adipocyte-specific *Tbc1d4*-deficiency could be confirmed, as WAT from aD4KO was lacking TBC1D4 in contrast to WAT from floxed mice (Figure 25). In comparison, *Soleus* muscle of aD4KO displayed a TBC1D4 band around 160 kDa.

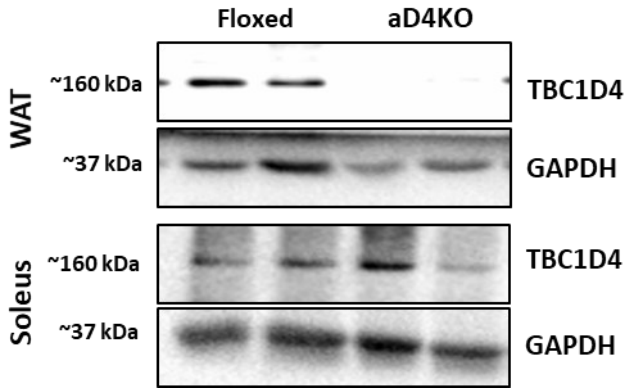

Figure 25: Validation of adipocyte-specific *Tbc1d4*-deficiency in aD4KO animals. Representative Western Blot of TBC1D4 in WAT and *Soleus* of aD4KO animals.

3.5.2 The impact of an adipocyte-specific *Tbc1d4* knockout on body composition in male mice after chronic exercise intervention

Body composition was measured by a NMR analyzer (Table 10). Body composition was analyzed before (week of life 8) and after (week of life 16) the chronic exercise intervention. The body composition analysis between pre and post exercise is displayed in the supplement (Supplemental Figure 5). Figure 26 displays the body composition of sedentary and trained male floxed controls and aD4KO mice after the exercise training. No differences in body weight between Floxed and aD4KO animals in the sedentary or trained state were detected (Figure 26A). Likewise, lean mass was unaltered between the genotypes or the training status (Figure 26B). Moreover, fat mass did not differ in sedentary and trained aD4KO compared to their Floxed littermates (Figure 26C).

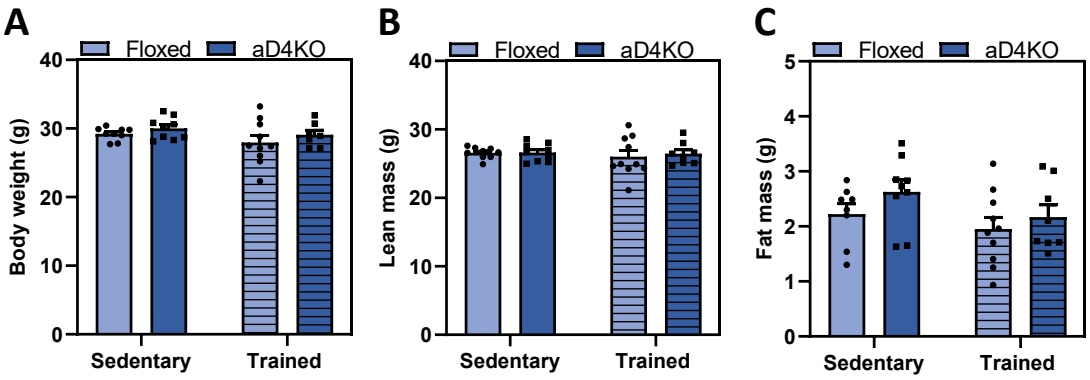

Figure 26: **Body composition of aD4KO mice**. Body weight (**A**), Lean (**B**) and Fat mass (**C**) of sedentary and trained Floxed and aD4KO mice. Data are shown as mean ± SEM (n=7-10). Floxed vs. aD4KO, 2-way ANOVA with Sidak post-test, sedentary vs. trained, 2-way ANOVA with Sidak post-test. Light blue bars represent floxed controls and dark blue bars display aD4KO mice. Additionally, striped bars show the trained condition.

3.5.3 The effect of adipocyte-specific *Tbc1d4* deficiency on whole-body glucose homeostasis after chronic exercise intervention

Glucose homeostasis was measured via an i.p.GTT after a fasting period of 16 hours and blood glucose levels were determined (2.2.2.5). All animals displayed rising blood glucose levels after glucose injection (Figure 27A). Interestingly, sedentary aD4KO exhibited significantly higher blood glucose levels 15 minutes and 30 minutes after the glucose injection compared to sedentary floxed mice. The impaired glucose tolerance was also reflected in the AUC, which was increased in sedentary aD4KO compared to their floxed littermates (Figure 27B). In the trained state, no differences in glucose

clearance between floxed and aD4KO animals were measured, which is presented in the AUC. Interestingly, due to the chronic exercise intervention, trained aD4KO displayed decreased blood glucose levels 15 minutes post glucose injection in comparison to their sedentary controls. These improvements were also observed in the AUC, which tended to be reduced in trained aD4KO compared to the sedentary state.

Insulin sensitivity was measured via an i.p.ITT (2.2.2.6). Blood glucose levels declined similarly during the time course in sedentary and trained Floxed and aD4KO mice (Figure 27C). This observation was also reflected in the AUC calculation. Baseline corrected glucose tolerance and insulin sensitivity are displayed in Supplemental Figure 6.

Fasting as well as postprandial blood glucose levels were measured via a fasting and refeeding experiment (2.2.2.9). After a fasting period of 16 hours, basal blood glucose levels were reduced in sedentary aD4KO mice compared to sedentary floxed animals (Figure 27D). Moreover, after the chronic exercise intervention, trained floxed animals displayed a significant reduction in basal blood glucose levels compared to their sedentary controls. One hour after refeeding, sedentary aD4KO mice displayed postprandial hyperglycemia compared to their respective floxed control littermates. Surprisingly, even after the chronic exercise intervention, aD4KO mice still exhibited postprandial hyperglycemia compared to trained floxed mice. Two hours after refeeding, trained aD4KO displayed increased blood glucose levels compared to trained floxed animals and sedentary aD4KO mice.

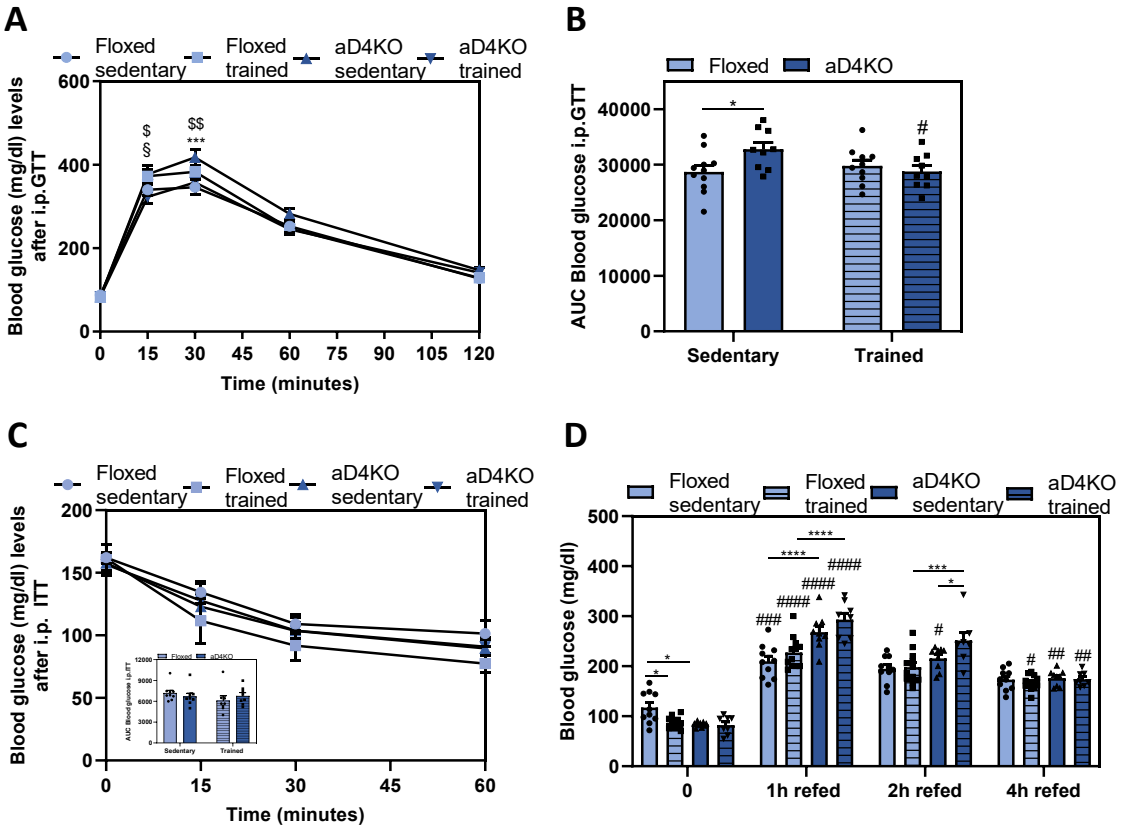

Figure 27: **Glucose homeostasis in aD4KO animals**. Blood glucose levels (**A**) after an i.p.GTT. Data are shown as mean ± SEM (n=9-11). § P<0.05, floxed sedentary vs. floxed trained at 15 min post injection, 2-way ANOVA with Tukey post-test; $ P<0.05, aD4KO sedentary vs. aD4KO trained at 15 min post injection, 2-way ANOVA with Tukey post-test; *** P<0.001, floxed sedentary vs. aD4KO sedentary at 30 min post injection, 2-way ANOVA with Tukey post-test; $$ P<0.01, aD4KO sedentary vs. aD4KO trained at 30 min post injection; Respective AUC (**B**) after an i.p.GTT. Data are shown as mean ± SEM (n=9-11). * P<0.05, floxed vs. aD4KO, 2-way ANOVA with Sidak post-test; # P<0.05, sedentary vs. trained, 2-way ANOVA with Sidak post-test. Blood glucose levels after an i.p. ITT and calculated AUC (**C**). Data are shown as mean ± SEM (n=8-9). Floxed vs. aD4KO, 2-way ANOVA with Sidak post-test; sedentary vs. trained, 2-way ANOVA with Sidak post-test. Blood glucose levels after a fasting and refeeding experiment (**D**). Data are shown as mean ± SEM (n=8-12). # P<0.05, ## P<0.01, ### P<0.001, #### P<0.0001, 16 h fasted vs. 1h refed vs. 2h refed vs. 4h refed, 2-way ANOVA with Tukey post-test; * P<0.05, *** P<0.001, **** P<0.0001, floxed sedentary vs. floxed trained vs. aD4KO sedentary vs. aD4KO trained, 2-way ANOVA with Tukey post-test. Light blue bars represent floxed control mice, whereas dark blue bars symbolize aD4KO animals. Additionally, striped bars demonstrate the trained status.

3.5.4 The effect of a adipocyte-specific *Tbc1d4* deficiency on exercise capacity after chronic exercise intervention

To evaluate the exercise capacity of aD4KO animals after a chronic exercise intervention, the time to exhaustion and VO_{2max} value were measured on calorimetric treadmills (2.2.2.7). Time to exhaustion was comparable between sedentary floxed and aD4KO mice (Figure 28A). In response to the chronic exercise intervention, time to exhaustion increased in floxed mice. In comparison, aD4KO did not improve their running capacity after the exercise training. Moreover, trained aD4KO displayed a

reduced exercise capacity compared to their respective floxed controls. In comparison, VO_{2max} value was unaltered between the genotypes and training status (Figure 28B).

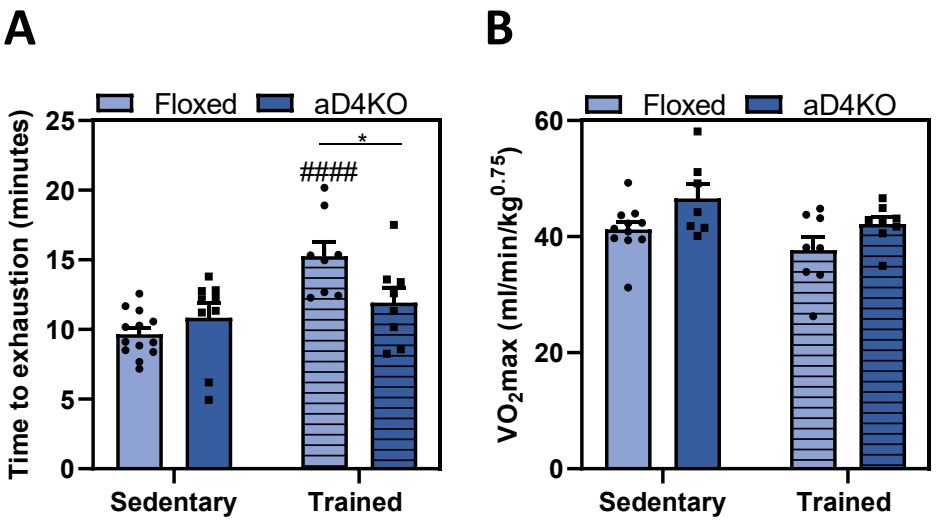

Figure 28: Exercise capacity of aD4KO mice. Time to exhaustion (**A**) and VO_{2max} value (**B**) determined during indirect calorimetry in sedentary and trained floxed and aD4KO mice. Data are shown as mean ± SEM (n=7-13). * P<0.05, floxed vs. aD4KO, 2-way ANOVA with Sidak post-test; #### P<0.0001, sedentary vs. trained, 2-way ANOVA with Sidak post-test. Light blue bars represent floxed control mice, whereas dark blue bars symbolize aD4KO animals. Additionally, striped bars demonstrate the trained status.

3.5.5 The contribution of adipose tissue TBC1D4 on insulin-stimulated glucose uptake into *Soleus* muscle and primary white adipocytes in male mice after chronic exercise intervention

Glucose uptake into oxidative *Soleus* muscle was measured *ex vivo* (2.2.2.10). No differences in the basal glucose transport were observed between the genotypes or the training status, respectively (Figure 29A). In response to insulin, sedentary and trained floxed and aD4KO animals displayed a significantly increased glucose transport. However, no differences were observed between the genotypes. Similar to the observed results in glucose transport, GLUT4 abundance in *Soleus* muscle was unaltered in floxed and aD4KO mice in both the sedentary and trained state (Figure 29C).

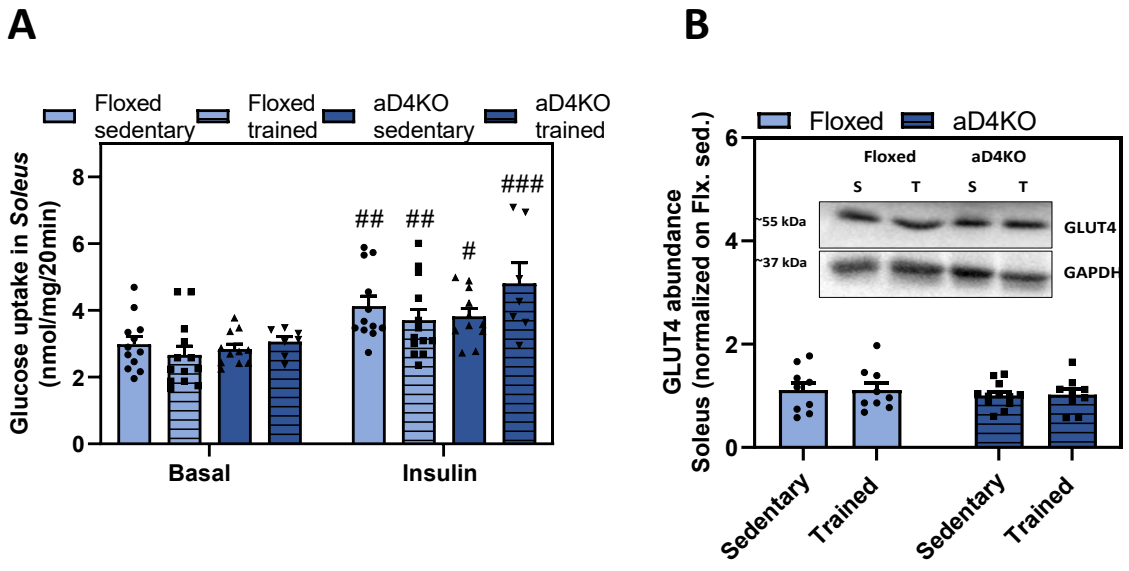

Figure 29: **Insulin-stimulated glucose uptake into *Soleus* muscle.** Insulin-stimulated glucose uptake into *Soleus* muscle (**A**). Data are shown as mean ± SEM (n=7-13). # P<0.05, ## P<0.01, ### P<0.001; Basal vs. Insulin, 2-way ANOVA with Sidak post-test; floxed sedentary vs. floxed trained vs. aD4KO sedentary vs. aD4KO trained, 2-way ANOVA with Tukey post-test. Outlier determined with GraphPad Grubb's outlier test. Western Blot quantification of GLUT4 (**B**) in sedentary and trained floxed and aD4KO mice. Protein abundance is normalized on GAPDH and given as ratio of sedentary floxed. Data are shown as mean ± SEM (n=9-12). Floxed vs. aD4KO, 2-way ANOVA with Sidak post-test; Sedentary vs. Trained, 2-way ANOVA with Sidak post-test. Light blue bars represent floxed control mice, whereas dark blue bars symbolize aD4KO animals. Additionally, striped bars demonstrate the trained status. S = sedentary, T = trained.

Insulin-stimulated glucose transport into primary white adipocytes was measured *ex vivo* with the help of [^{14}C]-D-glucose (2.2.2.11). Basal glucose uptake was unaltered between the genotypes and the training status (Figure 30A). In response to insulin, sedentary and trained floxed mice showed a significantly increased glucose transport. In comparison, sedentary aD4KO mice did not display an insulin response, furthermore, insulin-stimulated glucose uptake was significantly impaired compared to sedentary floxed animals. Unexpectedly, insulin-stimulated glucose uptake was still blunted in trained aD4KO animals. Further, glucose transport in trained aD4KO was significantly impaired compared to trained floxed mice. The blunted insulin-stimulated glucose uptake in aD4KO animals was accompanied by reduced GLUT4 protein abundance compared to floxed littermates (Figure 30B).

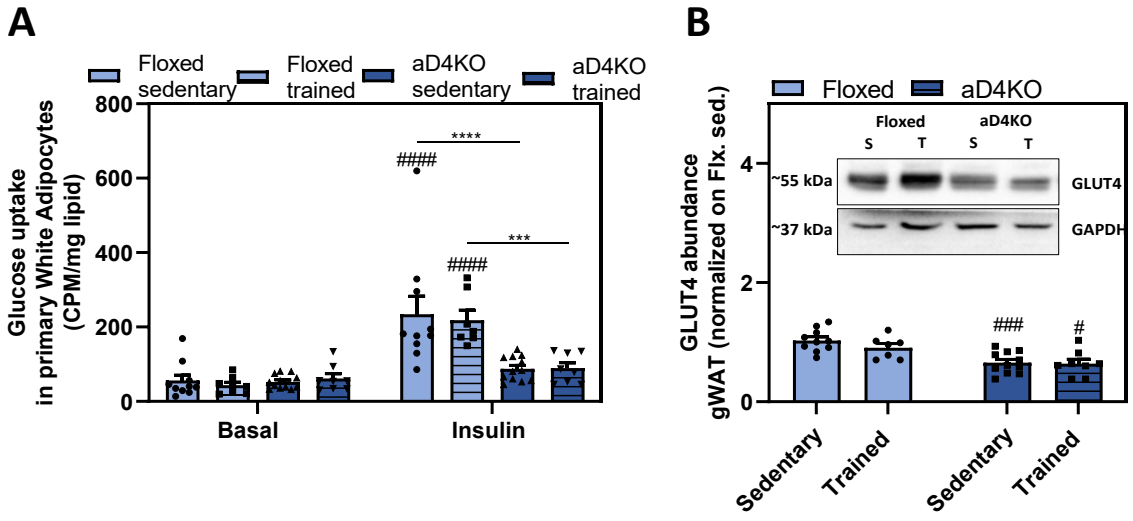

Figure 30: Insulin-stimulated glucose uptake into primary white adipocytes. Insulin-stimulated glucose uptake into primary white adipocytes (**A**). Data are shown as mean ± SEM (n=8-12). #### P<0.0001, Basal vs. Insulin, 2-way ANOVA with Sidak post-test; *** P<0.001, **** P<0.0001, floxed sedentary vs. floxed trained vs. aD4KO sedentary vs. aD4KO trained, 2-way ANOVA with Tukey post-test. Western Blot quantification of GLUT4 (**B**) in WAT of sedentary and trained floxed and aD4KO mice. Protein abundance is normalized on GAPDH and given as ratio of sedentary floxed. Data are shown as mean ± SEM (n=7-11). # P<0.05, ### P<0.001, floxed vs. aD4KO, 2-way ANOVA with Sidak post-test; sedentary vs. trained, 2-way ANOVA with Sidak post-test. Outlier were determined via GraphPad Grubb's outlier test. Light blue bars represent floxed control mice, whereas dark blue bars symbolize aD4KO animals. Additionally, striped bars indicate the trained status. S = sedentary, T = trained.

3.6 The impact of TBC1D4 knockout on the skeletal muscle transcriptome after chronic exercise intervention

The previously obtained results demonstrated that neither muscle-specific nor adipocyte-specific *Tbc1d4*-deficiency led to a full improvement in insulin-stimulated glucose uptake into primary white adipocytes after chronic exercise as demonstrated in the whole-body D4KO mice. These surprising results led to the assumption that *Tbc1d4*-deficient skeletal muscle secretes a factor in response to exercise that affects insulin sensitivity of *Tbc1d4*-deficient WAT. Therefore, an RNA sequencing approach (2.2.5.2) of *Gastrocnemius* muscle from sedentary and trained floxed and mD4KO mice, respectively was performed in order to gain further insights into the underlying cellular pathways.

3.6.1 Differentially regulated gene expression in *Tbc1d4*-deficient skeletal muscle after chronic exercise intervention

In order to elucidate which genes potentially play an important role in promoting insulin sensitivity in *Tbc1d4*-deficient mice, global gene expression of *Gastrocnemius* muscle was analyzed and visualized between sedentary and trained mD4KO mice and their corresponding floxed control animals (Figure 31). Outliers within the analyzed groups were identified with a Principal Component Analysis (PCA), which displays the variance (in percent) between samples in the same condition. Consequently, one sample in the sedentary mD4KO group was excluded from further analysis (Supplemental Figure 7). Comparing the different conditions in regard with genotype and training status, various differentially regulated genes were revealed (Figure 31A, $P < 0.05$). A comparable number of genes was differentially regulated due to the training intervention in both genotypes, with 475 genes in floxed control mice and 554 genes in mD4KO animals (Figure 31A). By comparing the genotypes, a smaller number of genes was differentially regulated at the sedentary state, with 760 differentially regulated transcripts (Figure 31A and C) and 1173 differentially regulated genes in the trained state between floxed and mD4KO mice (Figure 31A and D). The overlap of differentially regulated genes between floxed and mD4KO mice in the sedentary and trained state involves 158 genes (Figure 31B).

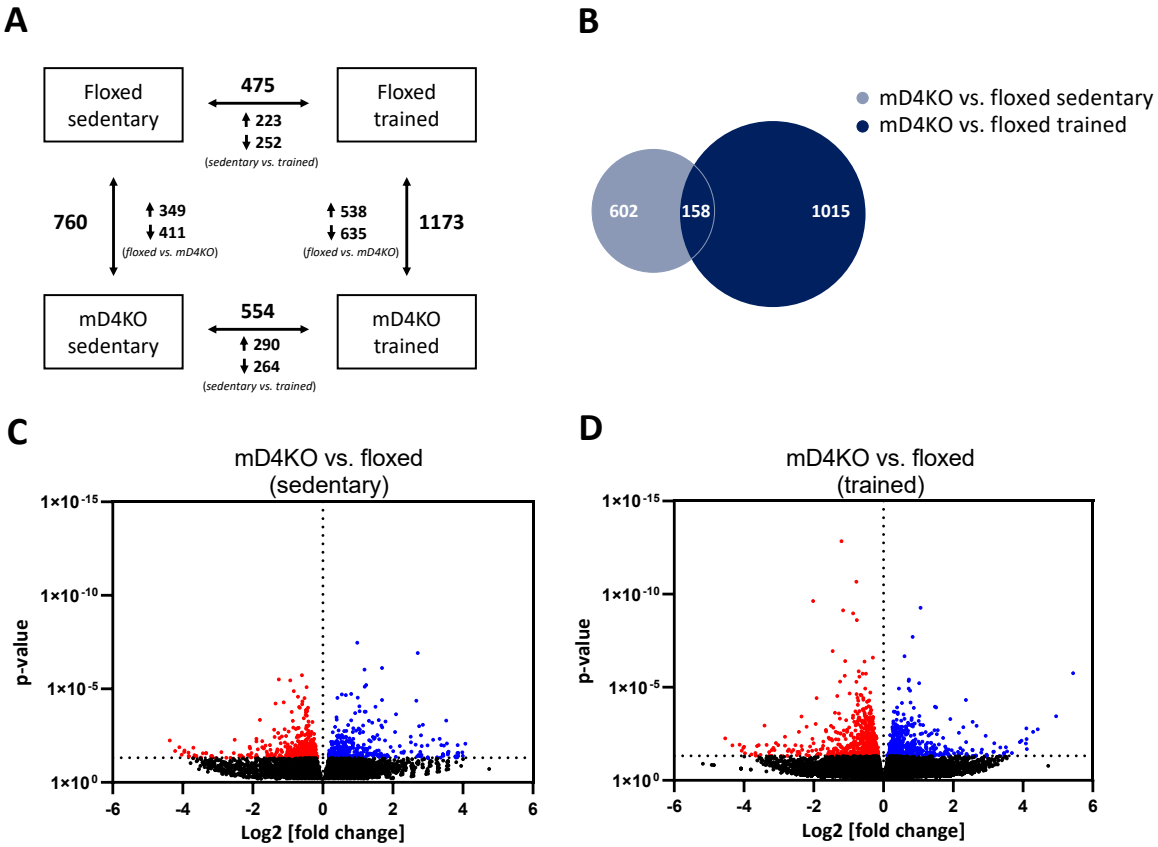

Figure 31: Differential gene expression in mD4KO and floxed mice in the sedentary and trained state. Skeletal muscle transcriptome of sedentary and trained floxed and mD4KO mice was analyzed using RNA Sequencing and subsequently tested for differential gene expression. Numbers of differentially expressed genes between the different experimental conditions (**A**). Overlap of differentially regulated genes due to the exercise training between the genotypes (**B**). Corresponding volcano plots displaying the size of differential regulation and size of significance (**C, D**). Significance threshold was set at $p < 0.05$ (n = 3-4).

After correction for multiple testing (adjusted p-value < 0.05), 15 genes were up- and 39 genes were downregulated in trained mD4KO compared to floxed littermates. The top 15 up- and downregulated genes are listed in Table 21 and Table 22, respectively. In order to further characterize the identified genes with regard to their cellular location, molecular function and biological process, respective gene ontology (GO) terms were included. Genes that are located within the extracellular space and/or are associated with intracellular transport, exocytosis and cell-cell signaling might be of special interest for further analysis, as these genes might be secreted itself or play a regulatory role in the processing of secreted factors. Thereby, they might alter the secretory profile of mD4KO mice after the chronic exercise training. Applying a filter regarding the cellular component, *Npnt* (Log2 Fold change = -1.155), *Angptl4* (Log2 Fold change = -1.111), *Glb1l2* (Log2 Fold change = -1.100) and *Apod* (Log2 Fold change = -0.722) were found to be in the extracellular space, matrix or region. In contrast, *Sytl2* (Log2 Fold change = 0.867), *Ccdc88c* (Log2 Fold change = 0.393) and *Arhgef17* (Log2 Fold change = 0.300) remained after filtering regarding “intracellular transport”, “exocytosis” and “cell-cell signaling”.

Interestingly, of these top regulated genes, only *Fgfbp1* (Log2 Fold change = -2.017) and *Adamts20* (Log2 Fold change = 0.774) displayed both criteria, as they were observed to be located in the extracellular space and associated with cell-cell signaling and signal transduction. Therefore, these two genes might be interesting target genes for further functional analysis.

Table 21: The 15 top downregulated genes in trained mD4KO compared to floxed littermates

Gene	Log2 Fold Change	Adj. P-value	GO term Cellular component	GO term Molecular function	GO term Biological process
Fgfbp1	-2.017	6.17E-07	Extracellular space	Growth factor binding	Cell-cell signaling, fibroblast growth factor signaling
Fos	-1.914	1.44E-02	Cytosol, nucleus	DNA binding, transcription factor	Skeletal muscle differentiation and proliferation
Dach2	-1.455	1.37E-04	Nucleus	DNA binding, transcription factor	Regulation of transcription
Cd28	-1.243	2.84E-03	Plasma membrane	Protein binding, protease binding	Immune response, T cell activation and proliferation
Tbc1d4	-1.200	7.45E-10	Cytosol	GTPase activator activity	Vesicle-mediated transport
Npnt	-1.155	1.44E-06	Extracellular matrix, plasma membrane	Integrin binding, calcium binding	Cell-cell adhesion, ECM organization
Angptl4	-1.111	1.74E-03	Extracellular space	Signaling receptor binding	Lipid metabolic process
Glb1l2	-1.100	3.59E-04	Extracellular region	Beta-galactosidase activity	Carbohydrate metabolic process
Odc1	-0.870	1.91E-06	Cytosol	Decarboxylase activity	Cell population proliferation
Cebpd	-0.805	4.73E-02	Nucleus	DNA binding, transcription factor	Regulation of cell differentiation
Slc40a1	-0.774	8.35E-08	Cytosol, plasma membrane	Metal ion binding, transmembrane transporter activity	Ion transport
Aldh1a1	-0.764	3.86E-06	Cytosol, nucleus	Dehydrogenase activity	Apoptotic process

Mafb	-0.740	1.44E-02	Nucleus	DNA binding, transcription factor	Regulation of transcription
Gfpt2	-0.735	2.75E-02	Cytosol	Transaminase activity, carbohydrate derivate binding	Energy reserve metabolic process
Apod	-0.722	1.80E-02	Cytoplasm, extracellular space	Cholesterol binding	Lipid transport

Table 22: The 15 top upregulated genes in trained mD4KO compared to floxed littermates.

Gene	Log2 Fold Change	Adj. P-value	GO term Cellular component	GO term Molecular function	GO term Biological process
Atp1a4	1.507	3.44E-02	Plasma membrane	ATP binding, ATP hydrolysis activity	Cellular ion homeostasis
Catsperg1	1.475	3. 33E-02	Motile cilium	Cell differentiation	-
Chrna1	1.061	1.22E-06	Plasma membrane, synapse	Acetylcholine binding	Signal transduction, skeletal muscle contraction
Sytl2	0.867	3.46E-02	Cytoplasm, plasma membrane	Small GTPase binding	Exocytosis, intracellular protein transport
Cited4	0.837	2.57E-05	Cytoplasm, nucleus	Transcription coactivator activity	Response to estrogen, DNA transcription
Adamts20	0.774	2.09E-02	Extracellular space	Endopeptidase activity	Signal transduction, ECM organization
Mpp3	0.764	7.13E-03	Plasma membrane	PDZ domain binding	-
Lrtm1	0.730	2.38E-03	Plasma membrane	Heparin binding	Negative chemotaxis, synapse assembly
Map3k7cl	0.726	5.81E-03	Cytosol, nucleus	-	-

Tspan13	0.601	2.44E-04	Plasma membrane	Calcium channel regulatory activity	Regulation of calcium ion transmembrane transport
Klhl40	0.533	2.19E-02	Cytoplasm	-	Skeletal muscle development
Rps6kc1	0.443	5.81E-03	Endosome, lysosome	ATP binding, protein serine kinase activity	Protein phosphorylation
Ccdc88c	0.393	3.44E-02	Cytoplasm	G-protein binding	Small GTPase mediated signal transduction
Pdlim3	0.330	4.88E-02	Cytosol	Actin binding	Muscle structure development
Arhgef17	0.300	4.86E-02	Cytosol	Guanyl-nucleotide exchange factor activity	Actin cytoskeleton organization, regulation of small GTPase mediated signal transduction

3.6.2 ConsensusPathDB enrichment analysis of *Tbc1d4*-deficient skeletal muscle after chronic exercise intervention

A gene set over-representation analysis using the tool "ConsensusPathDB" (CPDB) (Herwig et al., 2016) was performed across multiple publicly available databases and repositories (e.g. KEGG and Reactome), with the aim to elucidate canonical pathways that were exclusively over-represented in trained mD4KO animals compared to their trained floxed controls. Therefore, pathways that were already described in trained vs. sedentary floxed, trained vs. sedentary mD4KO and sedentary mD4KO vs. sedentary floxed were excluded (Supplemental Figure 9). Differentially expressed genes below a significance threshold of $p < 0.01$ were introduced into the overrepresentation analysis. The analysis revealed 11 pathways exclusively over-represented in trained mD4KO compared to trained floxed animals (adjusted p-value < 0.01) (Table 23). Table 23 is divided into the respective pathway name and underlying database. Furthermore, adjusted p-value and annotated pathway size are depicted, as well as the amount of containing candidate genes within the pathway. Among the enriched signaling pathways were the "Adipocytokine signaling pathway" (adj. p-value = 0.00235), the "PPAR signaling pathway" (adj. p-value = 0.0065) and the "Thermogenesis pathway" (adj. p-value = 0.00744).

Table 23: CPDB enrichment analysis floxed trained vs. mD4KO trained

Pathway	Database	Adj. p-value	Pathway size	Candidates contained (%)
Arrhythmogenic right ventricular cardiomyopathy	KEGG	3.78E-04	77	10 (12.99 %)
Dilated cardiomyopathy	KEGG	6.01E-04	94	10 (10.64 %)
Intracellular metabolism of fatty acids regulates insulin secretion	Reactome	6.01E-04	3	3 (100.00 %)
Metabolism	Reactome	2.33E-03	1702	52 (3.06 %)
Adipocytokine signaling pathway	KEGG	2.35E-03	71	8 (11.27 %)
Arginine and proline metabolism	KEGG	2.54E-03	54	7 (12.96 %)
Metabolism of polyamines	Reactome	3.22E-03	13	4 (30.77 %)
Diabetic cardiomyopathy	KEGG	4.19E-03	211	13 (6.16 %)
Cardiac muscle contraction	KEGG	6.09E-03	87	8 (9.20 %)
PPAR signaling pathway	KEGG	6.50E-03	89	8 (8.99 %)
Thermogenesis	KEGG	7.44E-03	230	13 (5.65 %)

3.6.3 Predicted upstream regulators of *Tbc1d4*-deficient skeletal muscle after a chronic exercise intervention

In order to identify potential upstream regulators involved in differential gene expression in trained mD4KO compared to their floxed littermates, an expression analysis was conducted using Ingenuity Pathway Analysis (IPA) (2.2.5.2). In total, 448 upstream regulators with a p-value < 0.01 were predicted to be affected in trained mD4KO compared to their floxed controls. Thereof, 39 upstream regulators were predicted to be inhibited, whereas nine upstream regulators were predicted to be activated (Z-Score > |2|). No prediction regarding their activation state could have been made for 400 of the affected upstream regulators. Figure 33A summarizes the 15 most significant (predicted) inhibited upstream regulators. Of these, the most inhibited upstream regulator was STAT3 (Z-Score = -3.285), followed by TCF7L2 (Z-Score = -3.046) and LIF (Z-Score = -2.882). In comparison, the predicted activated upstream regulators are displayed in Figure 33B. Here, the most predicted activated upstream

regulator was SIRT3 (Z-Score = 2.635), followed by APOE (Z-Score = 2.573) and TSC2 (Z-Score = 2.333). All predicted upstream regulators are listed in the supplement (Supplemental Table 2-5).

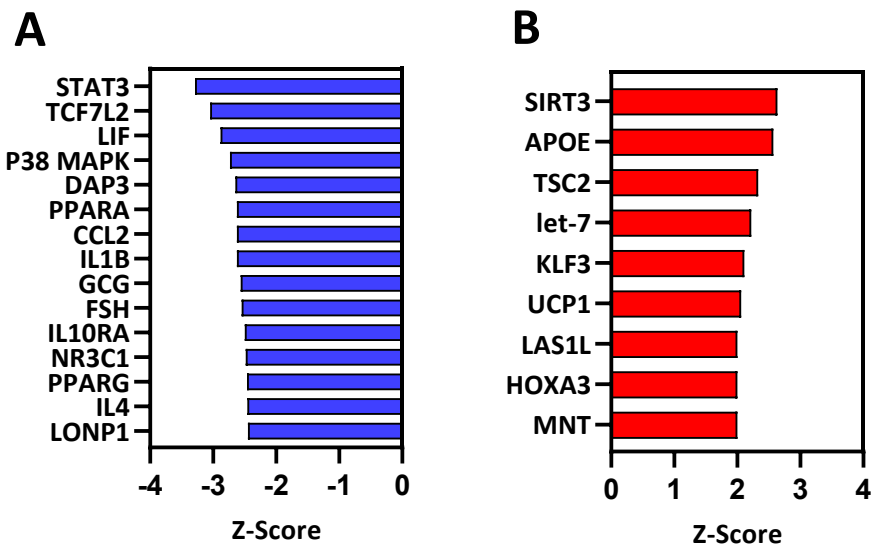

Figure 32: Predicted Upstream regulators. Predicted activated (**A**) and inhibited (**B**) upstream regulators in trained mD4KO mice compared to trained floxed controls.

3.6.4 Predicted molecular functions and diseases of *Tbc1d4*-deficient skeletal muscle after chronic exercise intervention

Next to the canonical pathways and upstream regulators, further over-representation analysis of diseases and molecular function were assessed using IPA. Based on this analysis molecular functions and diseases were identified that were affected in trained mD4KO compared to floxed littermates. Table 24 summarizes the 15 most significant predicted and inhibited and activated molecular functions in trained mD4KO mice compared to respective floxed littermates. Trained mD4KO mice displayed a predicted inhibited activity regarding “Organismal Development” (Z-Score = -2.401), “Gene expression” (Z-Score = -2.165) and “Molecular Transport” (Z-Score = 2.117) in contrast to the floxed controls. In comparison, “Organismal Survival” (Z-Score = 3.05) showed a predicted activation in trained mD4KO animals. A table with all significant annotated molecular functions and diseases is listed in the supplement (Supplemental Table 6-9).

Table 24: Predicted molecular functions

Diseases or Functions Annotation	Activation Z-score	p-value
Organismal Development	-2,401	2,10E-06
Embryonic Development,Organismal Development	-2,401	3,46E-06
Cell-To-Cell Signaling and Interaction,Cellular Assembly and Organization	-2,226	6,02E-06
Lipid Metabolism,Small Molecule Biochemistry	-2,54	1,50E-04
Carbohydrate Metabolism,Molecular Transport,Small Molecule Biochemistry	-2,201	2,60E-04
Lipid Metabolism,Small Molecule Biochemistry,Vitamin and Mineral Metabolism	-2,651	3,68E-04
Molecular Transport	-2,117	3,90E-04
Cellular Assembly and Organization,Cellular Function and Maintenance	-2,471	5,20E-04
Organismal Survival	3.05	6.54E-07

In conclusion, the present study shows that in contrast to the whole-body knockout, tissue-specific TBC1D4 ablation in skeletal muscle or adipose tissue alone did not lead to pronounced improvements in WAT after a chronic exercise intervention (Figure 33). While mD4KO mice displayed an impaired glucose transport and reduced GLUT4 abundance in skeletal muscle, aD4KO mice exhibited impairments in glucose uptake exclusively in the WAT. Both tissue-specific knockout mouse lines were characterized by postprandial hyperglycemia, but only mD4KO animals had improved postprandial glycemia in response to chronic exercise. However, aD4KO mice were glucose intolerant, which was restored after the training intervention. Therefore, both tissues in concordance might be responsible for the exercise-mediated improvements observed in trained whole-body D4KO mice. Furthermore, it is hypothesized that the *Tbc1d4*-deficient skeletal muscle secretes in response to chronic exercise a factor that affects insulin sensitivity of *Tbc1d4*-deficient WAT. The conducted transcriptome analysis in *Tbc1d4*-deficient skeletal muscle revealed that the TBC1D4 ablation, in concordance with chronic exercise, is associated with impairments in skeletal muscle development and lipid metabolism. Both physiological alterations could lead to changes in the secretory profile of *Tbc1d4*-deficient skeletal muscle, thereby further affecting insulin sensitivity of *Tbc1d4*-deficient WAT.

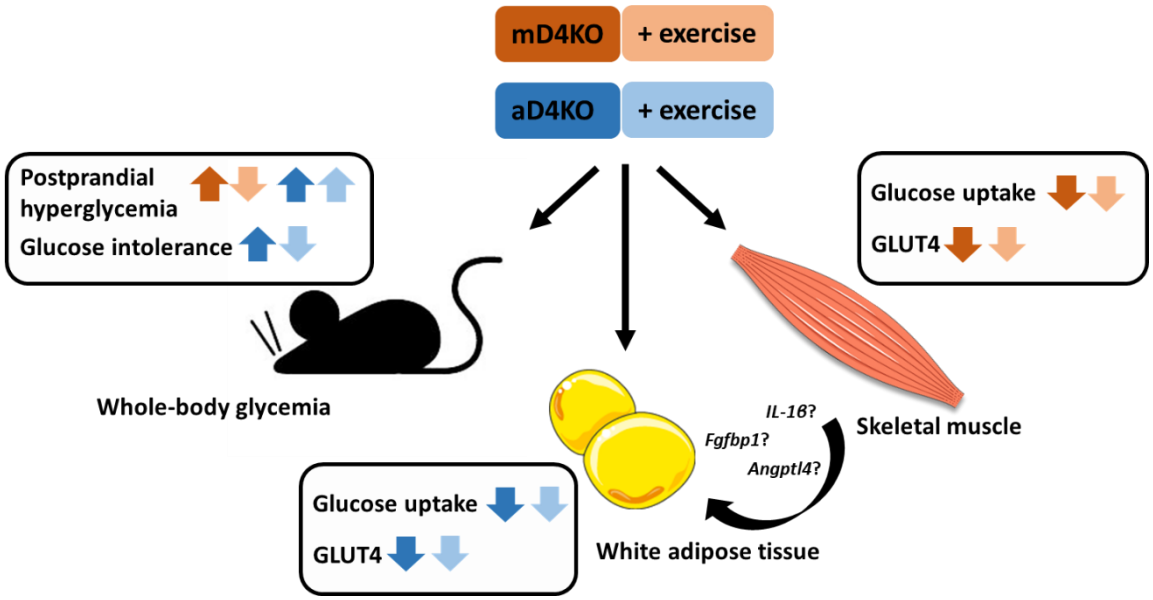

Figure 33: Key findings in tissue-specific *Tbc1d4*-deficient mice after chronic exercise training. mD4KO animals (orange arrows) display an impaired insulin-stimulated glucose uptake into oxidative skeletal muscle fibers, attributed due to a reduced GLUT4 protein abundance. However, chronic exercise intervention in these animals (light orange arrows) did not rescue glucose uptake into skeletal muscle or WAT. Furthermore, mD4KO mice exhibit postprandial hyperglycemia, which was restored after the chronic exercise training. The performed transcriptome analysis indicates that the *Tbc1d4*-deficient skeletal muscle might secrete in response to chronic exercise specific factors (*Fgfbp1*, *Il-1β*, *Angptl4*) that could further positively affect insulin sensitivity of *Tbc1d4*-deficient white adipocytes. In comparison, glucose uptake into primary white adipocytes was impaired in aD4KO mice (blue arrows), accompanied by reduced GLUT4 protein abundance. However, chronic exercise failed to rescue glucose transport and GLUT4 abundance in these animals (light blue arrows). Additionally, adipocyte-specific *Tbc1d4*-deficiency results in postprandial hyperglycemia and glucose intolerance, but only the latter one was rescued after chronic exercise. Modified from Springer 2018.

4 Discussion

Recently, a loss-of-function variant in the human *TBC1D4* gene (p.Arg684Ter) was identified in the indigenous Greenlandic population that confers *TBC1D4* deficiency specifically in skeletal muscle. Homozygous p.Arg684Ter allele carriers exhibit postprandial hyperglycemia and an increased risk to develop T2DM (Moltke et al., 2014). Whole-body *Tbc1d4*-deficient (D4KO) mice reflect the human phenotype in demonstrating postprandial hyperglycemia, caused by impaired insulin-stimulated glucose uptake into skeletal muscle and white adipose tissue (WAT), accompanied by reduced GLUT4 protein abundance (Chadt et al., 2015, de Wendt et al., 2021). Regular exercise training results in enhanced insulin-stimulated glucose uptake and a restored GLUT4 abundance into primary white adipocytes but not skeletal muscle (Springer PhD thesis, 2018). This project aims to elucidate the specific contribution of skeletal muscle and WAT to the observed exercise-mediated improvements in whole-body glycemia of D4KO mice. The present study indicates that both, skeletal muscle and WAT, in concordance are responsible for the TBC1D4-dependent improvements in whole-body glycemia in the trained state. We hypothesize that specific alterations in the secretory profile of *Tbc1d4*-deficient skeletal muscle after exercise training bridges the gap to *Tbc1d4*-deficient WAT, conferring enhanced insulin sensitivity in the latter.

4.1 Skeletal muscle-specific *Tbc1d4*-deficiency resembles in part whole-body TBC1D4 ablation after chronic exercise

4.1.1 Postprandial hyperglycemia in mD4KO mice is rescued after chronic exercise intervention

The current study shows that muscle-specific *Tbc1d4*-deficiency led to pronounced postprandial hyperglycemia. Thereby, mD4KO mice resemble homozygous allele carriers of a *TBC1D4* loss-of-function variant and whole-body D4KO mice (Moltke et al., 2014, de Wendt et al., 2021). Another study also demonstrated the significant contribution of skeletal muscle TBC1D4 in maintaining postprandial glycemia (Xie et al., 2016). However, Yang *et al.* provided evidence that the p.Arg684Ter mutation in *Tbc1d4* does not specifically account for impairments in the glycemic control in mice (Yang et al., 2021). They showed that a TBC1D4^{R691X} mutation (this residue is orthologous to human TBC1D4^{Arg684}) in mice, which selectively affects the long TBC1D4 variant, results in normal postprandial blood glucose levels (Yang et al., 2021). This might be due to alternative splicing in *Tbc1d4* that induces the expression of the short TBC1D4 isoform in skeletal muscle, which is usually expressed in WAT. As a consequence of

this compensatory response, TBC1D4^{R691X} mice displayed physiological protein levels of TBC1D4 and GLUT4, thereby maintaining normal postprandial glycemia (Yang et al., 2021). However, this compensation might be species dependent, as no compensatory expression of the short TBC1D4 isoform was observed in skeletal muscle of rats expressing a TBC1D4^{R693X} mutation (this residue is orthologous to murine TBC1D4^{R691X}). Thereby, TBC1D4^{R693X} knockin rats displayed postprandial hyperglycemia and decreased TBC1D4 and GLUT4 protein abundances (Yang et al., 2021).

Importantly, homozygous p.Arg684Ter allele carriers improved their postprandial blood glucose levels after a voluntary exercise intervention (Schnurr et al., 2021). These data implicate that already a moderate daily physical activity leads to pronounced improvements in whole-body glycemia, at least in homozygous allele carriers of a *TBC1D4* nonsense variant. Likewise, mD4KO mice displayed a similar response to the chronic exercise training. The initially observed postprandial hyperglycemia in mD4KO animals was rescued after the chronic exercise intervention. These data support the assumption that the benefit of physical activity on lowering postprandial blood glucose levels might be mediated via a TBC1D4-independent muscle-specific pathway and/or tissue crosstalk from skeletal muscle to other tissues with an intact TBC1D4 signaling (Schnurr et al., 2021).

4.1.2 Insulin-stimulated glucose uptake into oxidative skeletal muscle and WAT is not restored in mD4KO mice after chronic exercise

Similar to whole-body D4KO mice, insulin-stimulated glucose transport was reduced in *Soleus* muscle of mD4KO mice, accompanied by lower GLUT4 protein abundance. There is evidence that the inactivation of TBC1D4 promotes lysosomal degradation of GLUT4 (Xie et al., 2016). Likely the loss of the RabGAP function is responsible for the increased GLUT4 degradation in D4KO mice, since mice carrying a RabGAP-inactive TBC1D4^{R917K} mutant phenocopy D4KO animals (Xie et al., 2016). In contrast, glucose uptake into primary white adipocytes remained unaltered in mD4KO mice, presumably due to the intact TBC1D4 signaling in that tissue.

Interestingly, whole-body *Tbc1d4*-deficiency is associated with an exercise-mediated improved insulin-stimulated glucose uptake into *Soleus* muscle. However, glucose transport was not completely restored to WT levels (Springer PhD thesis, 2018). The trained female mD4KO cohort displayed a similar phenotype, demonstrated by an enhanced glucose transport. However, GLUT4 protein abundance was not increased in trained female mD4KO mice. Exercise training is known to be the most potent stimulus to increase skeletal muscle GLUT4 expression in humans and rodents (Richter and Hargreaves, 2013). Thus, already a single exercise bout in rats increased GLUT4 transcription and protein expression (Kuo

et al., 1999, Neufer and Dohm, 1993). Likewise chronic exercise training has been shown to enhance GLUT4 expression in skeletal muscle (Kim et al., 2004, Langfort et al., 2003). However, many different variables like the species, exercise mode, exercise intensity and duration and the diet might have an influence on exercise-induced effects on GLUT4 expression. Thus, not all studies observed an exercise-induced increased GLUT4 expression (Funai et al., 2009, Hansen et al., 1998, Steensberg et al., 2002). Another study suggested only high-intensity running capacity leads to an increased GLUT4 protein abundance in rats (Stephenson et al., 2013). Accordingly, the performed moderate treadmill exercise training in the present thesis might be not sufficient to induce an enhancement in GLUT4 abundance. Therefore, an increased exercise intensity or duration might increase the abundance of this glucose transporter. Noteworthy, Gurley and colleagues reported that restored GLUT4 levels after voluntary running was rather a posttranscriptional mechanism (Gurley et al., 2016). Thus, not the increased transcription, but enhanced translocation of intracellular GLUT4 storage vesicles to the plasma membrane might explain the improved glucose uptake in female mD4KO mice. Since only total GLUT4 protein abundance was measured in the present study, it was not distinguished between the amount of intracellular and plasma membrane-bound GLUT4, which could be an approach for further investigations.

Findings from our lab showed that chronic exercise on treadmills rescues insulin-stimulated glucose uptake into primary white adipocytes of D4KO animals, concomitant by an increased GLUT4 abundance (Springer PhD thesis, 2018). Since TBC1D4 is highly abundant in skeletal muscle and WAT, both tissues could contribute to this exercise-mediated improvement. Therefore, the individual contribution of skeletal muscle on adipose tissue insulin sensitivity was examined. Skeletal muscle contraction *per se* contributes to many exercise-mediated improvements, for instance through crosstalk with other organs (e.g. adipose tissue), mediated by the secretion of specific factors (Pedersen and Febbraio, 2008, Pedersen and Febbraio, 2012). We speculated that the secretory profile of skeletal muscle is altered due to the TBC1D4 ablation, thereby presumably inducing improvements in adipose tissue insulin sensitivity. However, the results of this thesis depict that glucose transport into primary white adipocytes was not affected by the skeletal muscle-specific TBC1D4 ablation in response to chronic exercise. Thus, the TBC1D4 depletion in skeletal muscle may be excluded as potential mediator of exercise-induced improvements in adipose tissue of whole-body D4KO mice.

4.1.3 Muscle-specific *Tbc1d4*-deficiency is not sufficient to induce glucose intolerance

The contribution of TBC1D4 on whole-body glucose tolerance is still not yet fully elucidated. Some studies have shown that female but not male whole-body D4KO mice display an impaired glucose

tolerance (Chadt et al., 2015, Wang et al., 2013, Lansey et al., 2012). Also an additional HFD challenge did not lead to remarkable impairments in the glucose tolerance in male D4KO mice (Springer PhD thesis, 2018). Previous investigations from our lab showed that only the additional ablation of the remaining RabGAP TBC1D1 led to reductions in glucose disposal (Chadt et al., 2015). In line with these results, the present study shows that the TBC1D4 knockout exclusively in skeletal muscle does not impair glucose tolerance. In contrast, Xie and colleagues demonstrated that muscle-specific *Tbc1d4*-deficiency led to pronounced impairments in glucose tolerance, suggesting skeletal muscle TBC1D4 is a significant contributor in whole-body glucose homeostasis (Xie et al., 2016). Of note, muscle-specific *Tbc1d4*-deficiency was achieved with the Cre/LoxP technology, using a Myf5 promoter to control Cre recombinase (Xie et al., 2016). *Myf5* is a myogenic regulatory factor that is expressed in the early phase of somite development and is restricted to the forming myotome (Tallquist et al., 2000). In the current project, Cre recombinase was under the control of an human skeletal actin promoter that is present in the myotome region of somites (Miniou et al., 1999). We speculate that TBC1D4 has already an important function during the early phases of skeletal muscle development. In the study of Xie *et al.*, TBC1D4 was already ablated in an earlier phase of myogenesis, due to the use of a Myf5 promotor (Xie et al., 2016). This early skeletal muscle TBC1D4 ablation might has affected glucose homeostasis in the adult state, indicating that a TBC1D4 knockout should rather be induced at a later time point, in order to avoid potential developmental impairments.

4.2 Adipose tissue-specific TBC1D4 ablation leads to impaired whole-body glycemia

4.2.1 *Tbc1d4*-deficiency in adipose tissue results in glucose intolerance that is restored after chronic exercise

The present study demonstrates for the first time that *Tbc1d4*-deficiency in adipose tissue leads to an impaired systemic glucose tolerance. This indicates that TBC1D4 in adipose tissue has a greater impact on whole-body glycemia than in skeletal muscle, as glucose tolerance remained unaltered in mD4KO mice. Although adipose tissue only accounts for less than 10 % of whole-body glucose uptake, it significantly mediates whole-body glucose homeostasis. Adipose tissue-specific GLUT4 knockout mice were characterized with glucose intolerance and insulin resistance. Furthermore, individual animals developed severe insulin resistance and a diabetes phenotype (Minokoshi et al., 2003, Abel et al., 2001). Abel and colleagues suggested that an inter-organ crosstalk between adipose tissue and skeletal muscle mediates this phenotype, as *in vivo* glucose uptake into skeletal muscle is markedly impaired

in adipose tissue-specific GLUT4 knockout mice (Abel et al., 2001). In contrast, skeletal muscle-specific GLUT4 depletion resulted in an unaltered skeletal muscle glucose uptake and a normal glucose tolerance, further emphasizing the important role of adipose tissue regulating whole-body glucose uptake (Fam et al., 2012).

For the first time in this study, aD4KO mice were placed on a chronic exercise intervention on treadmills. In response to the chronic exercise training, glucose intolerance in aD4KO mice was rescued. These results suggest that exercise-induced improvements in whole-body glycemia are attributed to the TBC1D4 ablation in adipose tissue, presumably mediated via a TBC1D4-independent signaling. Adipose tissue exerts a 'browning' ability, thereby inducing exercise-mediated improvements in whole-body glycemia (Scheel et al., 2022). For instance, scWAT browning after endurance exercise is associated with improvements in whole-body glycemia (Bostrom et al., 2012, Stanford et al., 2015). Interestingly, trained D4KO mice displayed a greater browning capacity in scWAT compared to WT animals. In fact, an increased mRNA expression of the browning markers *Ucp1*, *Cidea*, *Cox8b* and *P2rx5* were exclusively observed in trained D4KO mice, whereas WT animals showed increased *Ppargc1a* expression only (Springer PhD thesis, 2018). During or after acute and/or endurance exercise, WAT is secreting specific exerkines, which in turn improve whole-body glycemia (Rodriguez et al., 2020, Chow et al., 2022). Accordingly, adipose tissue derived exerkine transforming growth factor-β_2 (TGF-β_2) is associated with improvements in glucose tolerance, lipid oxidation and a possible reduction of adipose tissue inflammation (Takahashi et al., 2019). Moreover, the adipose tissue-released exerkine beta-aminoisobutyric acid significantly improves glucose tolerance in mice due to enhanced WAT browning trough a PPARα-mediated mechanism (Roberts et al., 2014). These data support the assumption that *Tbc1d4*-deficient adipose tissue may release a known or yet unknown adipokine during or after exercise that improves whole-body glucose tolerance.

4.2.2 Postprandial hyperglycemia in aD4KO mice is not rescued after chronic exercise training

aD4KO mice display postprandial hyperglycemia, however to a smaller extent than whole-body D4KO mice. We conclude that both, skeletal muscle and adipose tissue in concordance are responsible for the severe postprandial hyperglycemia observed in whole-body D4KO mice. Interestingly, a recent study did not observe increased postprandial blood glucose level in aD4KO mice (Xie et al., 2016). Xie and colleagues concluded that TBC1D4 in skeletal muscle is the main contributor in promoting postprandial hyperglycemia (Xie et al., 2016). However, this rather mild impact of adipose tissue-

specific *Tbc1d4*-deficiency on postprandial blood glucose levels might be the consequence of a small sample size (n=4) that was chosen in the study from Xie *et al*.

In response to the chronic exercise intervention, aD4KO mice still displayed postprandial hyperglycemia. This result indicates that exercise-mediated improvements in postprandial blood glucose levels are attributed to the TBC1D4 ablation specifically in skeletal muscle. A recent study demonstrated that voluntary regular activity improves postprandial blood glucose levels particularly in humans exhibiting a skeletal muscle-specific TBC1D4 ablation. In contrast, non-carriers or heterozygous carriers of this loss-of-function mutation displayed unaltered blood glucose levels (Schnurr et al., 2021). These data suggest that improvements in postprandial glycemia can be mediated via a pathway independent from skeletal muscle TBC1D4. However, the underlying mechanisms remain to be elucidated, but do point towards an inter-organ crosstalk from skeletal muscle to adipose tissue.

4.2.3 Chronic exercise intervention did not rescue impaired insulin-stimulated glucose uptake in aD4KO mice

The present study demonstrated impairments in adipose tissue glucose transport in aD4KO mice, with a simultaneous reduction in the GLUT4 abundance. In contrast, glucose uptake in the *Soleus* muscle remained unaltered due to the intact TBC1D4 signaling in skeletal muscle.

The chronic exercise intervention did not enhance insulin-stimulated glucose uptake in *Tbc1d4*-deficient primary white adipocytes. Thus, aD4KO mice do not reflect whole-body D4KO mice, where a chronic exercise intervention rescued the impaired glucose uptake into WAT (Springer PhD thesis, 2018). Consequently, the adipose tissue-specific TBC1D4 ablation is not responsible for improvements in insulin sensitivity after chronic exercise in whole-body D4KO mice. Further, our data are pointing toward a TBC1D4-independent tissue crosstalk between skeletal muscle and adipose tissue or a tissue crosstalk from skeletal muscle/adipose tissue to other tissues with an intact TBC1D4 signaling pathway, for instance the liver. Likewise, the liver contributes to the TBC1D4 knockout phenotype. Whole-body *Tbc1d4*-deficiency is associated with increased hepatic gluconeogenesis, indicated by pyruvate intolerance and increased expression of PEPCK, a key enzyme in gluconeogenesis (Wang et al., 2013). Furthermore, the liver secretes specific factors (hepatokines) in response to acute and chronic exercise, which in turn regulate metabolic pathways and inter-organ crosstalk (Priest and Tontonoz, 2019). Therefore, hepatokines might also be partially responsible for preventing or reverting obesity-associated metabolic dysfunction in target organs (Gonzalez-Gil and Elizondo-Montemayor, 2020).

Recent investigations have shown that the exercise-released hepatokine Angiopoietin-like protein 4 (ANGPTL4) may influence WAT and skeletal muscle metabolism to favor redistribution of lipid-derived metabolic fuel towards catabolic pathways (Weigert et al., 2019). We speculate that tissue-specific TBC1D4 depletion in either skeletal muscle or adipose tissue is not sufficient to induce the exercise-induced insulin-sensitizing effect in D4KO mice. Perhaps other organa (e.g. liver) are involved in exercise-induced improvements in RabGAP-deficient mice. However, it is also possible that a combined TBC1D4 ablation in skeletal muscle and adipose tissue is necessary, in order to improve insulin sensitivity in the latter one after chronic exercise. We hypothesize that *Tbc1d4*-deficient skeletal muscle might secrete a factor in response to chronic exercise that affects *Tbc1d4*-deficient WAT, thereby improving its insulin sensitivity.

TBC1D4 is mainly associated for regulating vesicle trafficking processes through its GAP activity towards several RabGTPases (e.g. Rab8a, Rab14) (Mafakheri et al., 2018). However, there is evidence that members of the TBC family not only regulate vesicle trafficking, but also the secretion of cargos. For instance, TBC1D4 regulates together with Rab14 the secretion of vesicles containing major histocompatibility complex class I molecules in macrophages (Weimershaus et al., 2018). Moreover exocytosis and secretion of matrix metalloproteinase 14 (MMP14) in cardiac muscle fibers is regulated by a subset of Rab proteins, including Rab5a, Rab8 and Rab14 (Bravo-Cordero et al., 2007, Wiesner et al., 2013). Thus, the impaired expression of MMPs and the altered ratio of MMPs and their corresponding inhibitors (TIMPs) might explain the marked increased cardiac ECM area in D4KO mice after ischemia/reperfusion events (Binsch et al., 2023). Furthermore, the TBC family members TBC1D10A and TBC1D10C regulate exosome secretion in oligodendrocytes via the RabGTPase Rab35, possibly by controlling the docking/tethering of endocytic vesicles with the plasma membrane. Thereby, oligodendrocytes secrete vesicles into the extracellular space, where they might play a role in neuron-glia communication (Hsu et al., 2010). Additionally, the catalytically inactive RabGAP TBC1D23 was identified as a vesicle-golgin adaptor GAP, required for endosome-to-Golgi trafficking (Shin et al., 2017, Navarro Negredo et al., 2018). The GAP domain of TBC1D23 binds to a conserved motif at the tip of golgin-245 and golgin-97 at the trans-Golgi, while the C-terminus binds to the WASH complex on endosome-derived vesicles. Thereby, TBC1D23 represents the link between trans-Golgi-network (TGN) golgins and endosome-derived vesicles (Shin et al., 2017). Interestingly, mutations of key residues of TBC1D23 lead to a dysregulated endosomal vesicle trafficking that contributes to pontocerebellar hypoplasia (Huang et al., 2019), further emphasizing the importance of an intact RabGAP signaling in vesicle trafficking. These data support the assumption that RabGAPs might regulate the secretion of specific factors by controlling docking/tethering of endocytic vesicles with

the plasma membrane in a RabGTPase-depending manner, and/or regulating vesicle trafficking during endosome-to-Golgi network.

4.3 Skeletal muscle-specific *Tbc1d4*-deficiency alters the skeletal muscle transcriptome in response to chronic exercise

The obtained *in vivo* measurements in the present thesis support the assumption of a so-far unrecognized exercise-stimulated tissue crosstalk between skeletal muscle and adipose tissue due to the *Tbc1d4*-deficiency. In order to investigate how skeletal muscle adapts to the *Tbc1d4*-deficiency with and without chronic exercise, and to identify potential factors enabling organ crosstalk, a RNA sequencing approach of trained and sedentary *Gastrocnemius* muscles of mD4KO mice and floxed controls was performed. Under the assumption that skeletal muscle *Tbc1d4*-deficiency alters organ crosstalk, differentially regulated genes were filtered regarding the GO terms cellular component, molecular function and biological processes. We assume that *Tbc1d4*-deficiency alters the expression of genes that are localized at endosomes, the trans-Golgi-network (TGN), the plasma membrane or the extracellular matrix. Furthermore, we assume that potential target genes are associated with exocytosis, signal transduction, intracellular protein transport, and small GTPase binding. Therefore, genes that cover one or more of these defined categories, will be further investigated in the following sections.

4.3.1 Deficiency of *Tbc1d4* is associated with impaired skeletal muscle development and differentiation

The obtained transcriptome results indicate that the *Tbc1d4*-deficiency in skeletal muscle *per se* is associated with impaired developmental processes, indicated by predicted inhibited tissue development, organismal development, cellular growth and proliferation. Previously, the closely related RabGAP TBC1D1 was rather associated with skeletal muscle development (Fontanesi et al., 2011). In contrast, TBC1D4 was related to muscle growth, due to its enhanced signaling upon the inactivation of the negative muscle growth and development regulator myostatin (Kocsis et al., 2017). However, the causal contribution of TBC1D4 in skeletal muscle development still needs to be elucidated, as it might be that the enhanced RabGAP signaling primarily supports the altered energy substrate metabolism of the growing muscle (Espelage et al., 2020). This assumption is further supported by a previous study showing that an impaired muscle stem cell differentiation in VPS39-

deficient mice is associated with a decreased insulin-stimulated TBC1D4 phosphorylation and a concomitant reduced glucose uptake (Davegardh et al., 2021).

Likewise in response to chronic exercise, the organismal development, cellular function and maintenance were predicted to be inhibited in mD4KO mice. Skeletal muscle possesses a remarkable regeneration capacity in response to tissue damage, for instance caused by exercise (Motohashi and Asakura, 2014, Almada et al., 2021). Within this process, satellite cells (SCs) cover an important role, as they are activated upon skeletal muscle regeneration, thereby giving rise to myogenic precursors (Motohashi and Asakura, 2014). After several rounds of proliferation and differentiation, most of these myogenic precursors form new muscle fibers (Motohashi and Asakura, 2014). Based on the transcriptome results in this thesis, it appears that the early SC activation, needed for efficient regenerative myogenesis, is impaired due to the TBC1D4 ablation in response to chronic exercise. This assumption is indicated by a significantly reduced expression level of the transcription factor *Fos*. Its activation is the earliest known transcriptional event of adult muscle stem cell activation. Moreover, the immediate and transient activity of *Fos* is required for muscle fibers regeneration after exercise-induced injury (Almada et al., 2021). Furthermore, this thesis provided evidence that the NAD-dependent deacetylase sirtuin-3 (SIRT3) is activated in trained mD4KO mice. Noteworthy, SIRT3 overexpression correlates with a decline in *Fos* gene expression (Palomer et al., 2020). Hence, the predicted SIRT3 activation most likely results in the repressed *Fos* expression.

Additionally, the transcriptome results in this thesis indicate towards an impaired mitogenic fibrobast growth factor (FGF) signaling of the trained *Tbc1d4*-deficient skeletal muscle. In this context, *Fibroblast growth factor-binding protein 1* (*Fgfbp1*) appeared to be significantly reduced in trained mD4KO mice. FGFBP1 chaperones mitogenic FGFs from their location in the extracellular matrix to target cells expressing FGF receptors (Schmidt et al., 2018, Li, 2019). In turn, these mitogenic FGFs overly regulate cellular proliferation, cell migration and tissue remodeling, thereby playing an important role in skeletal muscle maintenance and regeneration (Li, 2019, Zhang et al., 2006, Luo et al., 2006, Gospodarowicz et al., 1977). Interestingly, IPA predicted that the mitogenic and FGFBP1-target FGF2 is reduced in trained mD4KO mice. FGF2 has shown to enhance the number of proliferating cells by facilitating the recruitment of additional SC (Yablonka-Reuveni and Rivera, 1997).

4.3.2 Deficiency of *Tbc1d4* is associated with decreased lipid metabolism in response to chronic exercise training

Furthermore, the present transcriptome analysis demonstrates that the lipid metabolism pathway is decreased due to the TBC1D4 knockout in combination with a chronic exercise intervention. TBC1D4 represents an important signaling hub within skeletal muscle lipid metabolism, as it controls the uptake of long-chain fatty acids (LCFA) into skeletal muscle via the RabGTPases Rab8, Rab10 or Rab14 (Benninghoff et al., 2020, Miklosz et al., 2021). Thus, *Tbc1d4*-deficiency is associated with an increased LCFA uptake, due to the increased protein abundance of fatty acid transporter 4 (FATP4) and an enhanced expression level and translocation of FAT/CD36 (Benninghoff et al., 2020, Miklosz et al., 2021, Samovski et al., 2012). Accompanying the increased LCFA uptake, FAO is also enhanced in D4KO mice (Benninghoff et al., 2020, Chadt et al., 2015). This metabolic switch towards a preferable lipid usage likely compensates for the decreased carbohydrate consumption in these animals (Chadt et al., 2015). However, our data point towards a decreased LCFA uptake in trained mD4KO mice, indicated by a reduced gene expression of FAT/CD36. Furthermore, several Acyl-CoA synthestases displayed a reduced gene expression in these animals, suggesting a decreased FAO. Our results suggest that the metabolic switch toward an increased lipid combustion is reversed in trained *Tbc1d4*-deficient skeletal muscle. Consequently, the metabolism of carbohydrates might be enhanced, which could explain the decreased blood glucose levels in the postprandial state.

Additionally, the peroxisome proliferator-activated receptor (PPAR) signaling pathway appears to be decreased in mD4KO mice. This pathway is highly connected to lipid utilization, as PPARs are activated by fatty acids. Thereby, the expression of genes involved in lipid oxidation is regulated (Varga et al., 2011, Kersten and Stienstra, 2017). Interestingly, results of the present thesis predicted an inhibited activity of PPARα and PPARγ due to the *Tbc1d4*-deficiency and the exercise stimulus. These results further emphasize the assumption of a decreased lipid metabolism.

4.3.3 *Tbc1d4*-deficiency in skeletal muscle is associated with alterations in the expression of genes that regulate vesicle translocation and secretion

Comprehensive investigations have shown that TBC1D4 controls in skeletal muscle and adipose tissue the trafficking and plasma membrane fusion of glucose and fatty acid transporters (Chadt et al., 2015, Benninghoff et al., 2020). Furthermore, previous studies demonstrated an association between TBC1D4 and vesicle secretion in macrophages and cardiomyocytes (Weimershaus et al., 2018, Binsch et al., 2023). Hence, we hypothesize that TBC1D4 controls translocation and secretion of other cargo-

containing vesicles in a RabGTPase-dependent manner, thereby enabling tissue crosstalk. Our data show that *Tbc1d4*-deficient skeletal muscle displays an increased expression of the guanine exchange factor *Synaptotagmin-like protein 2* (*Sytl2*). *Sytl2* is the effector protein of Rab27, thereby transferring it into its more active GTP-bound conformational state (Yasuda and Fukuda, 2014). Rab27 and its effector proteins are specifically located on secretory vesicles and regulate a series of exocytic steps, such as vesicle maturation, movement along microtubules, and tethering to the plasma membrane (Izumi, 2021). Furthermore, Rab27 has been linked to control the exosome secretion pathway, by transferring multivesicular endosomes (MVEs) from microtubules to the actin-rich cortex and regulating the docking of MVEs to the plasma membrane (Ostrowski et al., 2010). However, the role of Rab27 and its effector proteins in the skeletal muscle secretory pathway is widely unknown. At least in melanocytes, TBC1D10 was identified as a GAP protein for Rab27 (Itoh and Fukuda, 2006). Of note, an *in vitro* GAP assay confirmed Rab27 as substrate of the GAP domain in TBC1D1 (Roach et al., 2007). Since TBC1D1 and TBC1D4 share 79 % homology in their RabGAP domains, it would be interesting to determine GAP activity of full-length TBC1D4 towards Rab27. Thus, we speculate that an increased *Sytl2*-mediated Rab27 activation leads to an increased vesicle trafficking in mD4KO mice, which in turn might account for an altered crosstalk between skeletal muscle and adipose tissue.

Beside the classical and unconventional protein secretion pathway, proteins can be secreted into the extracellular matrix via proteolytic ectodomain shedding (Lichtenthaler et al., 2018). Thereby, proteases cleave a membrane protein, leading to the secretion of the soluble extracellular domain (ectodomain) (Lichtenthaler et al., 2018, Kapeller et al., 1973, Black, 1980). In this regard, the soluble metalloproteinase *A disintegrin-like and metalloproteinase with thrombospondin type-1 motifs 20* (*Adamts20*) displayed an increased expression level in *Tbc1d4*-deficient skeletal muscle after chronic exercise. Several members of the ADAMTS family exert a protease activity and are involved in ectodomain shedding. Consequently, growth factors, cytokines, receptors and other molecules are activated or inactivated, which in turn enable them to control several processes (Wozniak et al., 2021, Bridges and Bowditch, 2005, Pluda et al., 2021, Bartens et al., 2016, Shimoda and Khokha, 2017). ADAMTS20 for instance cleaves the extracellular matrix component and proteoglycan versican, leading to its secretion (Silver et al., 2008). We speculate that the increased *Adamts20* expression in *Tbc1d4*-deficient skeletal muscle might enhance ectodomain shedding of bioactive molecules, which in turn alter skeletal muscle-adipose tissue crosstalk. Furthermore, ADAMTS20 regulates intercellular communication by being packaged in extracellular vesicles (EVs) and secreted into the extracellular matrix, as it was observed during ciliogenesis (Nandadasa et al., 2019). Thereby, ADAMTS20 exerts its shedding activity after being taken up by target cells (Valadi et al., 2007). Thus, *Adamts*20-EVs secretion

might be enhanced in trained mD4KO mice, which in turn could mediate tissue crosstalk from skeletal muscle as organ of origin.

The RabGAP TBC1D23 is associated to regulate vesicle trafficking by linking the trans-Golgi-network (TGN) and endosome-derived vesicles (Shin et al., 2017). Our data provide evidence that also TBC1D4 might connect the TGN and endosome-derived vesicles, by interacting with golgins that are located on the trans-Golgi. Golgins are peripheral membrane proteins of the TGN that may regulate membrane transport from the TGN (Gleeson et al., 2004). Golgin-7a is an interesting candidate gene, significantly increased in *Tbc1d4*-deficient skeletal muscle, although it did not meet our primary filter criteria (adjusted p-value <0.05). We assume that the GAP domain of TBC1D4 binds at the tip of golgin-7a at the TGN, thereby connecting TGN with endosome-derived vesicles in a similar manner as TBC1D23 does. This mechanism might be disturbed due to the TBC1D4 ablation, resulting in an altered vesicle trafficking.

4.3.4 *Tbc1d4*-deficiency in skeletal muscle leads to altered expression of genes associated with organ crosstalk after exercise

The conducted Ingenuity Pathway analysis in this thesis predicted that the activation of IL-1β is inhibited in trained mD4KO mice. IL-1β is involved in the development of obesity-associated insulin resistance and IL-1β treatment of human and murine adipose tissue displayed by decreased protein abundances of IRS1, PI3K, pAKT and GLUT4 (Jager et al., 2007, Gao et al., 2014). In contrast, blocking IL-1β signaling leads to improved glycemia in obese mice and ameliorated insulin signaling in human adipocytes (Owyang et al., 2010, McGillicuddy et al., 2011, Sauter et al., 2008). Thus, it is plausible that the inhibited IL-1β activity in trained mD4KO mice might lead to a positive effect on adipose tissue insulin sensitivity. Noteworthy, IL-1β appears to be a modulator of the myokine release. Alvarez *et al.* have shown that myoblast incubation with IL-1β leads to a reduced secretion of myostatin, irisin and osteonectin (Alvarez et al., 2020). These data suggest that the secretion of IL-1β-associated myokines is increased in trained mD4KO mice, which in turn could further affect insulin sensitivity in *Tbc1d4*-deficient WAT. Among those myokines, osteonectin has been shown to activate the PI3K/AKT signaling pathway and further promote AMPK-mediated GLUT4 expression in cultured myocytes and adipocytes, resulting in enhanced glucose uptake (Deng et al., 2022, Aoi et al., 2019, Song et al., 2010). Thus, analyzing the expression level of the IL-1β-associated myokine osteonectin in trained mD4KO mice would be an interesting approach.

As previously mentioned, the present thesis indicates that the lipid metabolism is decreased in trained mD4KO mice. Hence, the attenuated PPAR signaling might result in a gene repression of PPAR target genes. Indeed, the PPARα and PPARγ target *Angiopoetin-like 4* (*Angptl4*) displayed a significantly decreased expression in trained mD4KO mice. ANGPTL4 regulates the lipid metabolism by controlling the activity of lipoprotein lipase (Aryal et al., 2019). Furthermore, there is strong evidence that ANGPTL4 has a regulatory function in glucose metabolism, insulin resistance and T2DM. Carriers of an ANGPTL4 missense variant displayed lower fasting blood glucose levels, a greater insulin sensitivity, and had lower odds to develop T2DM (Gusarova et al., 2018). Additionally, an adipose tissue-specific *Angptl4*-deficiency in mice leads to an increased insulin-stimulated AKT phosphorylation in skeletal muscle and WAT, indicating an enhanced glucose transport (Aryal et al., 2018). Thus, the reduced *Angptl4* expression in trained mD4KO mice might account for improvements in postprandial blood glucose levels.

A transcriptome analysis was conducted in this thesis, aiming to elucidate how skeletal muscle adapts to the *Tbc1d4*-deficiency in the sedentary and trained state, and to identify potential factors that might explain how *Tbc1d4*-deficiency alters skeletal muscle tissue crosstalk. In our view, the greatest advantage of a transcriptome analysis is its sensitivity, as all skeletal muscle transcripts are depicted (Rao et al., 2018). Therefore, we were able to identify genes that might account for an altered vesicle trafficking and secretion. Alternatively, a secretome analysis would have perhaps revealed secreted proteins that could mediate organ crosstalk between *Tbc1d4*-deficient skeletal muscle and adipose tissue. However, this approach would not reflect the *in vivo* chronic exercise condition, as the experimental setting only allows to apply a contraction stimulus that resembles an acute exercise bout. Thus, the initial objective would not be pursued within this approach. Furthermore, the subsequent mass spectrometry analysis does not offer enough sensitivity, which makes it difficult to detect low-abundance proteins (Li et al., 2018, Momenbeitollahi et al., 2021). In addition, a secretome analysis does not provide insights into cellular changes. Thereby, *Tbc1d4*-mediated molecular mechanisms would not have been identified.

4.4 Tamoxifen-induced *Tbc1d4* gene knockout is not sufficient to affect metabolism and muscle function in adult mice

In order to analyze, whether a skeletal muscle-specific *Tbc1d4* ablation in the adult state is sufficient to alter the metabolism and muscle function, inducible mD4KO mice were generated and metabolically characterized. Therefore, a tamoxifen-induced Cre system was used, where the Cre recombinase is

modified and fused with the estrogen receptor containing a mutated ligand binding domain (CreER) (Mobley et al., 2020). In response to the tamoxifen treatment, male individuals developed structural abnormalities regardless of the genotype. We observed that a large amount of intestine herniated out of the abdominal cavity. This severe side effect was also seen in another study, where the low abdominal wall was broken after tamoxifen injection exclusively in male animals. These structural abnormalities in the male cohort were associated with decreased type II collagen content and increased MMP-2 and MMP-13 expression (Ma et al., 2015). As a consequence, male animals were excluded from the present thesis.

Tamoxifen was administered intraperitoneally in order to achieve a complete *Tbc1d4* gene knockout. After tamoxifen treatment, *Tbc1d4* gene knockout was achieved by only around 50 %, which might indicate that the tamoxifen dosage was too low to induce a sufficient gene knockout. However, if the tamoxifen dose is too high or the time of treatment too long, toxic side effects could occur (Gunschmann et al., 2014). At least in mouse myocardium, the dosage of 120 mg/kg injected on three consecutive days appeared to be sufficient to induce a *Serca2* knockout, where mRNA expression was reduced to <6 % after seven days (Andersson et al., 2010). However, this dosage might be not sufficient to induce a gene knockout in skeletal muscle. In comparison to an intraperitoneal injection, tamoxifen can also be administered via drinking water or food pellets, which is considered less stressful for the mice compared to an intraperitoneal injection. However, the efficiency of gene deletion depends on the individual drinking and eating behavior, which directly correlates to the final tamoxifen dosage in the target tissue (Yoshinobu et al., 2021). Moreover, the relatively low water solubility of tamoxifen limits the tamoxifen doses that can be administered via drinking water, making it more difficult to arrive a dose sufficient for gene knockout (Whitfield et al., 2015).

Likely due to the incomplete TBC1D4 ablation, GLUT4 protein content in the *Soleus* muscle was only reduced by about 25 %. In contrast, a 50 % reduction is observed in oxidative skeletal muscle of D4KO mice, generated by the conventional knockout system (Chadt et al., 2015, Springer PhD thesis, 2018). Furthermore, mD4KO.ind animals displayed normal postprandial blood glucose levels, while postprandial hyperglycemia is a prominent phenotype in D4KO mice (de Wendt et al., 2021). It is plausible that these mild phenotypes in mD4KO.ind mice occur due to an insufficient TBC1D4 knockout efficiency. Therefore, mD4KO.ind mice were excluded from further experimentation during this study. In order to guarantee a complete TBC1D4 ablation, all analyses were conducted using animals with a conventional muscle-specific TBC1D4 knockout.

In summary, the present thesis shows that tissue-specific TBC1D4 ablation in skeletal muscle or adipose tissue did not lead to pronounced improvements in adipose tissue insulin sensitivity after chronic exercise training. In fact, both tissue-specific knockout mouse lines were characterized by postprandial hyperglycemia, but only mD4KO mice improved their postprandial hyperglycemia in response to chronic exercise. However, aD4KO mice were glucose intolerant, which was restored after the training intervention. In conclusion, both tissues in concordance seem to be responsible for the exercise-mediated improvements observed in trained whole-body D4KO mice. The performed transcriptome analysis indicates that the *Tbc1d4*-deficiency in skeletal muscle is associated with impairments in skeletal muscle development and lipid metabolism. Further, TBC1D4 might bridges the gap between trans-Golgi-network and endosome-derived vesicles, perhaps regulating skeletal muscle crosstalk. Figure 34 postulates two possible mechanisms how TBC1D4 might regulate vesicle trafficking and secretion. However, further investigations are necessary to confirm the exact underlying mechanism.

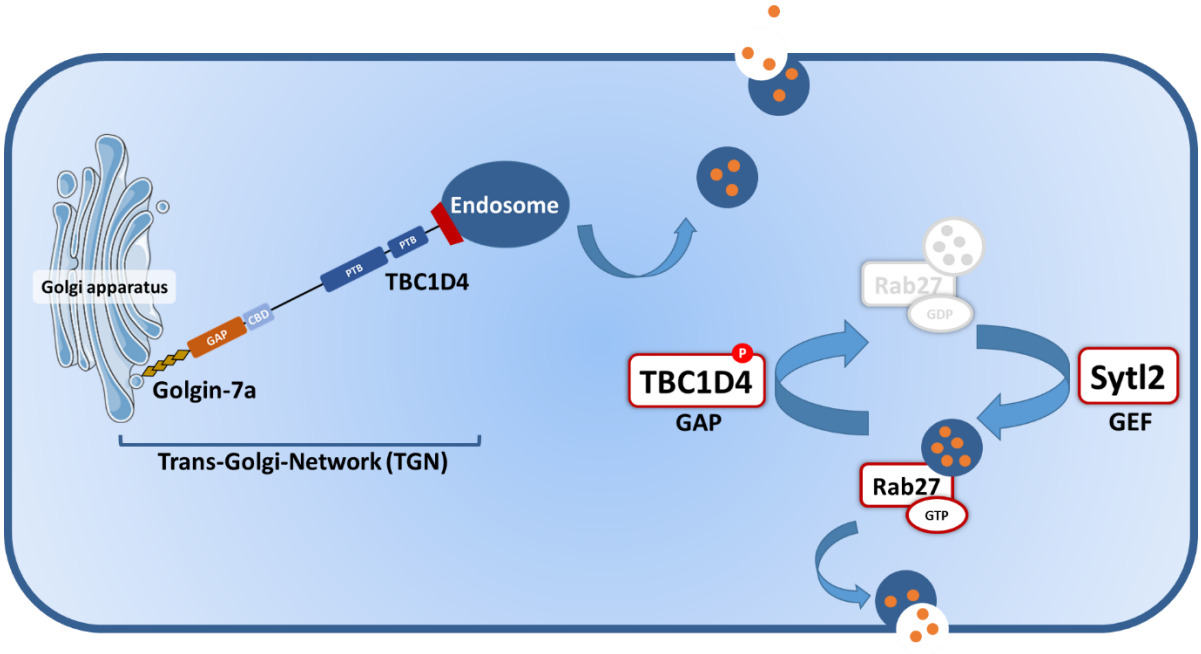

Figure 34: Postulated mechanisms how TBC1D4 regulates vesicle trafficking. Besides regulating vesicle transport of glucose and fatty acid transporters, TBC1D4 controls translocation and secretion of cargo-containing vesicles, presumably in interaction with Rab27 and its effector protein Sytl2. The GAP domain of TBC1D4 might bind at the tip of golgin-7a at the trans-Golgi, while the C-terminus of TBC1D4 presumably binds to a complex on endosome-derived vesicles. Thereby, TBC1D4 links trans-Golgi-network with endosome-derived vesicles. GEF = guanosine exchange factor, GAP = GTPase activating protein.

5 Outlook

The present thesis indicates that the TBC1D4 ablation presumably needs to be present in both, skeletal muscle and adipose tissue, in order to induce beneficial effects on adipose tissue insulin sensitivity after chronic exercise. Therefore, future investigations are necessary to analyze the transcripts of *Tbc1d4*-deficient WAT. Presumably an altered receptor abundance on the plasma membrane of WAT might alter the signal transduction that eventually affects glucose uptake.

The conducted transcriptome analysis revealed numerous differentially regulated genes due to the *Tbc1d4*-deficiency and in response to the chronic exercise training. These data underline the central role of TBC1D4 within the skeletal muscle exercise metabolism. Further, we provided evidence that TBC1D4 might regulate vesicle trafficking and postulate two underlying mechanisms. TBC1D4 might regulate vesicle trafficking by linking trans-Golgi-network and endosome-derived vesicles, presumably by interacting with golgin-7a that is located at the trans-Golgi. Therefore, it would be interesting to analyze whether GAP domain of TBC1D4 interacts with golgin-7a, to validate their connection. Moreover, our data point towards an enhanced activation of Rab27 due to the increased expression of its effector protein *Sytl2*. In this regard, an *in vitro* GAP assay could be performed to analyze, whether Rab27 is a substrate of full-length TBC1D4.

Furthermore, our data provided evidence that TBC1D4 ablation is associated with changes in the skeletal muscle secretion profile. One interesting identified candidate protein is IL1-β that was predicted to be inhibited in trained mD4KO mice and appears to be a modulator of the myokine release. Therefore, future investigations will aim to elucidate the secretory profile of IL1-β-associated myokines in mD4KO mice and their effect on *Tbc1d4*-deficient WAT. Since chronic exercise training leads to the secretion of hundreds of myokines (Severinsen and Pedersen, 2020), it is likely that several proteins display an altered secretory profile due to the *Tbc1d4*-deficiency in response to chronic exercise. Therefore, an immunology bead-based multiplex assay that targets several myokines, such as irisin, myostatin, FGF21 and osteonectin, will be performed with the plasma of sedentary and trained mD4KO mice.

6 References

AAGAARD, P. & ANDERSEN, J. L. 2010. Effects of strength training on endurance capacity in top-level endurance athletes. *Scand J Med Sci Sports,* 20 Suppl 2**,** 39-47.

AAGAARD, P., MAGNUSSON, P. S., LARSSON, B., KJAER, M. & KRUSTRUP, P. 2007. Mechanical muscle function, morphology, and fiber type in lifelong trained elderly. *Med Sci Sports Exerc,* 39**,** 1989-96.

ABDUL-GHANI, M. A. & DEFRONZO, R. A. 2010. Pathogenesis of insulin resistance in skeletal muscle. *J Biomed Biotechnol,* 2010**,** 476279.

ABEL, E. D., PERONI, O., KIM, J. K., KIM, Y. B., BOSS, O., HADRO, E., MINNEMANN, T., SHULMAN, G. I. & KAHN, B. B. 2001. Adipose-selective targeting of the GLUT4 gene impairs insulin action in muscle and liver. *Nature,* 409**,** 729-33.

ADEVA-ANDANY, M. M., GONZALEZ-LUCAN, M., DONAPETRY-GARCIA, C., FERNANDEZ-FERNANDEZ, C. & AMENEIROS-RODRIGUEZ, E. 2016. Glycogen metabolism in humans. *BBA Clin,* 5**,** 85-100.

AHLBORG, G., FELIG, P., HAGENFELDT, L., HENDLER, R. & WAHREN, J. 1974. Substrate turnover during prolonged exercise in man. Splanchnic and leg metabolism of glucose, free fatty acids, and amino acids. *J Clin Invest,* 53**,** 1080-90.

AHRÉN, B. 2013. Procedures and Evaluation of the Oral glucose Tolerance Test. *Encyclopedia of Human Nutrition*

ALDISS, P., BETTS, J., SALE, C., POPE, M., BUDGE, H. & SYMONDS, M. E. 2018. Exercise-induced 'browning' of adipose tissues. *Metabolism,* 81**,** 63-70.

ALMADA, A. E., HORWITZ, N., PRICE, F. D., GONZALEZ, A. E., KO, M., BOLUKBASI, O. V., MESSEMER, K. A., CHEN, S., SINHA, M., RUBIN, L. L. & WAGERS, A. J. 2021. FOS licenses early events in stem cell activation driving skeletal muscle regeneration. *Cell Rep,* 34**,** 108656.

ALVAREZ, A. M., DEOCESANO-PEREIRA, C., TEIXEIRA, C. & MOREIRA, V. 2020. IL-1beta and TNF-alpha Modulation of Proliferated and Committed Myoblasts: IL-6 and COX-2-Derived Prostaglandins as Key Actors in the Mechanisms Involved. *Cells,* 9.

AMEER, F., SCANDIUZZI, L., HASNAIN, S., KALBACHER, H. & ZAIDI, N. 2014. De novo lipogenesis in health and disease. *Metabolism,* 63**,** 895-902.

ANDERSEN, M. K. & HANSEN, T. 2018. Genetics of metabolic traits in Greenlanders: lessons from an isolated population. *J Intern Med,* 284**,** 464-477.

ANDERSSON, K. B., WINER, L. H., MORK, H. K., MOLKENTIN, J. D. & JAISSER, F. 2010. Tamoxifen administration routes and dosage for inducible Cre-mediated gene disruption in mouse hearts. *Transgenic Res,* 19**,** 715-25.

ANG, A. L., FOLSCH, H., KOIVISTO, U. M., PYPAERT, M. & MELLMAN, I. 2003. The Rab8 GTPase selectively regulates AP-1B-dependent basolateral transport in polarized Madin-Darby canine kidney cells. *J Cell Biol,* 163**,** 339-50.

AOI, W., HIRANO, N., LASSITER, D. G., BJORNHOLM, M., CHIBALIN, A. V., SAKUMA, K., TANIMURA, Y., MIZUSHIMA, K., TAKAGI, T., NAITO, Y., ZIERATH, J. R. & KROOK, A. 2019. Secreted protein acidic and rich in cysteine (SPARC) improves glucose tolerance via AMP-activated protein kinase activation. *FASEB J,* 33**,** 10551-10562.

ARYAL, B., PRICE, N. L., SUAREZ, Y. & FERNANDEZ-HERNANDO, C. 2019. ANGPTL4 in Metabolic and Cardiovascular Disease. *Trends Mol Med,* 25**,** 723-734.

ARYAL, B., SINGH, A. K., ZHANG, X., VARELA, L., ROTLLAN, N., GOEDEKE, L., CHAUBE, B., CAMPOREZ, J. P., VATNER, D. F., HORVATH, T. L., SHULMAN, G. I., SUAREZ, Y. & FERNANDEZ-HERNANDO, C. 2018. Absence of ANGPTL4 in adipose tissue improves glucose tolerance and attenuates atherogenesis. *JCI Insight,* 3.

ATKINSON, M. A., EISENBARTH, G. S. & MICHELS, A. W. 2014. Type 1 diabetes. *Lancet,* 383**,** 69-82.

BALDUCCI, S., ZANUSO, S., CARDELLI, P., SALVI, L., MAZZITELLI, G., BAZURO, A., IACOBINI, C., NICOLUCCI, A., PUGLIESE, G. & ITALIAN DIABETES EXERCISE STUDY, I. 2012. Changes in physical fitness predict improvements in modifiable cardiovascular risk factors independently of body

weight loss in subjects with type 2 diabetes participating in the Italian Diabetes and Exercise Study (IDES). *Diabetes Care,* 35**,** 1347-54.

BALDUCCI, S., ZANUSO, S., NICOLUCCI, A., FERNANDO, F., CAVALLO, S., CARDELLI, P., FALLUCCA, S., ALESSI, E., LETIZIA, C., JIMENEZ, A., FALLUCCA, F. & PUGLIESE, G. 2010. Anti-inflammatory effect of exercise training in subjects with type 2 diabetes and the metabolic syndrome is dependent on exercise modalities and independent of weight loss. *Nutr Metab Cardiovasc Dis,* 20**,** 608-17.

BARAZZONI, R., GORTAN CAPPELLARI, G., RAGNI, M. & NISOLI, E. 2018. Insulin resistance in obesity: an overview of fundamental alterations. *Eat Weight Disord,* 23**,** 149-157.

BARR, F. & LAMBRIGHT, D. G. 2010. Rab GEFs and GAPs. *Curr Opin Cell Biol,* 22**,** 461-70.

BARTENS, M. C., DRILLICH, M., RYCHLI, K., IWERSEN, M., ARNHOLDT, T., MEYER, L. & KLEIN-JOBSTL, D. 2016. Assessment of different methods to estimate bovine colostrum quality on farm. *N Z Vet J,* 64**,** 263-7.

BELL, J. A., REED, M. A., CONSITT, L. A., MARTIN, O. J., HAYNIE, K. R., HULVER, M. W., MUOIO, D. M. & DOHM, G. L. 2010. Lipid partitioning, incomplete fatty acid oxidation, and insulin signal transduction in primary human muscle cells: effects of severe obesity, fatty acid incubation, and fatty acid translocase/CD36 overexpression. *J Clin Endocrinol Metab,* 95**,** 3400-10.

BENJAMINI, Y. & HOCHBERG, Y. 1995. Controlling the False Discovery Rate: a Practical and Powerful Approach to Multiple Testing. *Journal of the Royal Statistical Society* 57**,** 289-300.

BENNINGHOFF, T., ESPELAGE, L., EICKELSCHULTE, S., ZEINERT, I., SINOWENKA, I., MULLER, F., SCHONDELING, C., BATCHELOR, H., CAMES, S., ZHOU, Z., KOTZKA, J., CHADT, A. & AL-HASANI, H. 2020. The RabGAPs TBC1D1 and TBC1D4 Control Uptake of Long-Chain Fatty Acids Into Skeletal Muscle via Fatty Acid Transporter SLC27A4/FATP4. *Diabetes,* 69**,** 2281-2293.

BERGMAN, B. C. & GOODPASTER, B. H. 2020. Exercise and Muscle Lipid Content, Composition, and Localization: Influence on Muscle Insulin Sensitivity. *Diabetes,* 69**,** 848-858.

BIENSO, R. S., OLESEN, J., GLIEMANN, L., SCHMIDT, J. F., MATZEN, M. S., WOJTASZEWSKI, J. F., HELLSTEN, Y. & PILEGAARD, H. 2015. Effects of Exercise Training on Regulation of Skeletal Muscle Glucose Metabolism in Elderly Men. *J Gerontol A Biol Sci Med Sci,* 70**,** 866-72.

BINSCH, C., BARBOSA, D. M., HANSEN-DILLE, G., HUBERT, M., HODGE, S. M., KOLASA, M., JERUSCHKE, K., WEISS, J., SPRINGER, C., GORRESSEN, S., FISCHER, J. W., LIENHARD, M., HERWIG, R., BORNO, S., TIMMERMANN, B., CREMER, A. L., BACKES, H., CHADT, A. & AL-HASANI, H. 2023. Deletion of Tbc1d4/As160 abrogates cardiac glucose uptake and increases myocardial damage after ischemia/reperfusion. *Cardiovasc Diabetol,* 22**,** 17.

BLACK, P. H. 1980. Shedding from normal and cancer-cell surfaces. *N Engl J Med,* 303**,** 1415-6.

BLUESTONE, J. A., HEROLD, K. & EISENBARTH, G. 2010. Genetics, pathogenesis and clinical interventions in type 1 diabetes. *Nature,* 464**,** 1293-300.

BOSTROM, P., WU, J., JEDRYCHOWSKI, M. P., KORDE, A., YE, L., LO, J. C., RASBACH, K. A., BOSTROM, E. A., CHOI, J. H., LONG, J. Z., KAJIMURA, S., ZINGARETTI, M. C., VIND, B. F., TU, H., CINTI, S., HOJLUND, K., GYGI, S. P. & SPIEGELMAN, B. M. 2012. A PGC1-alpha-dependent myokine that drives brown-fat-like development of white fat and thermogenesis. *Nature,* 481**,** 463-8.

BOUCHER, J., KLEINRIDDERS, A. & KAHN, C. R. 2014. Insulin receptor signaling in normal and insulin-resistant states. *Cold Spring Harb Perspect Biol,* 6.

BOULE, N. G., HADDAD, E., KENNY, G. P., WELLS, G. A. & SIGAL, R. J. 2001. Effects of exercise on glycemic control and body mass in type 2 diabetes mellitus: a meta-analysis of controlled clinical trials. *JAMA,* 286**,** 1218-27.

BRAVO-CORDERO, J. J., MARRERO-DIAZ, R., MEGIAS, D., GENIS, L., GARCIA-GRANDE, A., GARCIA, M. A., ARROYO, A. G. & MONTOYA, M. C. 2007. MT1-MMP proinvasive activity is regulated by a novel Rab8-dependent exocytic pathway. *EMBO J,* 26**,** 1499-510.

BRIDGES, L. C. & BOWDITCH, R. D. 2005. ADAM-Integrin Interactions: potential integrin regulated ectodomain shedding activity. *Curr Pharm Des,* 11**,** 837-47.

CAMPBELL, J. E. & NEWGARD, C. B. 2021. Mechanisms controlling pancreatic islet cell function in insulin secretion. *Nat Rev Mol Cell Biol,* 22**,** 142-158.

CANNON, B. & NEDERGAARD, J. 2004. Brown adipose tissue: function and physiological significance. *Physiol Rev,* 84**,** 277-359.

CARTEE, G. D. 2015. Roles of TBC1D1 and TBC1D4 in insulin- and exercise-stimulated glucose transport of skeletal muscle. *Diabetologia,* 58**,** 19-30.

CHADT, A., IMMISCH, A., DE WENDT, C., SPRINGER, C., ZHOU, Z., STERMANN, T., HOLMAN, G. D., LOFFING-CUENI, D., LOFFING, J., JOOST, H. G. & AL-HASANI, H. 2015. "Deletion of both Rab-GTPase-activating proteins TBC1D1 and TBC1D4 in mice eliminates insulin- and AICAR-stimulated glucose transport [corrected]. *Diabetes,* 64**,** 746-59.

CHAVEZ, J. A., ROACH, W. G., KELLER, S. R., LANE, W. S. & LIENHARD, G. E. 2008. Inhibition of GLUT4 translocation by Tbc1d1, a Rab GTPase-activating protein abundant in skeletal muscle, is partially relieved by AMP-activated protein kinase activation. *J Biol Chem,* 283**,** 9187-95.

CHEN, M. M., LI, Y., DENG, S. L., ZHAO, Y., LIAN, Z. X. & YU, K. 2022. Mitochondrial Function and Reactive Oxygen/Nitrogen Species in Skeletal Muscle. *Front Cell Dev Biol,* 10**,** 826981.

CHOMENTOWSKI, P., COEN, P. M., RADIKOVA, Z., GOODPASTER, B. H. & TOLEDO, F. G. 2011. Skeletal muscle mitochondria in insulin resistance: differences in intermyofibrillar versus subsarcolemmal subpopulations and relationship to metabolic flexibility. *J Clin Endocrinol Metab,* 96**,** 494-503.

CHOW, L. S., GERSZTEN, R. E., TAYLOR, J. M., PEDERSEN, B. K., VAN PRAAG, H., TRAPPE, S., FEBBRAIO, M. A., GALIS, Z. S., GAO, Y., HAUS, J. M., LANZA, I. R., LAVIE, C. J., LEE, C. H., LUCIA, A., MORO, C., PANDEY, A., ROBBINS, J. M., STANFORD, K. I., THACKRAY, A. E., VILLEDA, S., WATT, M. J., XIA, A., ZIERATH, J. R., GOODPASTER, B. H. & SNYDER, M. P. 2022. Exerkines in health, resilience and disease. *Nat Rev Endocrinol,* 18**,** 273-289.

COELHO, M., OLIVEIRA, T. & FERNANDES, R. 2013. Biochemistry of adipose tissue: an endocrine organ. *Arch Med Sci,* 9**,** 191-200.

COEN, P. M., HAMES, K. C., LEACHMAN, E. M., DELANY, J. P., RITOV, V. B., MENSHIKOVA, E. V., DUBE, J. J., STEFANOVIC-RACIC, M., TOLEDO, F. G. & GOODPASTER, B. H. 2013. Reduced skeletal muscle oxidative capacity and elevated ceramide but not diacylglycerol content in severe obesity. *Obesity (Silver Spring),* 21**,** 2362-71.

COGGAN, A. R., SWANSON, S. C., MENDENHALL, L. A., HABASH, D. L. & KIEN, C. L. 1995. Effect of endurance training on hepatic glycogenolysis and gluconeogenesis during prolonged exercise in men. *Am J Physiol,* 268**,** E375-83.

COLBERG, S. R., SIGAL, R. J., YARDLEY, J. E., RIDDELL, M. C., DUNSTAN, D. W., DEMPSEY, P. C., HORTON, E. S., CASTORINO, K. & TATE, D. F. 2016. Physical Activity/Exercise and Diabetes: A Position Statement of the American Diabetes Association. *Diabetes Care,* 39**,** 2065-2079.

COLBERG, S. R., SIMONEAU, J. A., THAETE, F. L. & KELLEY, D. E. 1995. Skeletal muscle utilization of free fatty acids in women with visceral obesity. *J Clin Invest,* 95**,** 1846-53.

COLLABORATION, N. C. D. R. F. 2016. Worldwide trends in diabetes since 1980: a pooled analysis of 751 population-based studies with 4.4 million participants. *Lancet,* 387**,** 1513-1530.

CONSITT, L. A., BELL, J. A. & HOUMARD, J. A. 2009. Intramuscular lipid metabolism, insulin action, and obesity. *IUBMB Life,* 61**,** 47-55.

CRYER, P. E. 2007. Hypoglycemia, functional brain failure, and brain death. *J Clin Invest,* 117**,** 868-70.

CZECH, M. P. 2017. Insulin action and resistance in obesity and type 2 diabetes. *Nat Med,* 23**,** 804-814.

CZECH, M. P. 2020. Mechanisms of insulin resistance related to white, beige, and brown adipocytes. *Mol Metab,* 34**,** 27-42.

DA SILVA ROSA, S. C., NAYAK, N., CAYMO, A. M. & GORDON, J. W. 2020. Mechanisms of muscle insulin resistance and the cross-talk with liver and adipose tissue. *Physiol Rep,* 8**,** e14607.

DANDONA, P., ALJADA, A., CHAUDHURI, A. & BANDYOPADHYAY, A. 2003. The potential influence of inflammation and insulin resistance on the pathogenesis and treatment of atherosclerosis-related complications in type 2 diabetes. *J Clin Endocrinol Metab,* 88**,** 2422-9.

DASH, S., SANO, H., ROCHFORD, J. J., SEMPLE, R. K., YEO, G., HYDEN, C. S., SOOS, M. A., CLARK, J., RODIN, A., LANGENBERG, C., DRUET, C., FAWCETT, K. A., TUNG, Y. C., WAREHAM, N. J., BARROSO, I., LIENHARD, G. E., O'RAHILLY, S. & SAVAGE, D. B. 2009. A truncation mutation in

TBC1D4 in a family with acanthosis nigricans and postprandial hyperinsulinemia. *Proc Natl Acad Sci U S A,* 106**,** 9350-5.

DASHTY, M. 2013. A quick look at biochemistry: carbohydrate metabolism. *Clin Biochem,* 46**,** 1339-52.

DAVEGARDH, C., SALL, J., BENRICK, A., BROHOLM, C., VOLKOV, P., PERFILYEV, A., HENRIKSEN, T. I., WU, Y., HJORT, L., BRONS, C., HANSSON, O., PEDERSEN, M., WURTHNER, J. U., PFEFFER, K., NILSSON, E., VAAG, A., STENER-VICTORIN, E., PIRCS, K., SCHEELE, C. & LING, C. 2021. VPS39-deficiency observed in type 2 diabetes impairs muscle stem cell differentiation via altered autophagy and epigenetics. *Nat Commun,* 12**,** 2431.

DE WENDT, C., ESPELAGE, L., EICKELSCHULTE, S., SPRINGER, C., TOSKA, L., SCHEEL, A., BEDOU, A. D., BENNINGHOFF, T., CAMES, S., STERMANN, T., CHADT, A. & AL-HASANI, H. 2021. Contraction-Mediated Glucose Transport in Skeletal Muscle is Regulated by a Framework of AMPK, TBC1D1/4 and Rac1. *Diabetes*.

DEFRONZO, R. A., FERRANNINI, E., GROOP, L., HENRY, R. R., HERMAN, W. H., HOLST, J. J., HU, F. B., KAHN, C. R., RAZ, I., SHULMAN, G. I., SIMONSON, D. C., TESTA, M. A. & WEISS, R. 2015. Type 2 diabetes mellitus. *Nat Rev Dis Primers,* 1**,** 15019.

DEN OTTER, W. & VAN BOXTEL, A. B. 1971. Relation between the glycogen content of the liver and liver weight, and its meaning for enzymology. *Experientia,* 27**,** 1271-2.

DENG, S., ZHANG, L., LI, J., JIN, Y. & WANG, J. 2022. Activation of the PI3K-AKT signaling pathway by SPARC contributes to the malignant phenotype of cholangiocarcinoma cells. *Tissue Cell,* 76**,** 101756.

DESPRES, J. P. & LEMIEUX, I. 2006. Abdominal obesity and metabolic syndrome. *Nature,* 444**,** 881-7.

DOBIN, A., DAVIS, C. A., SCHLESINGER, F., DRENKOW, J., ZALESKI, C., JHA, S., BATUT, P., CHAISSON, M. & GINGERAS, T. R. 2013. STAR: ultrafast universal RNA-seq aligner. *Bioinformatics,* 29**,** 15-21.

DOBROWSKY, R. T., KAMIBAYASHI, C., MUMBY, M. C. & HANNUN, Y. A. 1993. Ceramide activates heterotrimeric protein phosphatase 2A. *J Biol Chem,* 268**,** 15523-30.

DOKAS, J., CHADT, A., NOLDEN, T., HIMMELBAUER, H., ZIERATH, J. R., JOOST, H. G. & AL-HASANI, H. 2013. Conventional knockout of Tbc1d1 in mice impairs insulin- and AICAR-stimulated glucose uptake in skeletal muscle. *Endocrinology,* 154**,** 3502-14.

DUNSTAN, D. W., HOWARD, B., HEALY, G. N. & OWEN, N. 2012. Too much sitting--a health hazard. *Diabetes Res Clin Pract,* 97**,** 368-76.

EGAN, B. & ZIERATH, J. R. 2013. Exercise metabolism and the molecular regulation of skeletal muscle adaptation. *Cell Metab,* 17**,** 162-84.

EICKELSCHULTE, S., HARTWIG, S., LEISER, B., LEHR, S., JOSCHKO, V., CHOKKALINGAM, M., CHADT, A. & AL-HASANI, H. 2021. AKT/AMPK-mediated phosphorylation of TBC1D4 disrupts the interaction with insulin-regulated aminopeptidase. *J Biol Chem,* 296**,** 100637.

ELTON, C. W., TAPSCOTT, E. B., PORIES, W. J. & DOHM, G. L. 1994. Effect of moderate obesity on glucose transport in human muscle. *Horm Metab Res,* 26**,** 181-3.

EMERGING RISK FACTORS, C., SARWAR, N., GAO, P., SESHASAI, S. R., GOBIN, R., KAPTOGE, S., DI ANGELANTONIO, E., INGELSSON, E., LAWLOR, D. A., SELVIN, E., STAMPFER, M., STEHOUWER, C. D., LEWINGTON, S., PENNELLS, L., THOMPSON, A., SATTAR, N., WHITE, I. R., RAY, K. K. & DANESH, J. 2010. Diabetes mellitus, fasting blood glucose concentration, and risk of vascular disease: a collaborative meta-analysis of 102 prospective studies. *Lancet,* 375**,** 2215-22.

ESPELAGE, L., AL-HASANI, H. & CHADT, A. 2020. RabGAPs in skeletal muscle function and exercise. *J Mol Endocrinol,* 64**,** R1-R19.

EVANS, K. 2019. Diabetic ketoacidosis: update on management. *Clin Med (Lond),* 19**,** 396-398.

FAM, B. C., ROSE, L. J., SGAMBELLONE, R., RUAN, Z., PROIETTO, J. & ANDRIKOPOULOS, S. 2012. Normal muscle glucose uptake in mice deficient in muscle GLUT4. *J Endocrinol,* 214**,** 313-27.

FAYFMAN, M., PASQUEL, F. J. & UMPIERREZ, G. E. 2017. Management of Hyperglycemic Crises: Diabetic Ketoacidosis and Hyperglycemic Hyperosmolar State. *Med Clin North Am,* 101**,** 587-606.

FAZAKERLEY, D. J., KOUMANOV, F. & HOLMAN, G. D. 2022. GLUT4 On the move. *Biochem J,* 479**,** 445-462.

FEDORENKO, A., LISHKO, P. V. & KIRICHOK, Y. 2012. Mechanism of fatty-acid-dependent UCP1 uncoupling in brown fat mitochondria. *Cell,* 151**,** 400-13.

FERRO-NOVICK, S. & BROSE, N. 2013. Nobel 2013 Physiology or medicine: Traffic control system within cells. *Nature,* 504**,** 98.

FONTANESI, L., COLOMBO, M., TOGNAZZI, L., SCOTTI, E., BUTTAZZONI, L., DALL'OLIO, S., DAVOLI, R. & RUSSO, V. 2011. The porcine TBC1D1 gene: mapping, SNP identification, and association study with meat, carcass and production traits in Italian heavy pigs. *Mol Biol Rep,* 38**,** 1425-31.

FRAYN, K. N., ARNER, P. & YKI-JARVINEN, H. 2006. Fatty acid metabolism in adipose tissue, muscle and liver in health and disease. *Essays Biochem,* 42**,** 89-103.

FRIEDMAN, J. E., CARO, J. F., PORIES, W. J., AZEVEDO, J. L., JR. & DOHM, G. L. 1994. Glucose metabolism in incubated human muscle: effect of obesity and non-insulin-dependent diabetes mellitus. *Metabolism,* 43**,** 1047-54.

FRONTERA, W. R. & OCHALA, J. 2015. Skeletal muscle: a brief review of structure and function. *Calcif Tissue Int,* 96**,** 183-95.

FUNAI, K., SCHWEITZER, G. G., SHARMA, N., KANZAKI, M. & CARTEE, G. D. 2009. Increased AS160 phosphorylation, but not TBC1D1 phosphorylation, with increased postexercise insulin sensitivity in rat skeletal muscle. *Am J Physiol Endocrinol Metab,* 297**,** E242-51.

GALE, E. A. 2005. Type 1 diabetes in the young: the harvest of sorrow goes on. *Diabetologia,* 48**,** 1435-8.

GALICIA-GARCIA, U., BENITO-VICENTE, A., JEBARI, S., LARREA-SEBAL, A., SIDDIQI, H., URIBE, K. B., OSTOLAZA, H. & MARTIN, C. 2020. Pathophysiology of Type 2 Diabetes Mellitus. *Int J Mol Sci,* 21.

GAO, D., MADI, M., DING, C., FOK, M., STEELE, T., FORD, C., HUNTER, L. & BING, C. 2014. Interleukin-1beta mediates macrophage-induced impairment of insulin signaling in human primary adipocytes. *Am J Physiol Endocrinol Metab,* 307**,** E289-304.

GEE, H. Y., KIM, J. & LEE, M. G. 2018. Unconventional secretion of transmembrane proteins. *Semin Cell Dev Biol,* 83**,** 59-66.

GIBALA, M. J. & JONES, A. M. 2013. Physiological and performance adaptations to high-intensity interval training. *Nestle Nutr Inst Workshop Ser,* 76**,** 51-60.

GLEESON, P. A., LOCK, J. G., LUKE, M. R. & STOW, J. L. 2004. Domains of the TGN: coats, tethers and G proteins. *Traffic,* 5**,** 315-26.

GONZALEZ-GIL, A. M. & ELIZONDO-MONTEMAYOR, L. 2020. The Role of Exercise in the Interplay between Myokines, Hepatokines, Osteokines, Adipokines, and Modulation of Inflammation for Energy Substrate Redistribution and Fat Mass Loss: A Review. *Nutrients,* 12.

GOODPASTER, B. H. & SPARKS, L. M. 2017. Metabolic Flexibility in Health and Disease. *Cell Metab,* 25**,** 1027-1036.

GOSPODAROWICZ, D., ILL, C. R., HORNSBY, P. J. & GILL, G. N. 1977. Control of bovine adrenal cortical cell proliferation by fibroblast growth factor. Lack of effect of epidermal growth factor. *Endocrinology,* 100**,** 1080-9.

GRANATA, C., OLIVEIRA, R. S., LITTLE, J. P., RENNER, K. & BISHOP, D. J. 2016. Training intensity modulates changes in PGC-1alpha and p53 protein content and mitochondrial respiration, but not markers of mitochondrial content in human skeletal muscle. *FASEB J,* 30**,** 959-70.

GROOP, L. C., BONADONNA, R. C., DELPRATO, S., RATHEISER, K., ZYCK, K., FERRANNINI, E. & DEFRONZO, R. A. 1989. Glucose and free fatty acid metabolism in non-insulin-dependent diabetes mellitus. Evidence for multiple sites of insulin resistance. *J Clin Invest,* 84**,** 205-13.

GROOP, L. C., SALORANTA, C., SHANK, M., BONADONNA, R. C., FERRANNINI, E. & DEFRONZO, R. A. 1991. The role of free fatty acid metabolism in the pathogenesis of insulin resistance in obesity and noninsulin-dependent diabetes mellitus. *J Clin Endocrinol Metab,* 72**,** 96-107.

GROSSHANS, B. L., ORTIZ, D. & NOVICK, P. 2006. Rabs and their effectors: achieving specificity in membrane traffic. *Proc Natl Acad Sci U S A,* 103**,** 11821-7.

GUERREIRO, V. A., CARVALHO, D. & FREITAS, P. 2022. Obesity, Adipose Tissue, and Inflammation Answered in Questions. *J Obes,* 2022**,** 2252516.

GUNSCHMANN, C., CHITICARIU, E., GARG, B., HIZ, M. M., MOSTMANS, Y., WEHNER, M. & SCHARFENBERGER, L. 2014. Transgenic mouse technology in skin biology: inducible gene knockout in mice. *J Invest Dermatol,* 134**,** 1-4.

GURLEY, J. M., GRIESEL, B. A. & OLSON, A. L. 2016. Increased Skeletal Muscle GLUT4 Expression in Obese Mice After Voluntary Wheel Running Exercise Is Posttranscriptional. *Diabetes,* 65**,** 2911-9.

GUSAROVA, V., O'DUSHLAINE, C., TESLOVICH, T. M., BENOTTI, P. N., MIRSHAHI, T., GOTTESMAN, O., VAN HOUT, C. V., MURRAY, M. F., MAHAJAN, A., NIELSEN, J. B., FRITSCHE, L., WULFF, A. B., GUDBJARTSSON, D. F., SJOGREN, M., EMDIN, C. A., SCOTT, R. A., LEE, W. J., SMALL, A., KWEE, L. C., DWIVEDI, O. P., PRASAD, R. B., BRUSE, S., LOPEZ, A. E., PENN, J., MARCKETTA, A., LEADER, J. B., STILL, C. D., KIRCHNER, H. L., MIRSHAHI, U. L., WARDEH, A. H., HARTLE, C. M., HABEGGER, L., FETTEROLF, S. N., TUSIE-LUNA, T., MORRIS, A. P., HOLM, H., STEINTHORSDOTTIR, V., SULEM, P., THORSTEINSDOTTIR, U., ROTTER, J. I., CHUANG, L. M., DAMRAUER, S., BIRTWELL, D., BRUMMETT, C. M., KHERA, A. V., NATARAJAN, P., ORHO-MELANDER, M., FLANNICK, J., LOTTA, L. A., WILLER, C. J., HOLMEN, O. L., RITCHIE, M. D., LEDBETTER, D. H., MURPHY, A. J., BORECKI, I. B., REID, J. G., OVERTON, J. D., HANSSON, O., GROOP, L., SHAH, S. H., KRAUS, W. E., RADER, D. J., CHEN, Y. I., HVEEM, K., WAREHAM, N. J., KATHIRESAN, S., MELANDER, O., STEFANSSON, K., NORDESTGAARD, B. G., TYBJAERG-HANSEN, A., ABECASIS, G. R., ALTSHULER, D., FLOREZ, J. C., BOEHNKE, M., MCCARTHY, M. I., YANCOPOULOS, G. D., CAREY, D. J., SHULDINER, A. R., BARAS, A., DEWEY, F. E. & GROMADA, J. 2018. Genetic inactivation of ANGPTL4 improves glucose homeostasis and is associated with reduced risk of diabetes. *Nat Commun,* 9**,** 2252.

HANSEN, P. A., NOLTE, L. A., CHEN, M. M. & HOLLOSZY, J. O. 1998. Increased GLUT-4 translocation mediates enhanced insulin sensitivity of muscle glucose transport after exercise. *J Appl Physiol (1985),* 85**,** 1218-22.

HANSEN, S. L., BOJSEN-MOLLER, K. N., LUNDSGAARD, A. M., HENDRICH, F. L., NILAS, L., SJOBERG, K. A., HINGST, J. R., SERUP, A. K., OLGUIN, C. H., CARL, C. S., WERNBLAD, L. F., HENNEBERG, M., LUSTRUP, K. M., HANSEN, C., JENSEN, T. E., MADSBAD, S., WOJTASZEWSKI, J. F. P., RICHTER, E. A. & KIENS, B. 2020. Mechanisms Underlying Absent Training-Induced Improvement in Insulin Action in Lean, Hyperandrogenic Women With Polycystic Ovary Syndrome. *Diabetes,* 69**,** 2267-2280.

HARGETT, S. R., WALKER, N. N. & KELLER, S. R. 2016. Rab GAPs AS160 and Tbc1d1 play nonredundant roles in the regulation of glucose and energy homeostasis in mice. *Am J Physiol Endocrinol Metab,* 310**,** E276-88.

HARGREAVES, M. & SPRIET, L. L. 2020. Author Correction: Skeletal muscle energy metabolism during exercise. *Nat Metab,* 2**,** 990.

HASLAM, D. 2010. Obesity and diabetes: the links and common approaches. *Prim Care Diabetes,* 4**,** 105-12.

HAWLEY, J. A., HARGREAVES, M., JOYNER, M. J. & ZIERATH, J. R. 2014. Integrative biology of exercise. *Cell,* 159**,** 738-49.

HAWLEY, J. A. & LECKEY, J. J. 2015. Carbohydrate Dependence During Prolonged, Intense Endurance Exercise. *Sports Med,* 45 Suppl 1**,** S5-12.

HENRY, L. & SHEFF, D. R. 2008. Rab8 regulates basolateral secretory, but not recycling, traffic at the recycling endosome. *Mol Biol Cell,* 19**,** 2059-68.

HERS, H. G. 1976. The control of glycogen metabolism in the liver. *Annu Rev Biochem,* 45**,** 167-89.

HERWIG, R., HARDT, C., LIENHARD, M. & KAMBUROV, A. 2016. Analyzing and interpreting genome data at the network level with ConsensusPathDB. *Nat Protoc,* 11**,** 1889-907.

HSU, C., MOROHASHI, Y., YOSHIMURA, S., MANRIQUE-HOYOS, N., JUNG, S., LAUTERBACH, M. A., BAKHTI, M., GRONBORG, M., MOBIUS, W., RHEE, J., BARR, F. A. & SIMONS, M. 2010. Regulation of exosome secretion by Rab35 and its GTPase-activating proteins TBC1D10A-C. *J Cell Biol,* 189**,** 223-32.

HUANG, W., LIU, Z., YANG, F., ZHOU, H., YONG, X., YANG, X., ZHOU, Y., XUE, L., ZHANG, Y., LIU, D., MENG, W., ZHANG, W., ZHANG, X., SHEN, X., SUN, Q., LI, L., MA, C., WEI, Y., BILLADEAU, D. D.,

MO, X. & JIA, D. 2019. Structural and functional studies of TBC1D23 C-terminal domain provide a link between endosomal trafficking and PCH. *Proc Natl Acad Sci U S A,* 116**,** 22598-22608.

HUE, L. & TAEGTMEYER, H. 2009. The Randle cycle revisited: a new head for an old hat. *Am J Physiol Endocrinol Metab,* 297**,** E578-91.

HUGHES, D. C., ELLEFSEN, S. & BAAR, K. 2018. Adaptations to Endurance and Strength Training. *Cold Spring Harb Perspect Med,* 8.

HULVER, M. W., BERGGREN, J. R., CORTRIGHT, R. N., DUDEK, R. W., THOMPSON, R. P., PORIES, W. J., MACDONALD, K. G., CLINE, G. W., SHULMAN, G. I., DOHM, G. L. & HOUMARD, J. A. 2003. Skeletal muscle lipid metabolism with obesity. *Am J Physiol Endocrinol Metab,* 284**,** E741-7.

IBANEZ, J., IZQUIERDO, M., ARGUELLES, I., FORGA, L., LARRION, J. L., GARCIA-UNCITI, M., IDOATE, F. & GOROSTIAGA, E. M. 2005. Twice-weekly progressive resistance training decreases abdominal fat and improves insulin sensitivity in older men with type 2 diabetes. *Diabetes Care,* 28**,** 662-7.

IDF 2021. IDF Diabetes Atlas.

ITANI, S. I., ZHOU, Q., PORIES, W. J., MACDONALD, K. G. & DOHM, G. L. 2000. Involvement of protein kinase C in human skeletal muscle insulin resistance and obesity. *Diabetes,* 49**,** 1353-8.

ITOH, T. & FUKUDA, M. 2006. Identification of EPI64 as a GTPase-activating protein specific for Rab27A. *J Biol Chem,* 281**,** 31823-31.

IZUMI, T. 2021. In vivo Roles of Rab27 and Its Effectors in Exocytosis. *Cell Struct Funct,* 46**,** 79-94.

JACOBS, R. A., FLUCK, D., BONNE, T. C., BURGI, S., CHRISTENSEN, P. M., TOIGO, M. & LUNDBY, C. 2013. Improvements in exercise performance with high-intensity interval training coincide with an increase in skeletal muscle mitochondrial content and function. *J Appl Physiol (1985),* 115**,** 785-93.

JAGER, J., GREMEAUX, T., CORMONT, M., LE MARCHAND-BRUSTEL, Y. & TANTI, J. F. 2007. Interleukin-1beta-induced insulin resistance in adipocytes through down-regulation of insulin receptor substrate-1 expression. *Endocrinology,* 148**,** 241-51.

JAMES, D. E., BURLEIGH, K. M. & KRAEGEN, E. W. 1985. Time dependence of insulin action in muscle and adipose tissue in the rat in vivo. An increasing response in adipose tissue with time. *Diabetes,* 34**,** 1049-54.

JEDD, G., MULHOLLAND, J. & SEGEV, N. 1997. Two new Ypt GTPases are required for exit from the yeast trans-Golgi compartment. *J Cell Biol,* 137**,** 563-80.

JIN, Y., SULTANA, A., GANDHI, P., FRANKLIN, E., HAMAMOTO, S., KHAN, A. R., MUNSON, M., SCHEKMAN, R. & WEISMAN, L. S. 2011. Myosin V transports secretory vesicles via a Rab GTPase cascade and interaction with the exocyst complex. *Dev Cell,* 21**,** 1156-70.

JINDAL, A., GARCIA-TOUZA, M., JINDAL, N., WHALEY-CONNELL, A. & SOWERS, J. R. 2013. Diabetic kidney disease and the cardiorenal syndrome: old disease, new perspectives. *Endocrinol Metab Clin North Am,* 42**,** 789-808.

JOHANSEN, M. Y., MACDONALD, C. S., HANSEN, K. B., KARSTOFT, K., CHRISTENSEN, R., PEDERSEN, M., HANSEN, L. S., ZACHO, M., WEDELL-NEERGAARD, A. S., NIELSEN, S. T., IEPSEN, U. W., LANGBERG, H., VAAG, A. A., PEDERSEN, B. K. & RIED-LARSEN, M. 2017. Effect of an Intensive Lifestyle Intervention on Glycemic Control in Patients With Type 2 Diabetes: A Randomized Clinical Trial. *JAMA,* 318**,** 637-646.

JORGE, M. L., DE OLIVEIRA, V. N., RESENDE, N. M., PARAISO, L. F., CALIXTO, A., DINIZ, A. L., RESENDE, E. S., ROPELLE, E. R., CARVALHEIRA, J. B., ESPINDOLA, F. S., JORGE, P. T. & GELONEZE, B. 2011. The effects of aerobic, resistance, and combined exercise on metabolic control, inflammatory markers, adipocytokines, and muscle insulin signaling in patients with type 2 diabetes mellitus. *Metabolism,* 60**,** 1244-52.

KADOGLOU, N. P., ILIADIS, F., ANGELOPOULOU, N., PERREA, D., AMPATZIDIS, G., LIAPIS, C. D. & ALEVIZOS, M. 2007. The anti-inflammatory effects of exercise training in patients with type 2 diabetes mellitus. *Eur J Cardiovasc Prev Rehabil,* 14**,** 837-43.

KAHN, C. R., WANG, G. & LEE, K. Y. 2019. Altered adipose tissue and adipocyte function in the pathogenesis of metabolic syndrome. *J Clin Invest,* 129**,** 3990-4000.

KAPELLER, M., GAL-OZ, R., GROVER, N. B. & DOLJANSKI, F. 1973. Natural shedding of carbohydrate-containing macromolecules from cell surfaces. *Exp Cell Res,* 79**,** 152-8.

KELLERER, M., MUSHACK, J., SEFFER, E., MISCHAK, H., ULLRICH, A. & HARING, H. U. 1998. Protein kinase C isoforms alpha, delta and theta require insulin receptor substrate-1 to inhibit the tyrosine kinase activity of the insulin receptor in human kidney embryonic cells (HEK 293 cells). *Diabetologia,* 41**,** 833-8.

KELLEY, D. E., GOODPASTER, B., WING, R. R. & SIMONEAU, J. A. 1999. Skeletal muscle fatty acid metabolism in association with insulin resistance, obesity, and weight loss. *Am J Physiol,* 277**,** E1130-41.

KERSTEN, S. & STIENSTRA, R. 2017. The role and regulation of the peroxisome proliferator activated receptor alpha in human liver. *Biochimie,* 136**,** 75-84.

KHALAFI, M., RAVASI, A. A., MALANDISH, A. & ROSENKRANZ, S. K. 2022. The impact of high-intensity interval training on postprandial glucose and insulin: A systematic review and meta-analysis. *Diabetes Res Clin Pract,* 186**,** 109815.

KIM, H., KIM, M., IM, S. K. & FANG, S. 2018a. Mouse Cre-LoxP system: general principles to determine tissue-specific roles of target genes. *Lab Anim Res,* 34**,** 147-159.

KIM, H. J., LEE, J. S. & KIM, C. K. 2004. Effect of exercise training on muscle glucose transporter 4 protein and intramuscular lipid content in elderly men with impaired glucose tolerance. *Eur J Appl Physiol,* 93**,** 353-8.

KIM, J., GEE, H. Y. & LEE, M. G. 2018b. Unconventional protein secretion - new insights into the pathogenesis and therapeutic targets of human diseases. *J Cell Sci,* 131.

KIRWAN, J. P., SACKS, J. & NIEUWOUDT, S. 2017. The essential role of exercise in the management of type 2 diabetes. *Cleve Clin J Med,* 84**,** S15-S21.

KITABCHI, A. E., UMPIERREZ, G. E., MILES, J. M. & FISHER, J. N. 2009. Hyperglycemic crises in adult patients with diabetes. *Diabetes Care,* 32**,** 1335-43.

KITTAH, N. E. & VELLA, A. 2017. MANAGEMENT OF ENDOCRINE DISEASE: Pathogenesis and management of hypoglycemia. *Eur J Endocrinol,* 177**,** R37-R47.

KJOBSTED, R., CHADT, A., JORGENSEN, N. O., KIDO, K., LARSEN, J. K., DE WENDT, C., AL-HASANI, H. & WOJTASZEWSKI, J. F. P. 2019a. TBC1D4 Is Necessary for Enhancing Muscle Insulin Sensitivity in Response to AICAR and Contraction. *Diabetes,* 68**,** 1756-1766.

KJOBSTED, R., ROLL, J. L. W., JORGENSEN, N. O., BIRK, J. B., FORETZ, M., VIOLLET, B., CHADT, A., AL-HASANI, H. & WOJTASZEWSKI, J. F. P. 2019b. AMPK and TBC1D1 Regulate Muscle Glucose Uptake After, but Not During, Exercise and Contraction. *Diabetes,* 68**,** 1427-1440.

KLEINERT, M., PARKER, B. L., JENSEN, T. E., RAUN, S. H., PHAM, P., HAN, X., JAMES, D. E., RICHTER, E. A. & SYLOW, L. 2018. Quantitative proteomic characterization of cellular pathways associated with altered insulin sensitivity in skeletal muscle following high-fat diet feeding and exercise training. *Sci Rep,* 8**,** 10723.

KNUIMAN, P., HOPMAN, M. T. & MENSINK, M. 2015. Glycogen availability and skeletal muscle adaptations with endurance and resistance exercise. *Nutr Metab (Lond),* 12**,** 59.

KOCSIS, T., TRENCSENYI, G., SZABO, K., BAAN, J. A., MULLER, G., MENDLER, L., GARAI, I., REINAUER, H., DEAK, F., DUX, L. & KELLER-PINTER, A. 2017. Myostatin propeptide mutation of the hypermuscular Compact mice decreases the formation of myostatin and improves insulin sensitivity. *Am J Physiol Endocrinol Metab,* 312**,** E150-E160.

KOLNES, K. J., PETERSEN, M. H., LIEN-IVERSEN, T., HOJLUND, K. & JENSEN, J. 2021. Effect of Exercise Training on Fat Loss-Energetic Perspectives and the Role of Improved Adipose Tissue Function and Body Fat Distribution. *Front Physiol,* 12**,** 737709.

KONOPKA, A. R. & HARBER, M. P. 2014. Skeletal muscle hypertrophy after aerobic exercise training. *Exerc Sport Sci Rev,* 42**,** 53-61.

KOTANI, K., PERONI, O. D., MINOKOSHI, Y., BOSS, O. & KAHN, B. B. 2004. GLUT4 glucose transporter deficiency increases hepatic lipid production and peripheral lipid utilization. *J Clin Invest,* 114**,** 1666-75.

KRAMER, H. F., WITCZAK, C. A., TAYLOR, E. B., FUJII, N., HIRSHMAN, M. F. & GOODYEAR, L. J. 2006. AS160 regulates insulin- and contraction-stimulated glucose uptake in mouse skeletal muscle. *J Biol Chem,* 281**,** 31478-85.

KRAUSE, M. P., MILNE, K. J. & HAWKE, T. J. 2019. Adiponectin-Consideration for its Role in Skeletal Muscle Health. *Int J Mol Sci,* 20.

KUO, C. H., HUNT, D. G., DING, Z. & IVY, J. L. 1999. Effect of carbohydrate supplementation on postexercise GLUT-4 protein expression in skeletal muscle. *J Appl Physiol (1985),* 87**,** 2290-5.

LANGFORT, J., VIESE, M., PLOUG, T. & DELA, F. 2003. Time course of GLUT4 and AMPK protein expression in human skeletal muscle during one month of physical training. *Scand J Med Sci Sports,* 13**,** 169-74.

LANSEY, M. N., WALKER, N. N., HARGETT, S. R., STEVENS, J. R. & KELLER, S. R. 2012. Deletion of Rab GAP AS160 modifies glucose uptake and GLUT4 translocation in primary skeletal muscles and adipocytes and impairs glucose homeostasis. *Am J Physiol Endocrinol Metab,* 303**,** E1273-86.

LAURENS, C. & MORO, C. 2016. Intramyocellular fat storage in metabolic diseases. *Horm Mol Biol Clin Investig,* 26**,** 43-52.

LI, J., WANG, J., GREWAL, Y. S., HOWARD, C. B., RAFTERY, L. J., MAHLER, S., WANG, Y. & TRAU, M. 2018. Multiplexed SERS Detection of Soluble Cancer Protein Biomarkers with Gold-Silver Alloy Nanoboxes and Nanoyeast Single-Chain Variable Fragments. *Anal Chem,* 90**,** 10377-10384.

LI, L., PAN, R., LI, R., NIEMANN, B., AURICH, A. C., CHEN, Y. & ROHRBACH, S. 2011. Mitochondrial biogenesis and peroxisome proliferator-activated receptor-gamma coactivator-1alpha (PGC-1alpha) deacetylation by physical activity: intact adipocytokine signaling is required. *Diabetes,* 60**,** 157-67.

LI, X. 2019. The FGF metabolic axis. *Front Med,* 13**,** 511-530.

LI, Y., SOOS, T. J., LI, X., WU, J., DEGENNARO, M., SUN, X., LITTMAN, D. R., BIRNBAUM, M. J. & POLAKIEWICZ, R. D. 2004. Protein kinase C Theta inhibits insulin signaling by phosphorylating IRS1 at Ser(1101). *J Biol Chem,* 279**,** 45304-7.

LICHTENTHALER, S. F., LEMBERG, M. K. & FLUHRER, R. 2018. Proteolytic ectodomain shedding of membrane proteins in mammals-hardware, concepts, and recent developments. *EMBO J,* 37.

LITTLE, J. P., SAFDAR, A., WILKIN, G. P., TARNOPOLSKY, M. A. & GIBALA, M. J. 2010. A practical model of low-volume high-intensity interval training induces mitochondrial biogenesis in human skeletal muscle: potential mechanisms. *J Physiol,* 588**,** 1011-22.

LOVE, M. I., HUBER, W. & ANDERS, S. 2014. Moderated estimation of fold change and dispersion for RNA-seq data with DESeq2. *Genome Biol,* 15**,** 550.

LUO, Y., YE, S., KAN, M. & MCKEEHAN, W. L. 2006. Control of fibroblast growth factor (FGF) 7- and FGF1-induced mitogenesis and downstream signaling by distinct heparin octasaccharide motifs. *J Biol Chem,* 281**,** 21052-21061.

LUSTIG, R. H., COLLIER, D., KASSOTIS, C., ROEPKE, T. A., JI KIM, M., BLANC, E., BAROUKI, R., BANSAL, A., CAVE, M. C., CHATTERJEE, S., CHOUDHURY, M., GILBERTSON, M., LAGADIC-GOSSMANN, D., HOWARD, S., LIND, L., TOMLINSON, C. R., VONDRACEK, J. & HEINDEL, J. J. 2022. Obesity I: Overview and molecular and biochemical mechanisms. *Biochem Pharmacol***,** 115012.

MA, X., LIU, Y., WANG, Q., CHEN, Y., LIU, M., LI, X., XIANG, R., WEI, Y., DUAN, Y. & HAN, J. 2015. Tamoxifen induces the development of hernia in mice by activating MMP-2 and MMP-13 expression. *Biochim Biophys Acta,* 1852**,** 1038-48.

MACKRELL, J. G. & CARTEE, G. D. 2012. A novel method to measure glucose uptake and myosin heavy chain isoform expression of single fibers from rat skeletal muscle. *Diabetes,* 61**,** 995-1003.

MADDATU, J., ANDERSON-BAUCUM, E. & EVANS-MOLINA, C. 2017. Smoking and the risk of type 2 diabetes. *Transl Res,* 184**,** 101-107.

MAFAKHERI, S., CHADT, A. & AL-HASANI, H. 2018. Regulation of RabGAPs involved in insulin action. *Biochem Soc Trans,* 46**,** 683-690.

MAGKOS, F., HJORTH, M. F. & ASTRUP, A. 2020. Diet and exercise in the prevention and treatment of type 2 diabetes mellitus. *Nat Rev Endocrinol,* 16**,** 545-555.

MANOUSAKI, D., KENT, J. W., JR., HAACK, K., ZHOU, S., XIE, P., GREENWOOD, C. M., BRASSARD, P., NEWMAN, D. E., COLE, S., UMANS, J. G., ROULEAU, G., COMUZZIE, A. G. & RICHARDS, J. B. 2016. Toward Precision Medicine: TBC1D4 Disruption Is Common Among the Inuit and Leads to Underdiagnosis of Type 2 Diabetes. *Diabetes Care,* 39**,** 1889-1895.

MCCARTHY, J. J., SRIKUEA, R., KIRBY, T. J., PETERSON, C. A. & ESSER, K. A. 2012. Correction: Inducible Cre transgenic mouse strain for skeletal muscle-specific gene targeting. *Skelet Muscle,* 2**,** 22.

MCCONELL, G. K. 2020. It's well and truly time to stop stating that AMPK regulates glucose uptake and fat oxidation during exercise. *Am J Physiol Endocrinol Metab,* 318**,** E564-E567.

MCGARRY, J. D., KUWAJIMA, M., NEWGARD, C. B., FOSTER, D. W. & KATZ, J. 1987. From dietary glucose to liver glycogen: the full circle round. *Annu Rev Nutr,* 7**,** 51-73.

MCGILLICUDDY, F. C., HARFORD, K. A., REYNOLDS, C. M., OLIVER, E., CLAESSENS, M., MILLS, K. H. & ROCHE, H. M. 2011. Lack of interleukin-1 receptor I (IL-1RI) protects mice from high-fat diet-induced adipose tissue inflammation coincident with improved glucose homeostasis. *Diabetes,* 60**,** 1688-98.

MELLMAN, I. & WARREN, G. 2000. The road taken: past and future foundations of membrane traffic. *Cell,* 100**,** 99-112.

MENGESTE, A. M., RUSTAN, A. C. & LUND, J. 2021. Skeletal muscle energy metabolism in obesity. *Obesity (Silver Spring),* 29**,** 1582-1595.

MIINEA, C. P., SANO, H., KANE, S., SANO, E., FUKUDA, M., PERANEN, J., LANE, W. S. & LIENHARD, G. E. 2005. AS160, the Akt substrate regulating GLUT4 translocation, has a functional Rab GTPase-activating protein domain. *Biochem J,* 391**,** 87-93.

MIKLOSZ, A., LUKASZUK, B., SUPRUNIUK, E., GRUBCZAK, K., MONIUSZKO, M., CHOROMANSKA, B., MYSLIWIEC, P. & CHABOWSKI, A. 2021. Does TBC1D4 (AS160) or TBC1D1 Deficiency Affect the Expression of Fatty Acid Handling Proteins in the Adipocytes Differentiated from Human Adipose-Derived Mesenchymal Stem Cells (ADMSCs) Obtained from Subcutaneous and Visceral Fat Depots? *Cells,* 10.

MIKLOSZ, A., LUKASZUK, B., ZENDZIAN-PIOTROWSKA, M., KUREK, K. & CHABOWSKI, A. 2016. The Effects of AS160 Modulation on Fatty Acid Transporters Expression and Lipid Profile in L6 Myotubes. *Cell Physiol Biochem,* 38**,** 267-82.

MILES, J. M., RIZZA, R. A., HAYMOND, M. W. & GERICH, J. E. 1980. Effects of acute insulin deficiency on glucose and ketone body turnover in man: evidence for the primacy of overproduction of glucose and ketone bodies in the genesis of diabetic ketoacidosis. *Diabetes,* 29**,** 926-30.

MINIOU, P., TIZIANO, D., FRUGIER, T., ROBLOT, N., LE MEUR, M. & MELKI, J. 1999. Gene targeting restricted to mouse striated muscle lineage. *Nucleic Acids Res,* 27**,** e27.

MINOKOSHI, Y., KAHN, C. R. & KAHN, B. B. 2003. Tissue-specific ablation of the GLUT4 glucose transporter or the insulin receptor challenges assumptions about insulin action and glucose homeostasis. *J Biol Chem,* 278**,** 33609-12.

MOBLEY, C. B., VECHETTI, I. J., JR., VALENTINO, T. R. & MCCARTHY, J. J. 2020. CORP: Using transgenic mice to study skeletal muscle physiology. *J Appl Physiol (1985),* 128**,** 1227-1239.

MOLTKE, I., GRARUP, N., JORGENSEN, M. E., BJERREGAARD, P., TREEBAK, J. T., FUMAGALLI, M., KORNELIUSSEN, T. S., ANDERSEN, M. A., NIELSEN, T. S., KRARUP, N. T., GJESING, A. P., ZIERATH, J. R., LINNEBERG, A., WU, X., SUN, G., JIN, X., AL-AAMA, J., WANG, J., BORCH-JOHNSEN, K., PEDERSEN, O., NIELSEN, R., ALBRECHTSEN, A. & HANSEN, T. 2014. A common Greenlandic TBC1D4 variant confers muscle insulin resistance and type 2 diabetes. *Nature,* 512**,** 190-3.

MOMENBEITOLLAHI, N., CLOET, T. & LI, H. 2021. Pushing the detection limits: strategies towards highly sensitive optical-based protein detection. *Anal Bioanal Chem,* 413**,** 5995-6011.

MORIGNY, P., BOUCHER, J., ARNER, P. & LANGIN, D. 2021. Lipid and glucose metabolism in white adipocytes: pathways, dysfunction and therapeutics. *Nat Rev Endocrinol,* 17**,** 276-295.

MOTOHASHI, N. & ASAKURA, A. 2014. Muscle satellite cell heterogeneity and self-renewal. *Front Cell Dev Biol,* 2**,** 1.

MU, W. J., ZHU, J. Y., CHEN, M. & GUO, L. 2021. Exercise-Mediated Browning of White Adipose Tissue: Its Significance, Mechanism and Effectiveness. *Int J Mol Sci,* 22.

MUKUND, K. & SUBRAMANIAM, S. 2020. Skeletal muscle: A review of molecular structure and function, in health and disease. *Wiley Interdiscip Rev Syst Biol Med,* 12**,** e1462.

NANDADASA, S., KRAFT, C. M., WANG, L. W., O'DONNELL, A., PATEL, R., GEE, H. Y., GROBE, K., COX, T. C., HILDEBRANDT, F. & APTE, S. S. 2019. Secreted metalloproteases ADAMTS9 and ADAMTS20 have a non-canonical role in ciliary vesicle growth during ciliogenesis. *Nat Commun,* 10**,** 953.

NAVARRO NEGREDO, P., EDGAR, J. R., MANNA, P. T., ANTROBUS, R. & ROBINSON, M. S. 2018. The WDR11 complex facilitates the tethering of AP-1-derived vesicles. *Nat Commun,* 9**,** 596.

NEUFER, P. D. & DOHM, G. L. 1993. Exercise induces a transient increase in transcription of the GLUT-4 gene in skeletal muscle. *Am J Physiol,* 265**,** C1597-603.

NG, J. M., AZUMA, K., KELLEY, C., PENCEK, R., RADIKOVA, Z., LAYMON, C., PRICE, J., GOODPASTER, B. H. & KELLEY, D. E. 2012. PET imaging reveals distinctive roles for different regional adipose tissue depots in systemic glucose metabolism in nonobese humans. *Am J Physiol Endocrinol Metab,* 303**,** E1134-41.

NOVICK, P. 2016. Regulation of membrane traffic by Rab GEF and GAP cascades. *Small GTPases,* 7**,** 252-256.

OSTROWSKI, M., CARMO, N. B., KRUMEICH, S., FANGET, I., RAPOSO, G., SAVINA, A., MOITA, C. F., SCHAUER, K., HUME, A. N., FREITAS, R. P., GOUD, B., BENAROCH, P., HACOHEN, N., FUKUDA, M., DESNOS, C., SEABRA, M. C., DARCHEN, F., AMIGORENA, S., MOITA, L. F. & THERY, C. 2010. Rab27a and Rab27b control different steps of the exosome secretion pathway. *Nat Cell Biol,* 12**,** 19-30; sup pp 1-13.

OWYANG, A. M., MAEDLER, K., GROSS, L., YIN, J., ESPOSITO, L., SHU, L., JADHAV, J., DOMSGEN, E., BERGEMANN, J., LEE, S. & KANTAK, S. 2010. XOMA 052, an anti-IL-1{beta} monoclonal antibody, improves glucose control and {beta}-cell function in the diet-induced obesity mouse model. *Endocrinology,* 151**,** 2515-27.

PALOMER, X., ROMAN-AZCONA, M. S., PIZARRO-DELGADO, J., PLANAVILA, A., VILLARROYA, F., VALENZUELA-ALCARAZ, B., CRISPI, F., SEPULVEDA-MARTINEZ, A., MIGUEL-ESCALADA, I., FERRER, J., NISTAL, J. F., GARCIA, R., DAVIDSON, M. M., BARROSO, E. & VAZQUEZ-CARRERA, M. 2020. SIRT3-mediated inhibition of FOS through histone H3 deacetylation prevents cardiac fibrosis and inflammation. *Signal Transduct Target Ther,* 5**,** 14.

PAN, X. R., LI, G. W., HU, Y. H., WANG, J. X., YANG, W. Y., AN, Z. X., HU, Z. X., LIN, J., XIAO, J. Z., CAO, H. B., LIU, P. A., JIANG, X. G., JIANG, Y. Y., WANG, J. P., ZHENG, H., ZHANG, H., BENNETT, P. H. & HOWARD, B. V. 1997. Effects of diet and exercise in preventing NIDDM in people with impaired glucose tolerance. The Da Qing IGT and Diabetes Study. *Diabetes Care,* 20**,** 537-44.

PEDERSEN, B. K. & FEBBRAIO, M. A. 2008. Muscle as an endocrine organ: focus on muscle-derived interleukin-6. *Physiol Rev,* 88**,** 1379-406.

PEDERSEN, B. K. & FEBBRAIO, M. A. 2012. Muscles, exercise and obesity: skeletal muscle as a secretory organ. *Nat Rev Endocrinol,* 8**,** 457-65.

PEDERSEN, B. K., STEENSBERG, A., FISCHER, C., KELLER, C., KELLER, P., PLOMGAARD, P., WOLSK-PETERSEN, E. & FEBBRAIO, M. 2004. The metabolic role of IL-6 produced during exercise: is IL-6 an exercise factor? *Proc Nutr Soc,* 63**,** 263-7.

PERREAULT, L., NEWSOM, S. A., STRAUSS, A., KEREGE, A., KAHN, D. E., HARRISON, K. A., SNELL-BERGEON, J. K., NEMKOV, T., D'ALESSANDRO, A., JACKMAN, M. R., MACLEAN, P. S. & BERGMAN, B. C. 2018. Intracellular localization of diacylglycerols and sphingolipids influences insulin sensitivity and mitochondrial function in human skeletal muscle. *JCI Insight,* 3.

PESTA, D. H., GONCALVES, R. L. S., MADIRAJU, A. K., STRASSER, B. & SPARKS, L. M. 2017. Resistance training to improve type 2 diabetes: working toward a prescription for the future. *Nutr Metab (Lond),* 14**,** 24.

PETERSEN, M. C. & SHULMAN, G. I. 2018. Mechanisms of Insulin Action and Insulin Resistance. *Physiol Rev,* 98**,** 2133-2223.

PFEFFER, S. & AIVAZIAN, D. 2004. Targeting Rab GTPases to distinct membrane compartments. *Nat Rev Mol Cell Biol,* 5**,** 886-96.

PFEFFER, S. R. 2017. Rab GTPases: master regulators that establish the secretory and endocytic pathways. *Mol Biol Cell,* 28**,** 712-715.

PILEGAARD, H., SALTIN, B. & NEUFER, P. D. 2003. Exercise induces transient transcriptional activation of the PGC-1alpha gene in human skeletal muscle. *J Physiol,* 546**,** 851-8.

PLUDA, S., MAZZOCATO, Y. & ANGELINI, A. 2021. Peptide-Based Inhibitors of ADAM and ADAMTS Metalloproteinases. *Front Mol Biosci,* 8**,** 703715.

PRASAD, R. B. & GROOP, L. 2015. Genetics of type 2 diabetes-pitfalls and possibilities. *Genes (Basel),* 6**,** 87-123.

PRIEST, C. & TONTONOZ, P. 2019. Inter-organ cross-talk in metabolic syndrome. *Nat Metab,* 1**,** 1177-1188.

PRIGENT, M., BOY-MARCOTTE, E., CHESNEAU, L., GIBSON, K., DUPRE-CROCHET, S., TISSERAND, H., VERBAVATZ, J. M. & CUIF, M. H. 2011. The RabGAP proteins Gyp5p and Gyl1p recruit the BAR domain protein Rvs167p for polarized exocytosis. *Traffic,* 12**,** 1084-97.

RABOUILLE, C. 2017. Pathways of Unconventional Protein Secretion. *Trends Cell Biol,* 27**,** 230-240.

RABOUILLE, C., MALHOTRA, V. & NICKEL, W. 2012. Diversity in unconventional protein secretion. *J Cell Sci,* 125**,** 5251-5.

RAO, M. S., VAN VLEET, T. R., CIURLIONIS, R., BUCK, W. R., MITTELSTADT, S. W., BLOMME, E. A. G. & LIGUORI, M. J. 2018. Comparison of RNA-Seq and Microarray Gene Expression Platforms for the Toxicogenomic Evaluation of Liver From Short-Term Rat Toxicity Studies. *Front Genet,* 9**,** 636.

RAUN, S. H., HENRIQUEZ-OLGUIN, C., KARAVAEVA, I., ALI, M., MOLLER, L. L. V., KOT, W., CASTRO-MEJIA, J. L., NIELSEN, D. S., GERHART-HINES, Z., RICHTER, E. A. & SYLOW, L. 2020. Housing temperature influences exercise training adaptations in mice. *Nat Commun,* 11**,** 1560.

RICHTER, E. A. & HARGREAVES, M. 2013. Exercise, GLUT4, and skeletal muscle glucose uptake. *Physiol Rev,* 93**,** 993-1017.

RICHTER, E. A., SYLOW, L. & HARGREAVES, M. 2021. Interactions between insulin and exercise. *Biochem J,* 478**,** 3827-3846.

RIED-LARSEN, M., JOHANSEN, M. Y., MACDONALD, C. S., HANSEN, K. B., CHRISTENSEN, R., WEDELL-NEERGAARD, A. S., PILMARK, N. S., LANGBERG, H., VAAG, A. A., PEDERSEN, B. K. & KARSTOFT, K. 2019. Type 2 diabetes remission 1 year after an intensive lifestyle intervention: A secondary analysis of a randomized clinical trial. *Diabetes Obes Metab,* 21**,** 2257-2266.

RIIS, S., CHRISTENSEN, B., NELLEMANN, B., MOLLER, A. B., HUSTED, A. S., PEDERSEN, S. B., SCHWARTZ, T. W., JORGENSEN, J. O. L. & JESSEN, N. 2019. Molecular adaptations in human subcutaneous adipose tissue after ten weeks of endurance exercise training in healthy males. *J Appl Physiol (1985),* 126**,** 569-577.

RITOV, V. B. & KELLEY, D. E. 2001. Hexokinase isozyme distribution in human skeletal muscle. *Diabetes,* 50**,** 1253-62.

ROACH, W. G., CHAVEZ, J. A., MIINEA, C. P. & LIENHARD, G. E. 2007. Substrate specificity and effect on GLUT4 translocation of the Rab GTPase-activating protein Tbc1d1. *Biochem J,* 403**,** 353-8.

ROBERTS, L. D., BOSTROM, P., O'SULLIVAN, J. F., SCHINZEL, R. T., LEWIS, G. D., DEJAM, A., LEE, Y. K., PALMA, M. J., CALHOUN, S., GEORGIADI, A., CHEN, M. H., RAMACHANDRAN, V. S., LARSON, M. G., BOUCHARD, C., RANKINEN, T., SOUZA, A. L., CLISH, C. B., WANG, T. J., ESTALL, J. L., SOUKAS, A. A., COWAN, C. A., SPIEGELMAN, B. M. & GERSZTEN, R. E. 2014. beta-Aminoisobutyric acid induces browning of white fat and hepatic beta-oxidation and is inversely correlated with cardiometabolic risk factors. *Cell Metab,* 19**,** 96-108.

RODEN, M. 2005. Muscle triglycerides and mitochondrial function: possible mechanisms for the development of type 2 diabetes. *Int J Obes (Lond),* 29 Suppl 2**,** S111-5.

RODEN, M. 2012. Exercise in type 2 diabetes: to resist or to endure? *Diabetologia,* 55**,** 1235-9.

RODEN, M. & SHULMAN, G. I. 2019. The integrative biology of type 2 diabetes. *Nature,* 576**,** 51-60.

RODRIGUEZ, A., CATALAN, V., RAMIREZ, B., UNAMUNO, X., PORTINCASA, P., GOMEZ-AMBROSI, J., FRUHBECK, G. & BECERRIL, S. 2020. Impact of adipokines and myokines on fat browning. *J Physiol Biochem,* 76**,** 227-240.

ROMIJN, J. A., COYLE, E. F., SIDOSSIS, L. S., GASTALDELLI, A., HOROWITZ, J. F., ENDERT, E. & WOLFE, R. R. 1993. Regulation of endogenous fat and carbohydrate metabolism in relation to exercise intensity and duration. *Am J Physiol,* 265**,** E380-91.

RYNDERS, C. A., BLANC, S., DEJONG, N., BESSESEN, D. H. & BERGOUIGNAN, A. 2018. Sedentary behaviour is a key determinant of metabolic inflexibility. *J Physiol,* 596**,** 1319-1330.

SACKS, H. & SYMONDS, M. E. 2013. Anatomical locations of human brown adipose tissue: functional relevance and implications in obesity and type 2 diabetes. *Diabetes,* 62**,** 1783-90.

SAKAMOTO, K. & HOLMAN, G. D. 2008. Emerging role for AS160/TBC1D4 and TBC1D1 in the regulation of GLUT4 traffic. *Am J Physiol Endocrinol Metab,* 295**,** E29-37.

SALEEM, A., ADHIHETTY, P. J. & HOOD, D. A. 2009. Role of p53 in mitochondrial biogenesis and apoptosis in skeletal muscle. *Physiol Genomics,* 37**,** 58-66.

SALEEM, A. & HOOD, D. A. 2013. Acute exercise induces tumour suppressor protein p53 translocation to the mitochondria and promotes a p53-Tfam-mitochondrial DNA complex in skeletal muscle. *J Physiol,* 591**,** 3625-36.

SAMOVSKI, D., SU, X., XU, Y., ABUMRAD, N. A. & STAHL, P. D. 2012. Insulin and AMPK regulate FA translocase/CD36 plasma membrane recruitment in cardiomyocytes via Rab GAP AS160 and Rab8a Rab GTPase. *J Lipid Res,* 53**,** 709-17.

SANGWUNG, P., PETERSEN, K. F., SHULMAN, G. I. & KNOWLES, J. W. 2020. Mitochondrial Dysfunction, Insulin Resistance, and Potential Genetic Implications. *Endocrinology,* 161.

SANO, H., KANE, S., SANO, E., MIINEA, C. P., ASARA, J. M., LANE, W. S., GARNER, C. W. & LIENHARD, G. E. 2003. Insulin-stimulated phosphorylation of a Rab GTPase-activating protein regulates GLUT4 translocation. *J Biol Chem,* 278**,** 14599-602.

SARVAS, M., HARWOOD, C. R., BRON, S. & VAN DIJL, J. M. 2004. Post-translocational folding of secretory proteins in Gram-positive bacteria. *Biochim Biophys Acta,* 1694**,** 311-27.

SAUTER, N. S., SCHULTHESS, F. T., GALASSO, R., CASTELLANI, L. W. & MAEDLER, K. 2008. The antiinflammatory cytokine interleukin-1 receptor antagonist protects from high-fat diet-induced hyperglycemia. *Endocrinology,* 149**,** 2208-18.

SAWANO, S. & MIZUNOYA, W. 2022. History and development of staining methods for skeletal muscle fiber types. *Histol Histopathol***,** 18422.

SCHEEL, A. K., ESPELAGE, L. & CHADT, A. 2022. Many Ways to Rome: Exercise, Cold Exposure and Diet-Do They All Affect BAT Activation and WAT Browning in the Same Manner? *Int J Mol Sci,* 23.

SCHIAFFINO, S. 2018. Muscle fiber type diversity revealed by anti-myosin heavy chain antibodies. *FEBS J,* 285**,** 3688-3694.

SCHIAFFINO, S. & REGGIANI, C. 2011. Fiber types in mammalian skeletal muscles. *Physiol Rev,* 91**,** 1447-531.

SCHIENKIEWITZ, A., MENSINK, G., KUHNERT, R. & LANGE, C. 2017. Übergewicht und Adipositas bei Erwachsenen in Deutschland. *Journal of Health Monitoring*

SCHMIDT, M. O., GARMAN, K. A., LEE, Y. G., ZUO, C., BECK, P. J., TAN, M., AGUILAR-PIMENTEL, J. A., OLLERT, M., SCHMIDT-WEBER, C., FUCHS, H., GAILUS-DURNER, V., HRABE DE ANGELIS, M., GERMAN MOUSE CLINIC, C., TASSI, E., RIEGEL, A. T. & WELLSTEIN, A. 2018. The Role of Fibroblast Growth Factor-Binding Protein 1 in Skin Carcinogenesis and Inflammation. *J Invest Dermatol,* 138**,** 179-188.

SCHNURR, T. M., JORSBOE, E., CHADT, A., DAHL-PETERSEN, I. K., KRISTENSEN, J. M., WOJTASZEWSKI, J. F. P., SPRINGER, C., BJERREGAARD, P., BRAGE, S., PEDERSEN, O., MOLTKE, I., GRARUP, N., AL-HASANI, H., ALBRECHTSEN, A., JORGENSEN, M. E. & HANSEN, T. 2021. Physical activity attenuates postprandial hyperglycaemia in homozygous TBC1D4 loss-of-function mutation carriers. *Diabetologia,* 64**,** 1795-1804.

SEN, S. & DAS, C. 2018. Managing the sugar factory: New feather in the cap for nuclear factor Y. *J Biol Chem,* 293**,** 9651.

SEVERINSEN, M. C. K. & PEDERSEN, B. K. 2020. Muscle-Organ Crosstalk: The Emerging Roles of Myokines. *Endocr Rev,* 41.

SHAO, M., WANG, Q. A., SONG, A., VISHVANATH, L., BUSBUSO, N. C., SCHERER, P. E. & GUPTA, R. K. 2019. Cellular Origins of Beige Fat Cells Revisited. *Diabetes,* 68**,** 1874-1885.

SHIMODA, M. & KHOKHA, R. 2017. Metalloproteinases in extracellular vesicles. *Biochim Biophys Acta Mol Cell Res,* 1864**,** 1989-2000.

SHIN, J. J. H., GILLINGHAM, A. K., BEGUM, F., CHADWICK, J. & MUNRO, S. 2017. TBC1D23 is a bridging factor for endosomal vesicle capture by golgins at the trans-Golgi. *Nat Cell Biol,* 19**,** 1424-1432.

SHULMAN, G. I. 2014. Ectopic fat in insulin resistance, dyslipidemia, and cardiometabolic disease. *N Engl J Med,* 371**,** 1131-41.

SILVER, D. L., HOU, L., SOMERVILLE, R., YOUNG, M. E., APTE, S. S. & PAVAN, W. J. 2008. The secreted metalloprotease ADAMTS20 is required for melanoblast survival. *PLoS Genet,* 4**,** e1000003.

SMITH, P. K., KROHN, R. I., HERMANSON, G. T., MALLIA, A. K., GARTNER, F. H., PROVENZANO, M. D., FUJIMOTO, E. K., GOEKE, N. M., OLSON, B. J. & KLENK, D. C. 1985. Measurement of protein using bicinchoninic acid. *Anal Biochem,* 150**,** 76-85.

SMITH, U. & KAHN, B. B. 2016. Adipose tissue regulates insulin sensitivity: role of adipogenesis, de novo lipogenesis and novel lipids. *J Intern Med,* 280**,** 465-475.

SONG, H., GUAN, Y., ZHANG, L., LI, K. & DONG, C. 2010. SPARC interacts with AMPK and regulates GLUT4 expression. *Biochem Biophys Res Commun,* 396**,** 961-6.

SPRINGER PHD THESIS, C. 2018. Impact of exercise on glucose homeostasis in different mouse models for impaired insulin sensitivity. *Heinrich-Heine-Universität, Düsseldorf, Germany*

STANFORD, K. I., MIDDELBEEK, R. J. & GOODYEAR, L. J. 2015. Exercise Effects on White Adipose Tissue: Beiging and Metabolic Adaptations. *Diabetes,* 64**,** 2361-8.

STEENSBERG, A., VAN HALL, G., KELLER, C., OSADA, T., SCHJERLING, P., PEDERSEN, B. K., SALTIN, B. & FEBBRAIO, M. A. 2002. Muscle glycogen content and glucose uptake during exercise in humans: influence of prior exercise and dietary manipulation. *J Physiol,* 541**,** 273-81.

STENMARK, H. 2009. Rab GTPases as coordinators of vesicle traffic. *Nat Rev Mol Cell Biol,* 10**,** 513-25.

STEPHENSON, E. J., LESSARD, S. J., RIVAS, D. A., WATT, M. J., YASPELKIS, B. B., 3RD, KOCH, L. G., BRITTON, S. L. & HAWLEY, J. A. 2013. Exercise training enhances white adipose tissue metabolism in rats selectively bred for low- or high-endurance running capacity. *Am J Physiol Endocrinol Metab,* 305**,** E429-38.

STUART, C. A., HOWELL, M. E., BAKER, J. D., DYKES, R. J., DUFFOURC, M. M., RAMSEY, M. W. & STONE, M. H. 2010. Cycle training increased GLUT4 and activation of mammalian target of rapamycin in fast twitch muscle fibers. *Med Sci Sports Exerc,* 42**,** 96-106.

STUMVOLL, M., GOLDSTEIN, B. J. & VAN HAEFTEN, T. W. 2005. Type 2 diabetes: principles of pathogenesis and therapy. *Lancet,* 365**,** 1333-46.

SYLOW, L., TOKARZ, V. L., RICHTER, E. A. & KLIP, A. 2021. The many actions of insulin in skeletal muscle, the paramount tissue determining glycemia. *Cell Metab,* 33**,** 758-780.

TAKAHASHI, H., ALVES, C. R. R., STANFORD, K. I., MIDDELBEEK, R. J. W., NIGRO, P., RYAN, R. E., XUE, R., SAKAGUCHI, M., LYNES, M. D., SO, K., MUL, J. D., LEE, M. Y., BALAN, E., PAN, H., DREYFUSS, J. M., HIRSHMAN, M. F., AZHAR, M., HANNUKAINEN, J. C., NUUTILA, P., KALLIOKOSKI, K. K., NIELSEN, S., PEDERSEN, B. K., KAHN, C. R., TSENG, Y. H. & GOODYEAR, L. J. 2019. TGF-beta2 is an exercise-induced adipokine that regulates glucose and fatty acid metabolism. *Nat Metab,* 1**,** 291-303.

TALLQUIST, M. D., WEISMANN, K. E., HELLSTROM, M. & SORIANO, P. 2000. Early myotome specification regulates PDGFA expression and axial skeleton development. *Development,* 127**,** 5059-70.

TAYLOR, E. B., AN, D., KRAMER, H. F., YU, H., FUJII, N. L., ROECKL, K. S., BOWLES, N., HIRSHMAN, M. F., XIE, J., FEENER, E. P. & GOODYEAR, L. J. 2008. Discovery of TBC1D1 as an insulin-, AICAR-, and contraction-stimulated signaling nexus in mouse skeletal muscle. *J Biol Chem,* 283**,** 9787-96.

THOMPSON, D., KARPE, F., LAFONTAN, M. & FRAYN, K. 2012. Physical activity and exercise in the regulation of human adipose tissue physiology. *Physiol Rev,* 92**,** 157-91.

TREEBAK, J. T., PEHMOLLER, C., KRISTENSEN, J. M., KJOBSTED, R., BIRK, J. B., SCHJERLING, P., RICHTER, E. A., GOODYEAR, L. J. & WOJTASZEWSKI, J. F. 2014. Acute exercise and physiological insulin

induce distinct phosphorylation signatures on TBC1D1 and TBC1D4 proteins in human skeletal muscle. *J Physiol,* 592**,** 351-75.

TUOMILEHTO, J., LINDSTROM, J., ERIKSSON, J. G., VALLE, T. T., HAMALAINEN, H., ILANNE-PARIKKA, P., KEINANEN-KIUKAANNIEMI, S., LAAKSO, M., LOUHERANTA, A., RASTAS, M., SALMINEN, V., UUSITUPA, M. & FINNISH DIABETES PREVENTION STUDY, G. 2001. Prevention of type 2 diabetes mellitus by changes in lifestyle among subjects with impaired glucose tolerance. *N Engl J Med,* 344**,** 1343-50.

VALADI, H., EKSTROM, K., BOSSIOS, A., SJOSTRAND, M., LEE, J. J. & LOTVALL, J. O. 2007. Exosome-mediated transfer of mRNAs and microRNAs is a novel mechanism of genetic exchange between cells. *Nat Cell Biol,* 9**,** 654-9.

VAN LOON, L. J., GREENHAFF, P. L., CONSTANTIN-TEODOSIU, D., SARIS, W. H. & WAGENMAKERS, A. J. 2001. The effects of increasing exercise intensity on muscle fuel utilisation in humans. *J Physiol,* 536**,** 295-304.

VARGA, T., CZIMMERER, Z. & NAGY, L. 2011. PPARs are a unique set of fatty acid regulated transcription factors controlling both lipid metabolism and inflammation. *Biochim Biophys Acta,* 1812**,** 1007-22.

VIND, B. F., PEHMOLLER, C., TREEBAK, J. T., BIRK, J. B., HEY-MOGENSEN, M., BECK-NIELSEN, H., ZIERATH, J. R., WOJTASZEWSKI, J. F. & HOJLUND, K. 2011. Impaired insulin-induced site-specific phosphorylation of TBC1 domain family, member 4 (TBC1D4) in skeletal muscle of type 2 diabetes patients is restored by endurance exercise-training. *Diabetologia,* 54**,** 157-67.

VINIK, A. I., NEVORET, M. L., CASELLINI, C. & PARSON, H. 2013. Diabetic neuropathy. *Endocrinol Metab Clin North Am,* 42**,** 747-87.

VIOTTI, C. 2016. ER to Golgi-Dependent Protein Secretion: The Conventional Pathway. *Methods Mol Biol,* 1459**,** 3-29.

WALCH-SOLIMENA, C., COLLINS, R. N. & NOVICK, P. J. 1997. Sec2p mediates nucleotide exchange on Sec4p and is involved in polarized delivery of post-Golgi vesicles. *J Cell Biol,* 137**,** 1495-509.

WANG, H., ARIAS, E. B., PATAKY, M. W., GOODYEAR, L. J. & CARTEE, G. D. 2018. Postexercise improvement in glucose uptake occurs concomitant with greater gamma3-AMPK activation and AS160 phosphorylation in rat skeletal muscle. *Am J Physiol Endocrinol Metab,* 315**,** E859-E871.

WANG, H. Y., DUCOMMUN, S., QUAN, C., XIE, B., LI, M., WASSERMAN, D. H., SAKAMOTO, K., MACKINTOSH, C. & CHEN, S. 2013. AS160 deficiency causes whole-body insulin resistance via composite effects in multiple tissues. *Biochem J,* 449**,** 479-89.

WANG, W. & LO, A. C. Y. 2018. Diabetic Retinopathy: Pathophysiology and Treatments. *Int J Mol Sci,* 19.

WASSERMAN, D. H. 2009. Four grams of glucose. *Am J Physiol Endocrinol Metab,* 296**,** E11-21.

WATT, M. J. & HOY, A. J. 2012. Lipid metabolism in skeletal muscle: generation of adaptive and maladaptive intracellular signals for cellular function. *Am J Physiol Endocrinol Metab,* 302**,** E1315-28.

WEIGERT, C., HOENE, M. & PLOMGAARD, P. 2019. Hepatokines-a novel group of exercise factors. *Pflugers Arch,* 471**,** 383-396.

WEIMERSHAUS, M., MAUVAIS, F. X., SAVEANU, L., ADIKO, C., BABDOR, J., ABRAMOVA, A., MONTEALEGRE, S., LAWAND, M., EVNOUCHIDOU, I., HUBER, K. J., CHADT, A., ZWICK, M., VARGAS, P., DUSSIOT, M., LENNON-DUMENIL, A. M., BROCKER, T., AL-HASANI, H. & VAN ENDERT, P. 2018. Innate Immune Signals Induce Anterograde Endosome Transport Promoting MHC Class I Cross-Presentation. *Cell Rep,* 24**,** 3568-3581.

WHITFIELD, J., LITTLEWOOD, T. & SOUCEK, L. 2015. Tamoxifen administration to mice. *Cold Spring Harb Protoc,* 2015**,** 269-71.

WHO 2000. Obesity: preventing and managing the global epidemic: report of a WHO consultation.

WHO 2021. Obesity and overweight

WIESNER, C., EL AZZOUZI, K. & LINDER, S. 2013. A specific subset of RabGTPases controls cell surface exposure of MT1-MMP, extracellular matrix degradation and three-dimensional invasion of macrophages. *J Cell Sci,* 126**,** 2820-33.

WONG, N. D., ZHAO, Y., PATEL, R., PATAO, C., MALIK, S., BERTONI, A. G., CORREA, A., FOLSOM, A. R., KACHROO, S., MUKHERJEE, J., TAYLOR, H. & SELVIN, E. 2016. Cardiovascular Risk Factor Targets and Cardiovascular Disease Event Risk in Diabetes: A Pooling Project of the Atherosclerosis Risk in Communities Study, Multi-Ethnic Study of Atherosclerosis, and Jackson Heart Study. *Diabetes Care,* 39**,** 668-76.

WOZNIAK, J., FLOEGE, J., OSTENDORF, T. & LUDWIG, A. 2021. Key metalloproteinase-mediated pathways in the kidney. *Nat Rev Nephrol,* 17**,** 513-527.

WU, H. & BALLANTYNE, C. M. 2017. Skeletal muscle inflammation and insulin resistance in obesity. *J Clin Invest,* 127**,** 43-54.

WU, H. & BALLANTYNE, C. M. 2020. Metabolic Inflammation and Insulin Resistance in Obesity. *Circ Res,* 126**,** 1549-1564.

WU, M. V., BIKOPOULOS, G., HUNG, S. & CEDDIA, R. B. 2014. Thermogenic capacity is antagonistically regulated in classical brown and white subcutaneous fat depots by high fat diet and endurance training in rats: impact on whole-body energy expenditure. *J Biol Chem,* 289**,** 34129-40.

XIE, B., CHEN, Q., CHEN, L., SHENG, Y., WANG, H. Y. & CHEN, S. 2016. The Inactivation of RabGAP Function of AS160 Promotes Lysosomal Degradation of GLUT4 and Causes Postprandial Hyperglycemia and Hyperinsulinemia. *Diabetes,* 65**,** 3327-3340.

YABLONKA-REUVENI, Z. & RIVERA, A. J. 1997. Proliferative Dynamics and the Role of FGF2 During Myogenesis of Rat Satellite Cells on Isolated Fibers. *Basic Appl Myol,* 7**,** 189-202.

YANG, J. & HOLMAN, G. D. 2005. Insulin and contraction stimulate exocytosis, but increased AMP-activated protein kinase activity resulting from oxidative metabolism stress slows endocytosis of GLUT4 in cardiomyocytes. *J Biol Chem,* 280**,** 4070-8.

YANG, W. H., PARK, H., GRAU, M. & HEINE, O. 2020. Decreased Blood Glucose and Lactate: Is a Useful Indicator of Recovery Ability in Athletes? *Int J Environ Res Public Health,* 17.

YANG, X., CHEN, Q., OUYANG, Q., RONG, P., FENG, W., QUAN, C., LI, M., JIANG, Q., LIANG, H., ZHAO, T. J., WANG, H. Y. & CHEN, S. 2021. Tissue-Specific Splicing and Dietary Interaction of a Mutant As160 Allele Determine Muscle Metabolic Fitness in Rodents. *Diabetes,* 70**,** 1826-1842.

YASUDA, T. & FUKUDA, M. 2014. Slp2-a controls renal epithelial cell size through regulation of Rap-ezrin signaling independently of Rab27. *J Cell Sci,* 127**,** 557-70.

YOSHINOBU, K., ARAKI, M., MORITA, A., ARAKI, M., KOKUBA, S., NAKAGATA, N. & ARAKI, K. 2021. Tamoxifen feeding method is suitable for efficient conditional knockout. *Exp Anim,* 70**,** 91-100.

YU, C., CHEN, Y., CLINE, G. W., ZHANG, D., ZONG, H., WANG, Y., BERGERON, R., KIM, J. K., CUSHMAN, S. W., COONEY, G. J., ATCHESON, B., WHITE, M. F., KRAEGEN, E. W. & SHULMAN, G. I. 2002. Mechanism by which fatty acids inhibit insulin activation of insulin receptor substrate-1 (IRS-1)-associated phosphatidylinositol 3-kinase activity in muscle. *J Biol Chem,* 277**,** 50230-6.

ZANUSO, S., JIMENEZ, A., PUGLIESE, G., CORIGLIANO, G. & BALDUCCI, S. 2010. Exercise for the management of type 2 diabetes: a review of the evidence. *Acta Diabetol,* 47**,** 15-22.

ZERIAL, M. & MCBRIDE, H. 2001. Rab proteins as membrane organizers. *Nat Rev Mol Cell Biol,* 2**,** 107-17.

ZHANG, H., MA, J., TANG, K. & HUANG, B. 2021. Beyond energy storage: roles of glycogen metabolism in health and disease. *FEBS J,* 288**,** 3772-3783.

ZHANG, X., IBRAHIMI, O. A., OLSEN, S. K., UMEMORI, H., MOHAMMADI, M. & ORNITZ, D. M. 2006. Receptor specificity of the fibroblast growth factor family. The complete mammalian FGF family. *J Biol Chem,* 281**,** 15694-700.

ZHANG, X., YANG, S., CHEN, J. & SU, Z. 2018. Unraveling the Regulation of Hepatic Gluconeogenesis. *Front Endocrinol (Lausanne),* 9**,** 802.

ZHOU, Z., MENZEL, F., BENNINGHOFF, T., CHADT, A., DU, C., HOLMAN, G. D. & AL-HASANI, H. 2017. Rab28 is a TBC1D1/TBC1D4 substrate involved in GLUT4 trafficking. *FEBS Lett,* 591**,** 88-96.

ZICK, Y. 2005. Ser/Thr phosphorylation of IRS proteins: a molecular basis for insulin resistance. *Sci STKE,* 2005**,** pe4.

7 Supplement

7.1 Contribution to manuscripts

1) Mafakheri S, Flörke R, Kanngießer S, Hartwig S, **Espelage L**, De Wendt C, Schönberger T, Hamker N, Lehr S, Chadt A, Al-Hasani A (2018). AKT and AMP-activated protein kinase regulate TBC1D1 through phosphorylation and its interaction with the cytosolic tail of insulin-regulated aminopeptidase IRAP. *The Journal of biological chemistry*. doi: 10.1074/jbc.RA118.005040.

   Contribution: I was involved in the interpretation of the data.

2) **Espelage L**, Al-Hasani H, Chadt A (2020). RabGAPs in skeletal muscle function and exercise. *Journal of molecular endocrinology*. doi: 10.1530/JME-19-0143

   Contribution: I wrote the review.

3) Benninghoff T, **Espelage L**, Eickelschulte S, Zeinert I, Sinowenka I, Müller F, Schöndeling C, Batchelor H, Cames S, Zhou Z, Kotzka J, Chadt A, Al-Hasani, H (2020). The RabGAPs TBC1D1 and TBC1D4 Control Uptake of Long-Chain Fatty Acids Into Skeletal Muscle via Fatty Acid Transporter SLC27A4/FATP4. *Diabetes*. doi: 10.2337/db20-0180

   Contribution: Mouse hind limb *in vivo* electroporation (IVE) with *Fatp4* oligonucleotides was performed by myself. In addition, I verified the FATP4 knockdown efficiency via Western blot technology. Furthermore, I performed the *ex vivo* fatty acid oxidation (Figure 4D-F).

4) De Wendt C*, **Espelage L***, Eickelschulte S, Springer C, Toska L, Scheel A, Bedou Awovi Didi, Benninghoff T, Cames S, Stermann T, Chadt A, Al-Hasani H (2021). Contraction-Mediated Glucose Transport in Skeletal Muscle Is Regulated by a Framework of AMPK, TBC1D1/4, and Rac1. *Diabetes*. doi: 10.2337/db21-0587

   * equal contribution

   Contribution: Shared first author. The contraction-stimulated glucose uptake with prior Rac1 inhibition was performed by myself (Figure 6F). Furthermore, I analyzed and interpreted the data, as well wrote and edited large parts of the manuscript.

5) Scheel A, **Espelage L**, Chadt A (2022). Many Ways to Rome: Exercise, Cold Exposure and Diet-Do They All Affect BAT Activation and WAT Browning in the Same Manner? *International journal of molecular sciences*. doi: 10.3390/ijms23094759

   Contribution: I was involved in the writing process.

Further, parts of this thesis shall be published in a separate paper. The manuscript is currently under preparation:

6) **Espelage L**, Tautz M, Binsch C, Springer C, Scheel A, Saurbier S, Hartwig S, Lehr S, Cames S, Knebel B, Fahlbusch P, Al-Hasani H, Chadt A (in preparation). Working title: “Skeletal muscle and adipose tissue equally contribute to exercise-induced improvements of *Tbc1d4*-deficient mice”

7.2 Abbreviations

Acetyl-CoA	Acetyl coenzyme A
aD4KO	adipocyte-specific *Tbc1d4*-deficient mouse
ADP	Adenosine diphosphate
AMPK	AMP-activated protein kinase
ANGPTL4	Angiopoietin-like protein 4
APS	Ammonium persulfate
AS160	Akt substrate of 160 kDa
ATP	Adenosine triphosphate
AUC	Area under the curve
BAT	Brown adipose tissue
BCA	Bicinchonic acid assay
BeAT	Beige adipose tissue
Bp	Base pair
BSA	Bovine serum albumin
CBD	Calmodulin binding domain
CCL2	CC-chemokine ligand 2
CPDB	ConsensusPathDB
Cpm	Counts per minute
CPT-1	Carnitine palmitoyltransferase 1
CreER	Mutated estrogen receptor ligand binding domain
D4KO	*Tbc1d4*-deficient mouse
DAG	Diacylglycerol
DNL	*De novo* lipogenesis
dNTP	Deoxynucleoside triphosphate
ECM	Extracellular matrix
EDTA	Ethylenediaminetetraacetic acid

EGTA	Ethylene glycol bis (2-aminoethylether)-N, N, N', N'-tetra acetic acid
EtOH	Ethanol
ER	Endoplasmic reticulum
ESR1	Estrogen receptor α
ER	Extracellular vesicle
$FADH_2$	Flavin adenine dinucleotide
FABPpm	Fatty acid-binding protein
FAO	Fatty acid oxidation
FAT/CD36	Fatty acid translocase
FATP1	Fatty acid transporter protein 1
FATP4	Fatty acid transporter protein 4
FFA	Free fatty acids
FGF	Fibroblast growth factor
FGFBP1	Fibroblast growth factor-binding protein 1
Flp	Flippase
FRT	Flippase recognition target
G1P	Glucose-1-phosphate
G6P	Glucose-6-phosphate
GAP	GTPase activating protein
GAPDH	Glyceraldehyde 3-phosphate dehydrogenase
GEF	Guanine nucleotide exchange factor
GIP	Glucose-dependent insulinotropic polypeptide
GLP-1	Glucagon-like peptide-1
GLUT1	Glucose transporter type 1
GLUT4	Glucose transporter type 4
GO	Gene ontology
GS	Glycogen synthase
GSV	GLUT4 containing storage vesicle

GTT	Glucose tolerance test
HCL	Hydrochloric acid
HFD	High fat diet
HIIT	High intensity interval training
HEPES	4-(2-hydroxyethyl)-1-piperazineethanesulfonic acid
HRP	horseradish-peroxidase
HSA	Human-skeletal actin
HSP90	Heat shock protein 90
IL	Interleukin
IMCL	Intramyocellular lipids
I.p.	Intraperitoneal
IPA	Ingenuity Pathway Analysis
IR	Insulin receptor
IRAP	Insulin-regulated aminopeptidase
IRS	Insulin receptor substrate
ITT	Insulin tolerance test
KHB	Krebs-Henseleit buffer
KO	Knockout
KOMP	Knockout mouse project
KRBH	Krebs-Ringer-Bicarbonate HEPES buffer
LCFA	Long-chain fatty acids
LKB1	Liver kinase 1
mD4KO	Muscle-specific *Tbc1d4*-deficient mouse
MVE	Multivesicular endosome
NADH	Nicotinamide adenine dinucleotide
NEFA	Non-esterified free fatty acids
NMR	Nuclear magnetic resonance
NZO	New Zealand obese

PCA	Principal Component Analysis
PCR	Polymerase chain reaction
PDH	Pyruvate dehydrogenase
PI3K	Phosphatidylinositol-3'-kinase
PIP_2	Phosphatidylinositol (4,5)-bisphosphate
PIP_3	Phosphatidylinositol (3,4,5)-trisphosphate
PGC1α	Peroxisome proliferator-activated receptor gamma coactivator 1-alpha
PKB	Protein kinase B
PPAR	Peroxisome proliferator-activated receptor
PTB	Phosphotyrosine binding domain
Rab	Ras related in brain
RabGAP	Rab-GTPase-activating protein
RER	Respiratory exchange ratio
RT	Room temperature
SC	Satellite cells
scWAT	Subcutaneous white adipose tissue
SD	Standard diet
SDS	Sodium dodecyl sulfate
SEM	Standard error oft he mean
Ser	Serine
T1DM	Type 1 diabetes mellitus
T2DM	Type 2 diabetes mellitus
TCA	tricarboxylic acid
TEMED	N, N, N', N'-Tetramethylendiamine
TGF-β_2	Transforming growth factor-β_2
TGN	Trans-Golgi-Network
Thr	Threonine
UCP1	Uncoupling protein 1

UDP	Uridine diphoshate
UPS	Unconventional protein secretion
visWAT	Visceral white adipose tissue
VO_{2max}	Maximal oxygen consumption
WAT	White adipose tissue
WHO	World Health Organization
WT	Wildtype

7.3 Supplemental Tables

Supplemental Table 1: Treadmill training protocol used for mD4KO and aD4KO mice.

Week	Training	Monday	Tuesday	Wednesday	Thursday	Friday
1	Warm-up	5 min 6 m/min		5 min 6 m/min	5 min 6 m/min	
	Training	5 min 6-9 m/min 5 min 9-10 m/min 10 min 10 m/min		5 min 6-9 m/min 5 min 9-10 m/min 10 min 10/m/min 10 min12 m/min	5 min 6-9 m/min 5 min 9-10 m/min 10 min 10 m/min 10 min 12 m/min	
	Duration and incline	20 min at 5 °		30 min at 5 °	30 min at 5 °	
2	Warm-up	2 min 6-9 m/min 3min 9-10 m/min		2 min 6-9 m/min 3min 9-10 m/min	2 min 6-9 m/min 3min 9-10 m/min	
	Training	5 min 6-9 m/min 10 min 10 m/min 20 min 12 m/min 10 min 15 m/min		5 min 6-9 m/min 10 min 10 m/min 10 min 12 m/min 20 min 15 m/min 10 min 18 m/min	5 min 6-9 m/min 10 min 10 m/min 10 min 12 m/min 20 min 15 m/min 15 min 18 m/min	
	Duration	45 min at 10 °		55 min at 10 °	60 min at 13 °	
3	Warm-up	5 min 9-10 m/min		5 min 9-10 m/min	5 min 9-10 m/min	
	Training	5 min 12 m/min 20 min 15 m/min 20 min 18 m/min 15 min 18-22 m/min		5 min 12 m/min 10 min 15 m/min 25 min 18 m/min 20 min 18-22 m/min	5 min 12 m/min 5 min 15 m/min 25 min 18 m/min 25 min 18-22 m/min	
	Duration	60 min at 13 °		60 min at 13 °	60 min at 13 °	
4	Warm-up	5 min 9-10 m/min		5 min 9-10 m/min	5 min 9-10 m/min	
	Training	5 min 12 m/min 5 min 15 m/min 25 min 18 m/min 25 min 18-22 m/min		5 min 12 m/min 5 min 15 m/min 25 min 18 m/min 25 min 18-22 m/min	5 min 12 m/min 5 min 15 m/min 25 min 18 m/min 25 min 18-22 m/min	
	Duration	60 min at 13 °		60 min at 13 °	60 min at 13 °	
5	Warm-up	5 min 9-10 m/min		5 min 9-10 m/min	5 min 9-10 m/min	
	Training	5 min 12 m/min 5 min 15 m/min 25 min 18 m/min		5 min 12 m/min 5 min 15 m/min 25 min 18 m/min	5 min 12 m/min 5 min 15 m/min 25 min 18 m/min	

		25 min 18-22 m/min		25 min 18-22 m/min	25 min 18-22 m/min	
	Duration	60 min at 13 °		60 min at 13 °	60 min at 13 °	

Supplemental Table 2: Upstream regulators floxed sedentary vs. trained

Floxed sedentary vs. trained		
Upstream Regulator	**Activation z-score**	**p-value of overlap**
ESRRA	-2,33	1,14E-06
SOX7	-2,00	6,44E-06
MTOR	-2,65	9,09E-05
GATA6	-2,41	1,84E-04
mir-223	-2,00	2,65E-03
DHX36	2,22	1,06E-07
DNMT3B	2,45	6,06E-06
dihydrotestosterone	2,00	7,41E-06
U0126	2,16	3,46E-04
STAT5A	2,21	9,29E-04
SB-431542	2,00	2,00E-03

Supplemental Table 3: Upstream regulators mD4KO sedentary vs. trained

mD4KO sedentary vs. trained		
Upstream Regulator	**Activation z-score**	**p-value of overlap**
bufalin	-2,00	1,58E-07
4-hydroxytamoxifen	-2,53	9,12E-07
troglitazone	-2,25	4,17E-06
GPER1	-2,15	5,45E-06
MEF2C	-2,38	1,85E-05
CREB1	-2,55	2,31E-05
cycloheximide	-2,20	2,91E-05
bezafibrate	-2,20	4,86E-05
dalfampridine	-2,00	1,13E-04
estrogen receptor	-2,00	6,37E-04
FOXO1	-2,58	7,97E-04
NRG1	-2,20	8,90E-04
pirinixic acid	-2,09	2,52E-03
Growth hormone	-2,16	3,26E-03
TCR	-2,21	4,54E-03
RARB	-2,00	6,00E-03
RORA	2,43	2,41E-07
NR1H2	2,15	4,55E-06
SFTPA1	2,24	1,80E-05
ANLN	2,00	4,78E-05
DNMT3A	2,24	1,37E-04
ACOX1	2,24	3,22E-04
PELP1	2,00	2,54E-03

Supplemental Table 4: Upstream regulators sedentary mD4KO vs. floxed

sedentary mD4KO vs. floxed		
Upstream Regulator	**Activation z-score**	**p-value of overlap**
IL10RA	-2,71	2,70E-05
TWIST1	-2,54	6,28E-08
BNIP3L	-2,45	6,01E-06
EDN1	-2,39	1,01E-03
CCR2	-2,38	6,47E-11
epicatechin	-2,24	8,86E-04
IL6R	-2,22	5,72E-04
IGFBP2	-2,18	6,43E-05
SP1	-2,17	5,21E-04
MSTN	-2,17	2,28E-04
dexamethasone	-2,16	1,16E-10
NPM1	-2,12	4,01E-06
SMAD3	-2,08	3,69E-04
SUCNR1	-2,00	1,37E-05
acetaldehyde	-2,00	1,69E-05
vismodegib	-2,00	2,31E-04
BMP10	-2,00	5,62E-03
miR-335-3p	2,00	5,54E-05
miR-338-3p	2,00	1,52E-04
CCN5	2,00	6,85E-04
COL18A1	2,00	4,63E-03
ShK-223	2,00	7,99E-03
sunitinib	2,05	5,89E-07
miR-29b-3p	2,19	8,86E-04
MM-589	2,19	1,97E-05
PTC-209	2,19	2,45E-05
10E,12Z-octadecadienoic acid	2,20	7,38E-03
4-(2-aminoethyl)benzenesulfonylfluoride	2,24	5,35E-06
ciprofloxacin	2,24	2,51E-04
let-7a-5p)	2,25	1,34E-04
ramipril	2,45	8,59E-08

Supplemental Table 5: Upstream regulators trained mD4KO vs. floxed

trained mD4KO vs. floxed		
Upstream Regulator	**Activation z-score**	**p-value of overlap**
IL10RA	-2,50	4,14E-06
NR3C1	-2,48	2,51E-03
PPARG	-2,46	4,93E-04
IL4	-2,46	9,04E-05
LONP1	-2,45	2,70E-04
PTH	-2,44	3,75E-06
Creb	-2,43	4,46E-05
EGF	-2,43	3,22E-11
AR	-2,43	8,65E-08
cholecalciferol	-2,43	8,48E-03
CREB1	-2,41	7,04E-07
CREBBP	-2,41	1,01E-03
FASN	-2,41	2,86E-04
STAT5A	-2,39	1,17E-04
FGF2	-2,39	1,79E-08
pCPT-cAMP	-2,37	5,22E-08
L-glutamic acid	-2,35	2,40E-03
MITF	-2,33	1,87E-04
cyclic AMP	-2,32	9,38E-04
FOXO3	-2,24	1,80E-05
MMP9	-2,24	4,08E-03
TWNK	-2,24	1,03E-05
MKNK1	-2,22	1,24E-04
ALKBH7	-2,21	2,72E-07
FGF21	-2,21	1,50E-03
tetradecanoylphorbol acetate	-2,21	3,91E-06
cobalt chloride	-2,20	9,36E-03
PIK3R1	-2,20	1,05E-03
PDGF BB	-2,20	1,89E-07
fluoxetine	-2,20	4,93E-03
isobutylmethylxanthine	-2,18	1,49E-04
GW501516	-2,18	7,26E-05
fluticasone propionate	-2,13	2,05E-03
EGR2	-2,10	2,93E-04
ERK	-2,10	5,91E-06
glucocorticoid	-2,08	2,45E-03
RXRA	-2,01	2,42E-04
dalfampridine	-2,00	8,35E-03
GC-GCR dimer	-2,00	6,01E-04
ALKBH1	-2,00	4,61E-05
NSUN3	-2,00	1,93E-06

Supplemental Table 6: Molecular functions in floxed sedentary vs. trained

Floxed sedentary vs. trained		
Molecular function	**Activation z-score**	**p-value**
Cellular Movement,Hematological System Development and Function,Immune Cell Trafficking	-2,54	6,94E-04
Cell Death and Survival,Cellular Development,Nervous System Development and Function,Tissue Development,Tissue Morphology	2,00	1,74E-04
Cell Death and Survival,Skeletal and Muscular Disorders	2,07	2,18E-06
Cell Death and Survival	2,11	7,27E-06

Supplemental Table 7: Molecular functions in mD4KO sedentary vs. trained

mD4KO sedentary vs. trained		
Molecular function	**Activation z-score**	**p-value**
Organismal Development	-2,43	2,31E-04
Cardiovascular Disease,Organismal Injury and Abnormalities	2,00	4,22E-04
Cellular Development,Cellular Growth and Proliferation,Embryonic Development	2,03	6,90E-04
Cancer,Dermatological Diseases and Conditions,Organismal Injury and Abnormalities	2,18	5,33E-06
Cardiovascular Disease	2,21	2,57E-04
Cardiovascular Disease,Organismal Injury and Abnormalities	2,22	2,72E-05
Nervous System Development and Function,Tissue Morphology	2,34	2,55E-04

Supplemental Table 8: Molecular functions in sedentary mD4KO vs. floxed

sedentary mD4KO vs. floxed		
Molecular function	**Activation z-score**	**p-value**
Cellular Growth and Proliferation	-3,54	3,51E-05
Cellular Development,Cellular Growth and Proliferation,Nervous System Development and Function,Tissue Development	-2,63	3,21E-05
Cellular Assembly and Organization,Cellular Function and Maintenance	-2,41	6,41E-06
Cell Death and Survival	-2,30	1,52E-07
Cellular Movement	-2,24	9,62E-09
Cell-To-Cell Signaling and Interaction,Hematological System Development and Function,Immune Cell Trafficking	-2,23	1,24E-06
Cancer,Neurological Disease,Organismal Injury and Abnormalities	-2,22	3,33E-07
Cardiovascular System Development and Function,Embryonic Development,Organ Development,Organismal Development,Tissue Development	-2,20	6,31E-06
Cellular Movement	-2,16	1,48E-06
Embryonic Development,Organismal Development	-2,16	7,22E-07
Tissue Development	-2,03	8,49E-06
Organismal Survival	2,08	1,17E-08
Cellular Movement,Immune Cell Trafficking	2,20	4,86E-05
Gastrointestinal Disease,Hepatic System Disease,Organismal Injury and Abnormalities	2,56	7,42E-09

Supplemental Table 9: Molecular functions in trained mD4KO vs. floxed

trained mD4KO vs. floxed		
Molecular function	**Activation z-score**	**p-value**
Infectious Diseases	-2,64	9,12E-04
Cellular Assembly and Organization,Cellular Function and Maintenance	-2,57	1,69E-03
Lipid Metabolism,Small Molecule Biochemistry,Vitamin and Mineral Metabolism	-2,48	1,13E-03
Lipid Metabolism,Small Molecule Biochemistry	-2,41	1,60E-03
Organismal Development	-2,24	1,93E-03
Cellular Development,Connective Tissue Development and Function,Tissue Development	-2,22	1,75E-03
Cell Death and Survival	-2,20	2,01E-03
Cell Morphology,Cellular Development,Cellular Growth and Proliferation,Nervous System Development and Function,Organismal Development,Tissue Development	-2,19	1,43E-03

7.4 Supplemental Figures

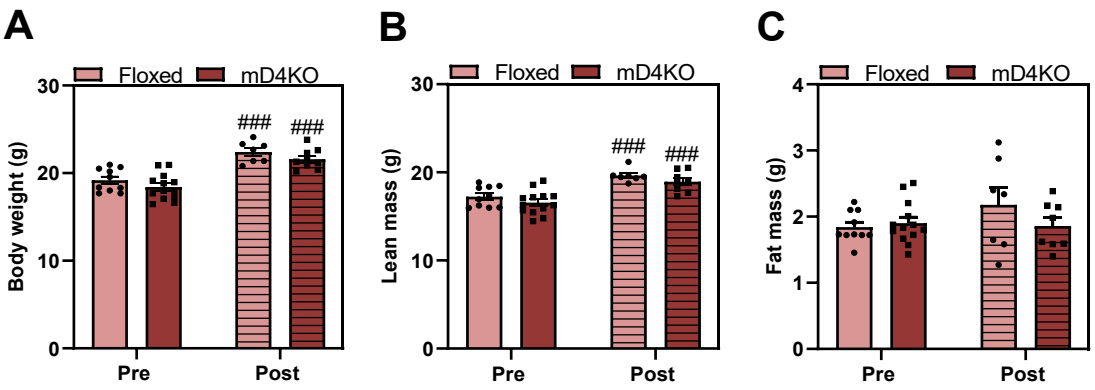

Supplemental Figure 1: Body composition of female mD4KO mice pre and post chronic exercise training. Body weight (**A**), lean (**B**) and fat (**C**) mass of floxed controls and mD4KO littermates pre and post chronic exercise training. Data are shown as mean ± SEM (n=8-13). Floxed vs. mD4KO, 2-way ANOVA with Sidak post-test; ### P<0.001, pre vs. post, 2-way ANOVA with Sidak post-test. Pink bars represent floxed controls, whereas red bars display mD4KO mice. Additionally, striped bars symbolize the trained situation.

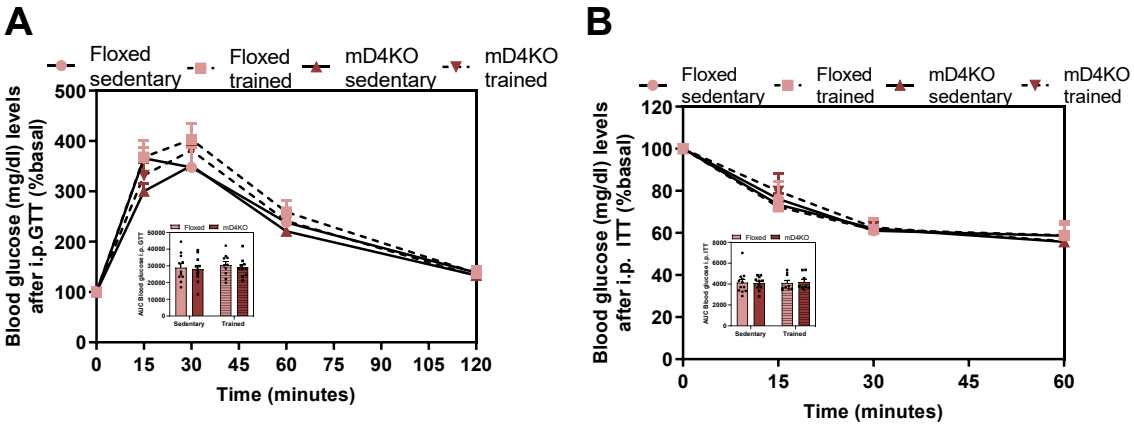

Supplemental Figure 2: Glucose and insulin tolerance in female mD4KO mice baseline corrected. Baseline corrected blood glucose levels and respective AUC after an i.p.GTT (**A**). Data are shown as mean ± SEM (n=9-11). Floxed sedentary vs. floxed trained vs. mD4KO sedentary vs. mD4KO trained, 2-way ANOVA with Tukey post-test. Blood glucose levels and AUC baseline corrected after an i.p.ITT (**B**). Data are shown as ± SEM (n=8-12). Floxed sedentary vs. floxed trained vs. mD4KO sedentary vs. mD4KO trained, 2-way ANOVA with Tukey post-test. Pink bars represent floxed controls, whereas dark red bars display mD4KO mice. Additionally, striped pattern represents the trained condition.

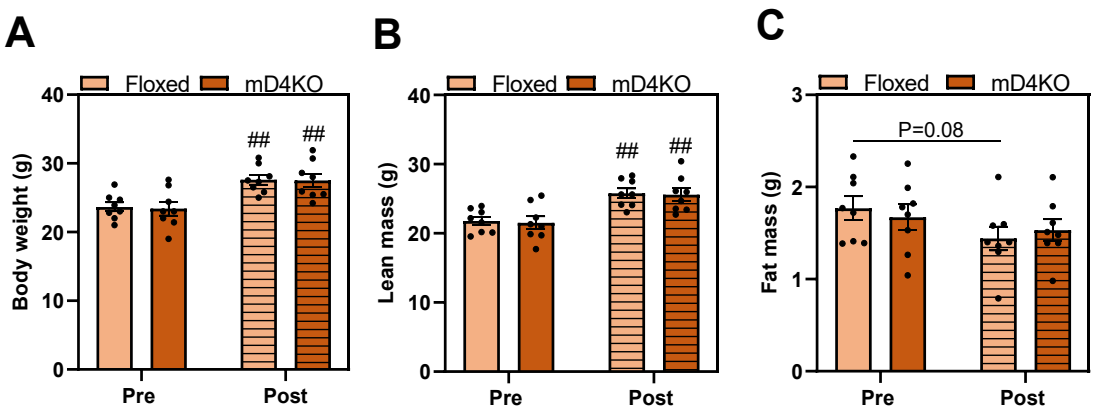

Supplemental Figure 3: Body composition of male mD4KO mice pre and post chronic exercise training. Body weight (**A**), lean (**B**) and fat (**C**) mass of floxed controls and mD4KO littermates pre and post chronic exercise training. Data are shown as mean ± SEM (n=8). Floxed vs. mD4KO, 2-way ANOVA with Sidak post-test; ### P<0.001, pre vs. post, 2-way ANOVA with Sidak post-test. Light orange bars represent floxed controls, whereas dark orange bars display mD4KO mice. Additionally, striped bars symbolize the trained situation.

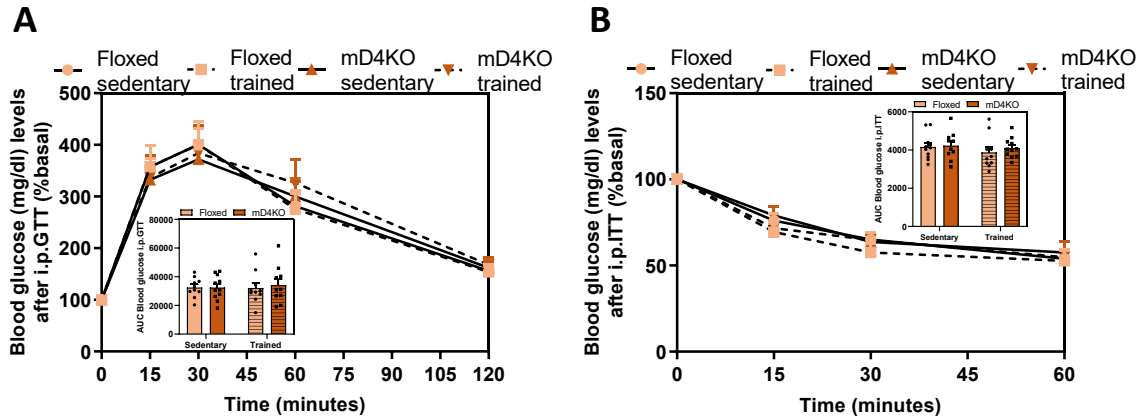

Supplemental Figure 4: Glucose and insulin tolerance in male mD4KO mice baseline corrected. Baseline corrected blood glucose levels and respective AUC after an i.p.GTT (**A**). Data are shown as mean ± SEM (n=10-11). Floxed sedentary vs. floxed trained vs. mD4KO sedentary vs. mD4KO trained, 2-way ANOVA with Tukey post-test. Blood glucose levels and AUC baseline corrected after an i.p.ITT (**B**). Data are shown as ± SEM (n=10-11). Floxed sedentary vs. floxed trained vs. mD4KO sedentary vs. mD4KO trained, 2-way ANOVA with Tukey post-test. Light orange bars represent floxed controls, whereas dark orange bars display mD4KO mice. Additionally, striped pattern represents the trained condition.

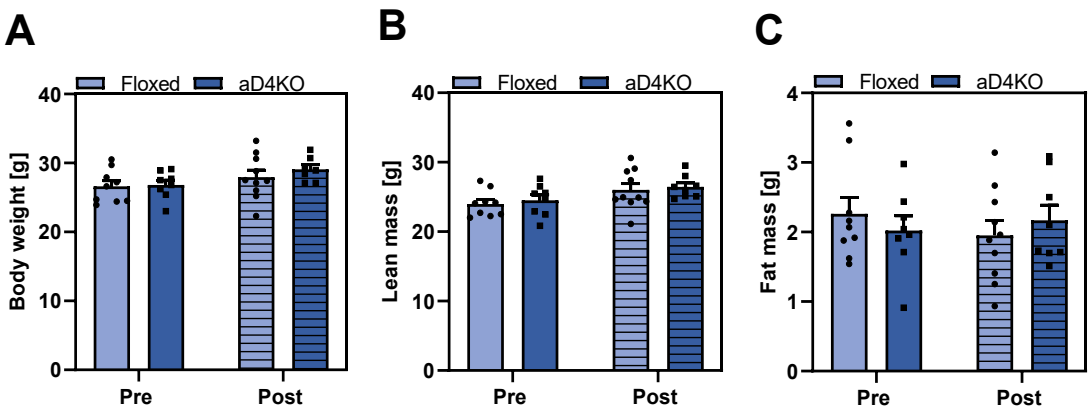

Supplemental Figure 5: Body composition of aD4KO mice pre and post chronic exercise training. Body weight (**A**), lean (**B**) and fat (**C**) mass of floxed controls and aD4KO littermates pre and post chronic exercise training. Data are shown as mean ± SEM (n=7-10). Floxed vs. aD4KO, 2-way ANOVA with Sidak post-test; Pre vs. post, 2-way ANOVA with Sidak post-test. Light blue bars represent floxed controls, whereas dark blue bars display mD4KO mice. Additionally, striped bars symbolize the trained situation.

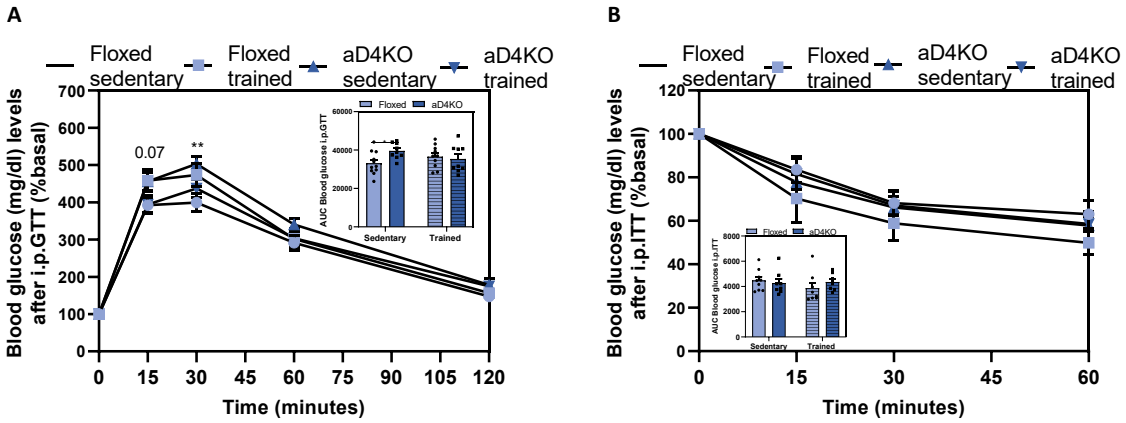

Supplemental Figure 6: Glucose and insulin tolerance in aD4KO mice baseline corrected. Baseline corrected blood glucose levels and respective AUC after an i.p.GTT (**A**). Data are shown as mean ± SEM (n=9-11). * P<0.05, *** P<0.001, floxed sedentary vs. aD4KO sedentary, 2-way ANOVA with Tukey post-test; # P<0.05, floxed sedentary vs. floxed trained, 2-way ANOVA with Tukey post-test. Blood glucose levels and AUC baseline corrected after an i.p.ITT (**B**). Data are shown as ± SEM (n=8-9). Floxed sedentary vs. floxed trained vs. aD4KO sedentary vs. aD4KO trained, 2-way ANOVA with Tukey post-test. Light blue bars represent floxed controls, whereas dark blue bars display aD4KO mice. Additionally, striped pattern represents the trained condition.

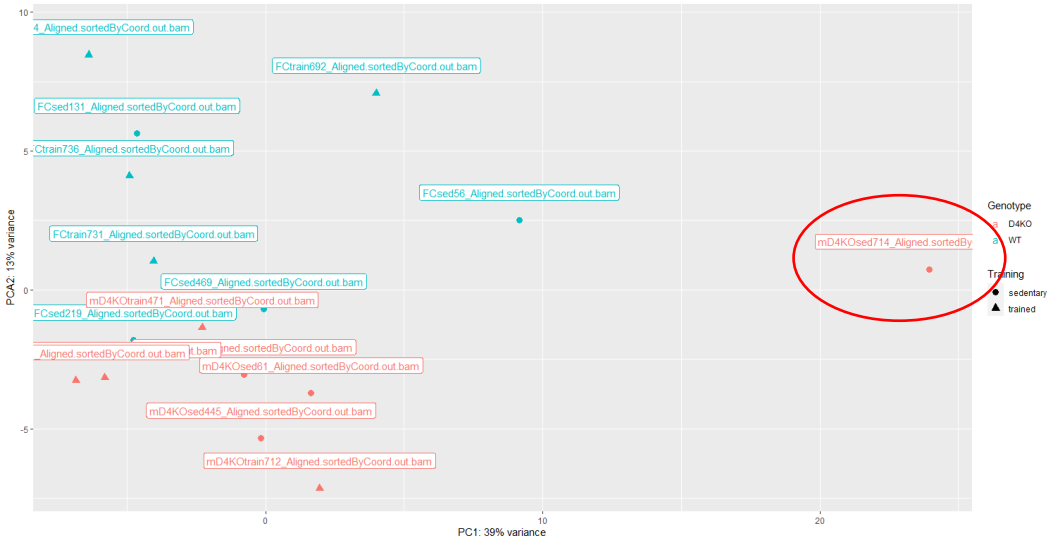

Supplemental Figure 7: Principal Component Analysis (PCA). The PCA displays the variance between RNA sequencing samples in the same condition. Dots display the sedentary and triangle the trained state. The red color scheme represents mD4KO animals and the blue color displays the floxed controls. One sample in the sedentary mD4KO group was identiefied as outlier and excluded from further analysis, marked with a red circle.

A

Floxed sedentary vs. trained			
Pathway	**Adj. p-value**	**Pathway Size**	**Candidates contained (%)**
Chemokine receptors bind chemokines	5,95E-04	52	5 (9,61 %)
Cytokine-cytokine receptor interaction	8,79E-04	292	9 (3,08 %)
Muscle contraction	4,32E-03	155	6 (3,87 %)
NF-kappa B signaling pathway	8,79E-04	105	6 (5,71 %)
Striated Muscle Contraction	8,49E-05	31	5 (16,13 %)
Viral protein interaction with cytokine and cytokine receptor	4,32E-03	95	5 (5,26 %)

B

mD4KO sedentary vs. trained			
Pathway	**Adj. p-value**	**Pathway Size**	**Candidates contained (%)**
Hypertrophic cardiomyopathy	2,66E-02	91	5 (5,49 %)

C

sedentary mD4KO vs. Floxed			
Pathway	**Adj. p-value**	**Pathway Size**	**Candidates contained (%)**
AGE-RAGE signaling pathway in diabetic complications	2,46E-03	101	7 (6.93 %)
Collagen degradation	1,44E-03	19	4 (21,05 %)
Degradation of the extracellular matrix	3,64E-04	94	8 (8,51 %)
ECM-receptor interaction	2,89E-06	88	10 (11,36 %)
Extracellular matrix organization	3,22E-10	254	20 (7,87 %)
Focal adhesion	9,41E-05	201	12 (5,97 %)
Human papillomavirus infection	8,01E-03	359	12 (3,34 %)
Integrin cell surface interactions	1,11E-03	55	6 (10,91 %)
PI3K-Akt signaling pathway	2,46E-03	359	13 (3,62 %)
Post-translational protein phosphorylation	4,19E-03	112	7 (6,25 %)
Regulation of Insulin-like Growth Factor (IGF) transport and uptake by Insulin-like Growth Factor Binding Proteins (IGFBPs)	1,30E-03	118	8 (6,78 %)

Supplemental Figure 8: CPDB Pathway analysis. Significantly affected pathways in floxed sedentary vs. trained (**A**), mD4KO sedentary vs. trained (**B**), sedentary mD4KO vs. floxed (**C**). Significance threshold adj. p-value < 0.05.

7.5 List of Figures

7.6 List of Tables

Danksagung

Eine lange, lehrreiche und aufregende Zeit mit vielen Höhen und den ein oder anderen Tiefen geht nun zu Ende. Ohne die Hilfe und Unterstützung vieler Personen wäre die vorliegende Arbeit nicht zustandegekommen. Dafür möchte ich mich an dieser Stelle bedanken.

Zunächst danke ich Prof. Dr. Hadi Al-Hasani für die Möglichkeit, meine Doktorarbeit an seinem Institut für Klinische Biochemie und Pathobiochemie am Deutschen Diabetes Zentrum zu schreiben. Zudem bedanke ich mich für die Möglichkeit meine Forschungsergebnisse auf nationalen und internationalen Kongressen präsentieren zu dürfen.

Des Weiteren bedanke ich mich bei Prof. Dr. Christine R. Rose für die Übernahme des Zweitgutachtens.

Als nächstes gilt mein großer Dank Dr. Alexandra Chadt, die mir trotz des alltäglichen Chaos bei jeglichen Fragen selbstverständlich zur Seite stand, immer ein offenes Ohr hatte und zudem zu allen aufkommenden Problemen eine passende Lösung parat hatte. Zusätzlich danke ich ihr für ihre Ideen und Anregungen, die das Projekt maßgeblich vorangebracht haben.

Für ihre tatkräftige Unterstützung bei den unzähligen *ex vivo* Versuchen im Isotopenlabor danke ich Anette Kurowski und Heidrun Podini. Außerdem bedanke ich mich herzlich bei Birgit Knobloch für ihre Hilfe bei der Arbeit mit den Mäusen.

Des Weiteren bedanke ich mich bei Svenja Saurbier und Marina Tautz, die ich während ihrer Zeit als Masterandinnen unterstützen durfte. Es hat mir große Freude bereitet mit euch zusammen zu arbeiten.

Ebenfalls möchte ich mich besonders bei allen aktuellen und ehemaligen Mitarbeiter:innen des Instituts für Klinische Biochemie und Pathobiochemie bedanken: Dr. Christian Springer, Dr. Delsi Altenhofen, Dr. Christian Binsch, Dr. Samaneh Eickelschulte, Dr. Matthias Dille, Dr. Tim Benninghoff, Dr. Christian de Wendt, Sarah Görigk, Jenny Khuong, Didi Bedou, Anna Scheel, Pia Marlene Förster, Katharina Kaiser, Sebastian Sill, Aleksandra Nikolic, Angelika Horrighs, Antonia Osmers, Dagmar Grittner, Carina Heitmann und Delia Bahn. Es ist einfach Erfolge gemeinsam zu feiern, aber ich weiß es umso mehr zu schätzen, dass ihr mich auch bei den ein oder anderen Hindernissen und Tiefen unterstützt habt. Ohne unser gemeinsames Lachen während den Mittagspausen wäre meine Zeit hier nur halb so schön gewesen.

Mein allerherzlichster Dank geht an meine Eltern, die mich in jeder Phase unterstützen, meine Sorgen und Ängste teilen und mir dennoch das Gefühl geben alles schaffen zu können. Danke, dass ihr immer für mich da seid und ich mich auf euch verlassen kann!

Zum Schluss möchte ich meine immense Dankbarkeit gegenüber dir, Eduard, zeigen. Ich weiß, die letzten Jahre waren sehr ausdauernd und anstrengend, in der ich mich häufig bei dir beschwert habe. Danke, für deine Ruhe und Geduld. Danke, dass du mich immer wieder aufbaust und ich mich auf dich verlassen kann. Wie schön, dass ich dich in meinem Leben habe.

Erklärung

Ich versichere an Eides Statt, dass die Dissertation von mir selbstständig und ohne unzulässige fremde Hilfe unter Beachtung der „Grundsätze zur Sicherung guter wissenschaftlicher Praxis an der Heinrich-Heine-Universität Düsseldorf“ erstellt worden ist.

Ferner versichere ich, dass die Dissertation bisher keiner anderen Fakultät vorgelegt worden ist.

Düsseldorf, den 16.03.2023

_____

Lena Espelage